Cell Imprinted Polymers Integrated with Microfluidic Biosensors for Electrical and Electrochemical Detection of Bacteria in Water

Shiva Akhtarian

A DISSERTATION SUBMITTED TO

THE FACULTY OF GRADUATE STUDIES

IN PARTIAL FULFILLMENT OF THE REQUIREMENTS

FOR THE DEGREE OF DOCTOR OF PHILOSOPHY

GRADUATE PROGRAM IN MECHANICAL ENGINEERING

YORK UNIVERSITY

TORONTO, ONTARIO

January 2024

Abstract

There is a growing demand for sensors that enable rapid, cost-effective, and laboratory-free detection of microorganisms in clinical, food and environmental samples. Traditional methods are slow, expensive, and require specialized personnel. Biosensors offer a promising alternative but face challenges like instability, high cost, short lifespan, and complex synthesis of the biorecognition elements. Molecularly imprinted polymers (MIPs) provide a more robust, cost-effective solution by embedding the target analyte's imprint into a polymer matrix. While MIPs are effective for small molecules, designing them for biological cells is more complex due to their structural diversity. Noncovalent interactions, preferred in synthesizing cell-imprinted polymers (CIPs), enable easier binding and dissociation. Selecting suitable functional monomers is crucial, as their interactions with cell surface molecules determine imprinting success. However, the effects of CIP composition on the bacterial capture efficiency remain unexplored. Furthermore, integrating CIPs into microfluidic and electrochemical sensing platforms is vital for portable, real-time detection systems.

This research aimed to improve the understanding of the CIPs' effectiveness in capturing bacteria to develop effective bacteria sensing platforms using microfluidic devices. In **Objective 1**, we optimized a polymerization methodology for uniform functionalization of stainless steel microwires reproducible CIP coatings, imprinted with *E. coli* as the template. In **Objective 2**, we assessed *E. coli* rebinding performance which demonstrated 76±5 % uptake efficiency with the optimized composition. In **Objective 3**, we integrated CIPs into a conductometric-based microfluidic sensor. Resistance changes normalization and subsequent analysis of the dose-response curve revealed a dynamic range of 10^4 to 10^7 CFU/mL, with limit of detection (LOD) of 2.1×10^5 CFU/mL. Specificity experiments demonstrated specificity of the sensor towards

imprinted *E. coli* cells. Further improvements were made by modifying the sensor design to a three-electrode configuration and employing electrochemical impedance spectroscopy (EIS). The charge-transfer resistance changes normalization and the subsequent analysis revealed an enhanced LOD of 2×10^2 CFU/mL, with a broader dynamic range of 10^2 to 10^7 CFU/mL. The proposed sensor has the potential to offer a cost-effective, durable, portable, and real-time solution for the detection of waterborne pathogens. Future impacts include enhancing bacterial detection in environmental monitoring, food safety, and healthcare.

Acknowledgements

Completing this research and writing this thesis has undoubtably been one of the most challenging yet rewarding experiences of my academic journey. As I reflect on this accomplishment, I am filled with immense gratitude for all the people who have supported me along the way.

First and foremost, I would like to express my deepest appreciation to my supervisors, Professor Pouya Rezai and Professor Satinder Kaur Brar. Their guidance, encouragement, and unwavering support have been pivotal in shaping both my research and my growth as a scholar. Their expertise, thoughtful insights, and mentorship have made this thesis possible, and I am forever grateful for the opportunity to work under their direction.

I am also sincerely thankful to my committee members, Professors Jennifer Chen and Sunny Leung, for their invaluable feedback and collaborative spirit throughout this process. Their guidance, specially during committee meetings and my comprehensive exam, has been essential in refining my work and broadening my perspective.

I would like to express my deepest gratitude to my husband, Alireza, whose unwavering love, support, and companionship have sustained me through this journey. Meeting and marrying him midway through my studies has been a true blessing. I also want to extend my heartfelt thanks to my parents and my brother, Sina, for their endless support, love, and believe in me, despite the physical distance between us. I owe everything to them; without their support, I would not be where I am today.

Finally, I would like to acknowledge the financial support and recognitions I received throughout my PhD including SME Toronto Chapter 26 Joseph R. Benedetto Scholarship, the Ontario Onsite Wastewater Association (OOWA) University Scholarship, the Manulife Graduate

Scholarship, the Parya Scholarship, and from the York University for the Susan Mann Dissertation Scholarship and Provost Dissertation Scholarship, the 2024 Mechanical Engineering PhD Excellence Award for Graduate Research, the York Graduate Scholarship, the Academic Excellence Award, and the Francis Tetteh Memorial Award.

Table of Contents

List of Tables

List of Figures

Abbreviations

AAM: Acrylamide

AIBN: N-N’-bis isobutyronitrile

BAs: Biological agents

BCE: Bacteria capture efficiency

CBR: cell binding ratio

CIP: Cell imprinted polymer

CNTs: carbon nanotubes

DC: Direct Current

DHEBA: Dihydroxyethylene-bisacrylamide

DI: Deionized

DMSO: Dimethyl sulfoxide

DOE: Design of experiment

EBs: Electrochemical biosensors

EIS: Electrochemical impedance spectroscopy

FETs: Field-effect transistors

EGDMA: Ethylene glycol dimethacrylate

FMs: functional monomers

FRET: Fluorescent resonance energy transfer

GFP: Green fluorescent protein

HAV: Hepatitis A virus

HEMA: Hydroxyethyl methacrylate

HIV: Human immunodeficiency virus

Ips: Imprinted polymers

JEV: Japanese encephalitis virus

LOC: Lab-on-a-chip

LOD: Limit of detection

LOQ: Limit of quantification

LPS: Lipopolysaccharides

LV: Leprosy virus

MAA: Methacrylic acid

MBAA: N, N-methylenebisacrylamide

MEMS: Micro-Electro-Mechanical Systems

MIP: Molecularly imprinted polymer

MIT: Molecular imprinting technique

MMA: Methyl methacrylate

MWs: microwires (MWs)

NIP: Non-imprinted polymers

PBS: Phosphate-buffered saline

PDMS: Polydimethylsiloxane

PON: Point-of-Need

QCM: Quartz crystal microbalance

RE: Reference electrode

RFP: Red fluorescent protein

RSM: Response surface methodology

RV: Rabies virus

SAMs: Self-assembly monolayers

SD: standard deviation

SEM: Scanning electron microscopy

SPME: Solid phase microextraction

SS: Stainless-steel

TEOS: tetraethyl orthosilicate

TFMAA: Trifluoro methacrylic acid

TMV: Tobacco mosaic virus

TRIM: Trimethylolpropane trimethacrylate

TRL: Technology Readiness Level

2-VP: 2-vinyl pyridine

4-VP: 4-vinyl pyridine

WE: Working electrode

Chapter 1[i]

1. Motivation and introduction

The demand for diagnostic devices that allow for rapid, affordable, and laboratory-free detection of pathogenic and indicator microorganisms is increasingly evident. This need is critical for applications in clinical settings, food safety, and environmental monitoring, where timely identification of microorganisms can significantly impact public health and safety [1]–[4]. For instance, various infectious diseases are caused by different bacterial microorganisms (e.g., *Escherichia coli O157:H7* and *methicillin-resistant Staphylococcus aureus (MRSA)*) present in the soil, food and water resources [2], [3], [5]. The conventional methods of detecting these microorganisms are cell culturing techniques, molecular tests and immunological assays [3], [4]. However, these methods are laboratory-based, time-consuming and require costly and complex

[i] Some content of this chapter has been published in "Akhtarian, S., Doostmohammadi, A., Youssef, K., Kraft, G., Kaur Brar, S. and Rezai, P., 2023. Metal microwires functionalized with cell-imprinted polymer for capturing bacteria in water. ACS Applied Polymer Materials, 5(5), pp.3235-3246". Permissions for the use of the text has been received from American Chemical Society.

equipment and trained personnel to be performed[6]. These limitations and challenges indicate the need to develop reliable rapid, low-cost, and miniaturized detection techniques to detect pathogenic and indicator microorganisms [7].

In this context, biosensors have emerged as highly sensitive bioanalytical devices [8]. Biosensors consist of two main components: bio receptor (recognition elements) and transducers. This configuration integrates the transducer's sensitivity with the bioreceptor's selectivity, facilitating the precise detection of target analytes [9]. Upon selective binding of the recognition element to the target analyte, a transducer is required to transform the binding event on the bio receptor into a measurable signal [10]. The most used transduction mechanisms include optical [11]–[15], electrical, electrochemical [16] and mass-based (i.e., Quartz Crystal Microbalance (QCM))[17] transducers. Electrical and Electrochemical biosensors (EBs) are claimed to be the most sensitive and reliable types of transducers [18]. Additionally, they are rapid, cost-effective, and capable of being miniaturized, which are major requirements in developing point-of-need (PoN) sensors for monitoring non-patient samples such as air and water [19]. This category of transducers can quantitatively detect the biological target by enabling the direct and label-free conversion of biological recognition into a target concentration-related electrical signal read-out [20]. To achieve this, the bio receptor is required to be immobilized on an electrical interface, such as electrodes, nanowire arrays, and field-effect transistors (FETs) [9].

The common strategy in developing electrochemical biosensors for detecting microorganisms is using recognition elements such as antibodies, enzymes, and active proteins [21]. However, despite their high sensitivity and specificity, these sensing elements have major inherent limitations, such as thermal and chemical instability, very high cost, low reproducibility, short on-

shelf lifetime, and complicated synthesis and integration process [22]. Many bacteria electrochemical biosensors have been developed using bio-recognition materials such as bacteriophages, aptamers, and antibodies [23], [24]. While these biosensors show excellent detection performance in laboratory conditions, their real-world deployment is limited due to their high cost and the instability of bio-receptors when exposed to environmental changes, particularly in extreme temperature and humidity conditions.

Molecularly imprinted polymers (MIPs) and Cell-Imprinter Polymers (CIPs) are new class of synthetic recognition materials with low cost. It has been proved that they offer physically and chemically stable and selective recognition sites similar to the biological receptors, such as antibodies, enzymes, and active proteins [24], [25]. The method of synthesizing MIPs is called the molecular imprinting technique (MIT). CIPs are synthesized using MIT too, with a target cell serving as the template during fabrication rather than a molecule.

Although MIPs have various advantages over conventional receptors, there are some limitations and challenges in developing MIP-based sensors. The main challenges include lack of a general preparation procedure (especially with biological agents (BAs) as a target), the complexity of integration with a transducer, and difficulty of binding transformation into an electrical read-out signal [26]. This is also true for the case of BA-imprinted polymers that have been synthesized during the last few years.

This research aims to help gain a fundamental understanding of CIPs in microfluidic biosensing applications by developing and optimizing a methodology for the controllable synthesis of BA-specific CIP coatings on the surface of conductive microwire (MW) electrodes. The prepared CIP-

MWs will be integrated within a novel microfluidic biosensing platform for further electrical transduction of target binding to the synthesized CIPs.

1.1. Biosensors

Biosensors have emerged as complementary sensing platforms to the in-lab diagnostic methods and have developed into rapid, sensitive, and reliable sensing tools for recognizing biomarkers. Moreover, offering an easy operation, requiring minimal sample pre-treatment and low-cost instrumentation, makes this technique suitable for developing miniaturized PON devices [1], [27].

Generally, biosensors consist of two main components: bioreceptors and transducers. Bioreceptors or recognition elements can selectively bind to the target biomarkers, and transducers are responsible for transforming the binding event into a measurable signal. The performance of a biosensor, such as sensitivity, selectivity, speed, limit of detection (LOD), limit of quantification (LOQ) and stability, is directly related to the type and performance of these bioreceptors and transducers [9], [28].

Biosensors can be classified into four main groups of antibodies- or immune-based, antigen-based, DNA-based, and cell-based, according to the type of their affinity agents and their interactions as illustrated in Fig. 1-1. All the recognition elements mentioned above are chemical or biological receptors, and because of their biological origins, they have various inherent limitations. These limitations include thermal and chemical instability, high cost, low reproducibility, and complicated synthesis and integration process [17]. On the other hand, synthetic receptors can offer a favourable alternative to their biological counterparts. In this context, molecular imprinting has emerged as an efficient and versatile method for synthesizing

robust, cost-effective receptors called MIPs, which are recognized for their high specificity as innovative synthetic recognition materials [26]. It has been reported that they offer selectivity comparable to biological receptors, such as antibodies, enzymes, and active proteins, while generally demonstrating higher physical and chemically stability [24], [25], [29]. Imprinted polymers were selected as synthetic bioreceptors in this project due to their enhanced stability and versatility, and will be reviewed in more detail in future sections.

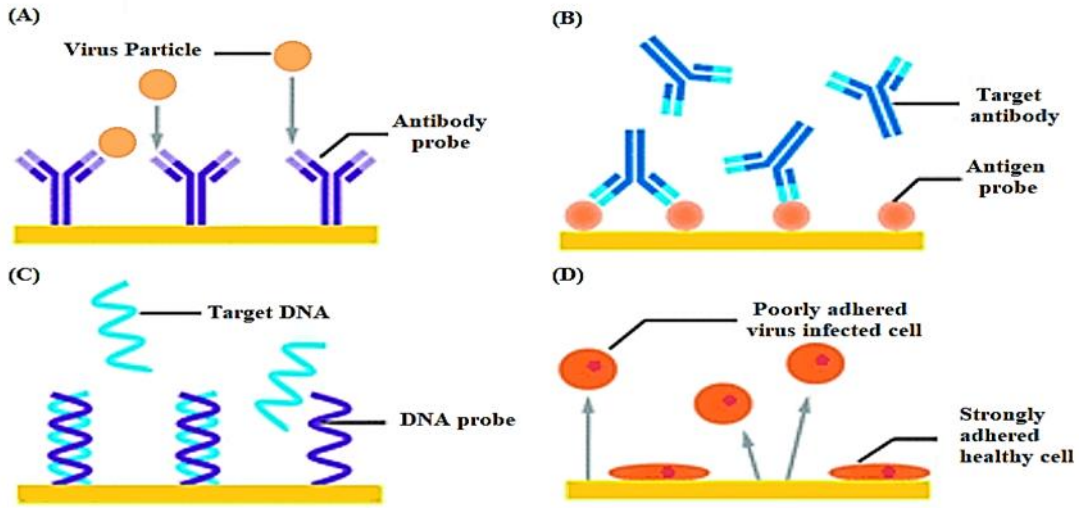

Fig. 1-1. Schematic of different categories of biosensors based on the nature of their affinity reactions. (A) antibody or immune-, (B) antigen- (C) DNA-, and (D) cell-based biosensors [30]. *Reprinted with permission from Royal Society of Chemistry.*

1.2. Developing biosensors with microfluidics technology

To integrate the two main components of biosensors (i.e., bioreceptor and transducer), microfluidic-based approaches have been used during the last few decades [31]. Microfluidic-based detection platforms and microfluidics integrated biosensors are extensively utilized in the creation of Lab-on-a-chip (LOC) and point of care (POC) devices [32], [33]. These systems enable

the efficient analysis of samples by miniaturizing laboratory processes, allowing for rapid and on-site testing and diagnosis. Microfluidics technology enables the creation of portable, cost-effective, and rapid response sensors with reduced reaction times by manipulating very tiny amounts of samples within channels and chambers on a scale of a few to hundred micrometres [34]. Fig. 1-2 demonstrates an overview schematic of a microfluidic-based biosensor for detecting BAs. The system comprises three key components: the sample point, where biological samples are introduced; the sensing point, which incorporates recognition elements to interact with the target analytes; and the signal/output unit, which converts these interactions into measurable signals—whether optical, electrical, or electrochemical—enabling effective detection. This integrated platform allows for efficient and rapid identification of target biological substances, significantly enhancing diagnostic capabilities across various applications.

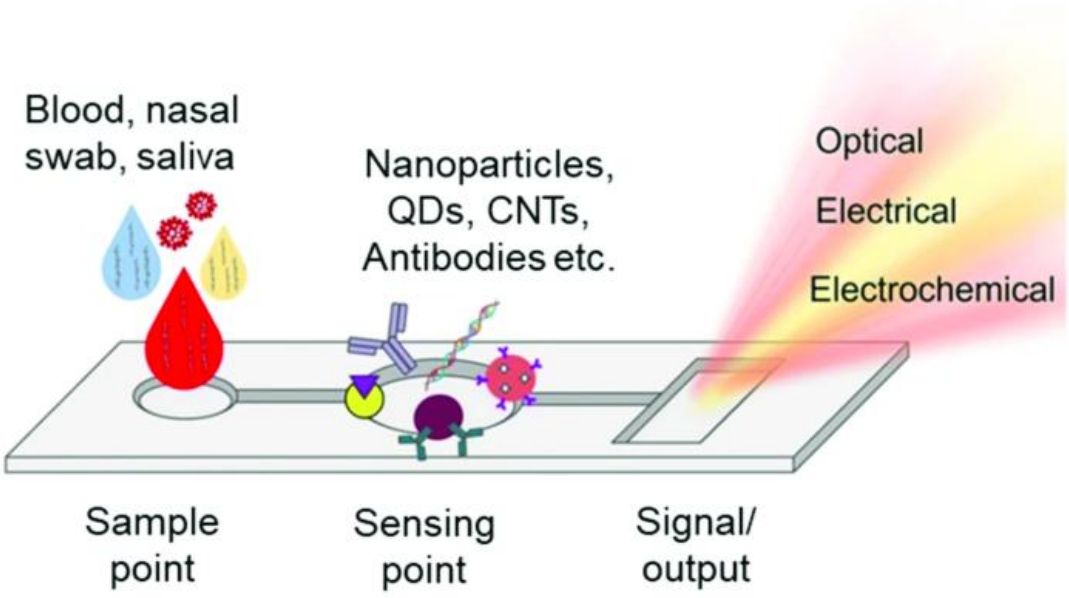

Fig. 1-2. Overview of a microfluidic biosensor for detecting biological agents (BAs) [35], *Open Access.*

Numerous fabrication methods have been used to develop microfluidic-based sensors, such as injection moulding, soft lithography, photolithography, and 3D printing [36]. However, the soft lithography method based on polydimethylsiloxane (PDMS) elastomer has attracted great attention due to the exceptional properties of PDMS such as biocompatibility, transparency, and simple fabrication method [37].

Microfluidic-based sensors usually include the sensing element and the transduction unit to transform the sensing event into a readable signal. However, in some microfluidic sensors, the transduction unit is not integrated into the microfluidic device, and the measurement takes place off-chip using external equipment [38]. Fig. 1-3 represents two main units of a microfluidic biosensor, i.e., the sensing and detection units. The sensing unit comprises elements such as functionalized nanoparticles, biological entities, and metallic electrodes. For the detection unit, electrochemical and optical detection systems are the most widely utilized methods in microfluidic sensors [34]. Microfluidic detection platforms also enable the possibility of performing various analyses within the same chip or by small modifications of the microchannel patterns. Therefore, microfluidic-based detection platforms and LOC devices have been widely studied and evaluated for substituting conventional laboratory-based techniques [39].

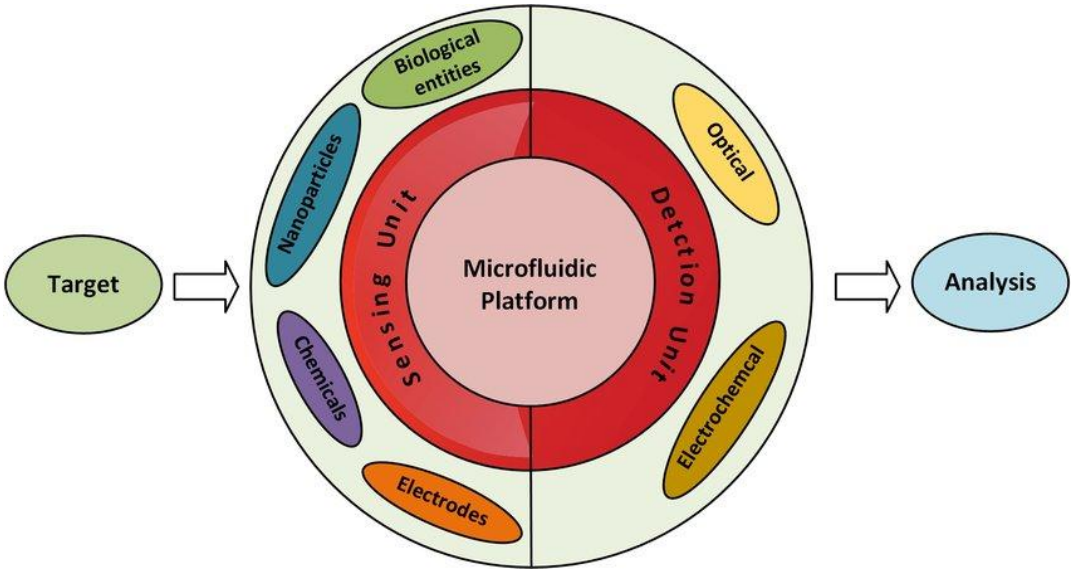

Fig. 1-3. Illustration of different components of microfluidic-based sensory systems [39], *Open Access*

1.3. Molecularly imprinted polymers (MIPs) and cell imprinted polymers (CIPs)

MIPs (Fig. 1-4) are polymeric networks formed in the presence of molecules that they are designed to detect, called the template molecules. Other main components of MIPs formulation are functional monomers, cross-linkers, initiators, and solvents [40]. The method of synthesizing MIPs is called the molecular imprinting technique (MIT). In this method shown in Fig. 1-4, a cross-linked polymer matrix is formed in the presence of the target molecule/cell, usually called "template." The formation of this network between the functional monomers of MIPs and the template molecules during the polymerization process is the main idea behind MIP's selective binding ability to that specific template. After polymerization and removing the template molecule, its imprint remains on the resultant polymer network. This imprint retains the morphological/physical, chemical, and functional properties of the target molecule and thus can

selectively bind to it in complex samples, such as environmental samples and biological fluids [40].

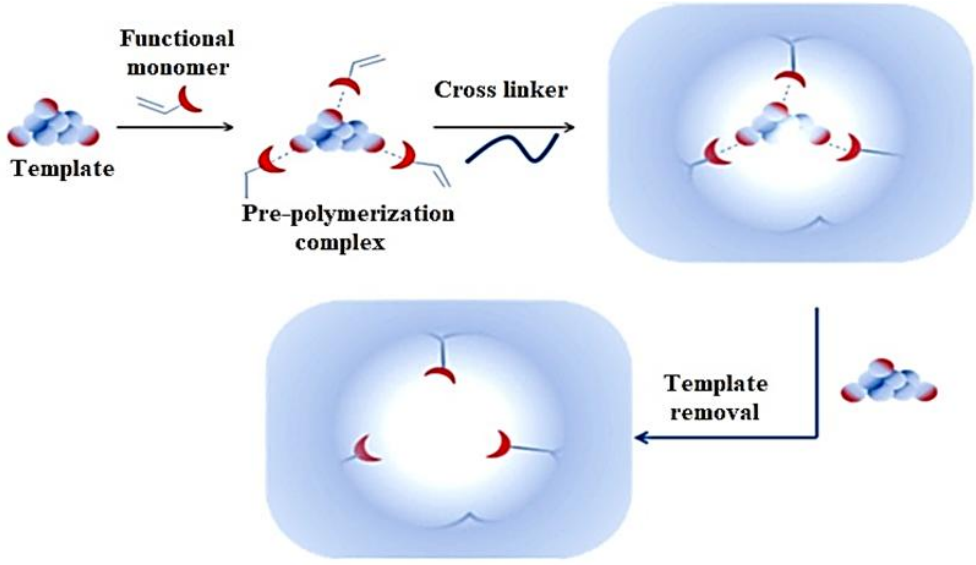

Fig. 1-4. Schematic of molecular imprinting technique [41], *Open Access.*

The versatility of MIPs has been confirmed since they can provide recognition sites for a wide range of target molecules in different shapes, sizes, functionalities, and even BAs [17]. Moreover, the preparation/ synthesis of MIPs is simple, and their properties can be tuned with engineering techniques to achieve desired binding and recognition characteristics for applications in biosensors and bioassays [17], [42]. Therefore, MIPs can be synthesized and employed as recognition elements to detect emerging BAs.

The main components of MIPs formulation can be listed as functional monomers, cross-linkers, initiators, and orogenic solvents. The formulation of MIPs and synthesis parameters define the final MIPs' morphology and binding performance. The selection of appropriate functional monomers is the first step in synthesizing MIPs since it defines the nature of the interaction between MIP and template molecule, and thus it directly affects the binding and specificity

properties of the final synthesized MIPs. This selection is made based on the nature and strength of interactions between functional monomers and templates [40].

CIPs have emerged as polymeric bio-recognition materials offering competitive affinity to target cells, along with the added advantage of low-cost, robustness and stability in different environmental conditions. CIPs are synthesized using MIT too, with a target cell serving as the template during fabrication.

The integration of MIPs and CIPs into microfluidic biosensors represents a significant advancement, as it combines the advantages of microfluidic biosensing—including rapid sample analysis, reduced reagent consumption, and portability—with the specific recognition capabilities and stability of MIPs and CIPs, which offer enhanced selectivity, robustness, versatility, and low-cost in biosensing [43], [44].

The nature of interactions between MIPs and templates (target BAs) during polymerization and subsequent binding (recognition) steps can be covalent, semi-covalent, or non-covalent. These interactions are defined by the binding properties between the functional monomers of MIPs and functional groups of templates. For example, in the non-covalent approach, the interactions between functional groups of MIPs and templates are non-covalent, such as electrostatic, hydrogen, hydrophobic and π-π interactions. Among different interactions, the non-covalent approach is more popular since a variety of the suitable functional monomers for that are available, and its experimental procedure is quite simple and straightforward [45].

Table 1-1 compares imprinted polymers (synthetic receptors) with biological receptors in biosensor applications [26]. While MIPs offer several advantages, such as high stability across

various temperatures and pH levels, low-cost synthesis, and compatibility with miniaturization, they also come with limitations including the lack of general synthesis method and need for the optimization of synthesis parameters to achieve desired properties which can be complex and time-consuming [46]. This complexity is further amplified with CIPs, where the abundant surface functionality and larger template sizes introduce additional challenges. During synthesis, larger-sized templates have a higher tendency to become entrapped within the bulk polymer or to undergo incomplete template removal and denaturation [47]. To address these challenges, advanced strategies for imprinting have been adopted, such as surface imprinting, which creates an accessible cavity for the target analyte. The synthesis and template elution processes become more complicated, molecular modeling, and computational screening less applicable or effective in optimizing CIPs for specific applications [47]. As such, the effective application of CIPs requires careful consideration of these advantages and disadvantages, highlighting the need for ongoing research to optimize their use in biosensing applications.

Table 1-1. Comparison between synthetic receptors and biological receptors in biosensor applications [26]. *Reproduced with permission from Chemical Society reviews.*

Polymeric recognition elements	**Biological recognition elements**
High stability in different temperatures, PH, and pressures	Not stable, having specific operational requirements
Low-cost, reusable	High price and complex preparation
Can be used in organic solvents	Weak performance in non-aqueous media

Can be prepared for almost many target, and binding properties can be tuned	Exist for a limited number of targets and mostly need animal-based sources
Compatible with micromachining techniques	Poor compatibility with miniaturization

The next section discusses the effect of each component and polymerization and synthesis parameters on MIPs synthesis and functionality. Although many researchers have tried to study and realize the effect of various parameters in synthesizing MIPs, it is still difficult to understand them rationally. However, based on previous studies, some findings can be highlighted.

1.3.1. Functional monomer

The selection of functional monomers is the first step in synthesizing molecular or cellular imprinted polymers (IPs) since it defines the nature of the interaction between IP and template, and thus it directly affects the binding and specificity properties of the final synthesized IPs [48]. Table 1-2 includes the most frequently used functional monomers' chemical formula and structures. Commonly used functional monomers in IPs synthesis are sulphonic acids, carboxylic acids, and heteroaromatic bases [40]. One of the most extensively used functional monomers in synthesizing IPs is methacrylic acid (MAA) since it can act as both hydrogen bond donor and acceptor [49], [50].

In general, the responsibility of functional monomers is to provide required functionalities for self-assembly and formation of IP-template complex either by non-covalent or covalent interactions. The strength of the interactions between the template and monomer determines the affinity and selectivity of the formed recognition sites in IPs [50]. A stronger interaction leads to a more stable template–IP complex, which contributes to high binding capacity in the synthesized

receptors [49], [51]. Generally, selecting the functional monomers for small molecules is performed by combinational or computational method. However, unlike small molecules whose recognition is achieved based on electrostatic interactions, recognizing cells and large BAs relies on weaker interactions, i.e., hydrogen bonds, ionic bonds, and Van der Waals interactions combined with shape complementarity. Therefore, imprinting of large BAs and cells is often effectively performed by selecting functional monomers with specific functional groups, which can form non-covalent bonds with the template [40].

Table 1-2. Chemical structure and formula of the most used functional monomers in Ips [50], [52].

Functional monomer	**Chemical formula**	**Chemical structure**
Acrylamide (AAM)	C3H5NO	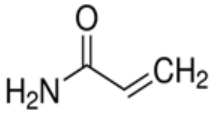
Methacrylic acid (MAA)	C4H6O2	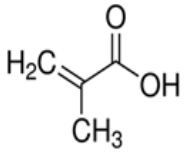
2-vinyl pyridine (2-VP)	C7H7N	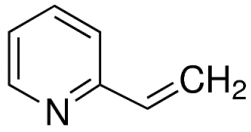
4-vinyl pyridine (4-VP)	C7H7N	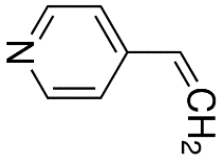
Methyl methacrylate (MMA)	C5H8O2	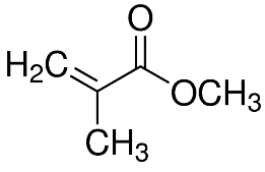

Hydroxyethyl methacrylate (HEMA)	C6H10O3	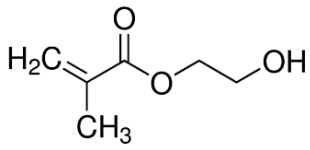
Trifluoro methacrylic acid (TFMAA)	C5H5F3O2	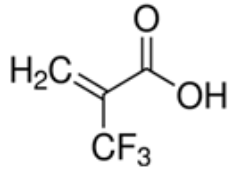

For imprinting the BAs, proteins, and large molecules, it has been shown that MIPs synthesized with multiple functional monomers with suitable side chains could give efficient imprinting and rebinding performance [53]–[56]. Different sidechains during the preparation of MIPs allow them to have both polar and hydrophobic functionalities to interact with amino acids presented on the BA's surface. Each monomer is likely to be compatible with a set of amino acid sidechains depending on the polarity and shape of the monomer and particular amino acids. By mixing the monomers with the BA template prior to polymerization, it is assumed that a monomer will have a chance to move along the template surface until it is held by a suitable amino sidechain. After polymerization and cross-linking, this will create MIPs network partially optimized for the BA surface [40]. For instance, one study [53] used co-polymers consisting of AAM, MAA, and MMA as monomers. However, the resulting MIPs were not capable of differentiating between the 5 different virus sub-types. This led to the modification of that monomer system by including VP as an additional monomer resulting in a dramatic increase in the selectivity displayed by the MIP for the influenza A virus sub-types. The sensitivity and selectivity of the method was further refined by adjusting the ratio between the different monomers and the cross-linker.

1.3.2. Cross-linker

Cross-linker is another important component in synthesizing IPs and has at least two polymerizable double bonds. Generally, cross-linker affects the physical properties of synthesized IP rather than the interaction between template and IP [49], [51]. The type of cross-linker and its molar ratio to functional monomer affect the final polymer complex's morphology and mechanical stability in retaining its recognition ability and binding sites [57]. In general, higher cross-linker ratios are used to achieve permanent macroporous polymers with sufficient mechanical stability. The most frequently used cross-linkers in synthesizing IPs and their chemical formula and structures are included in Table 1-3. It has been observed that optimizing the cross-linker amount improves the binding properties of synthesized IP and decreases non-specific interactions [58]. Also, changing the type of cross-linker in a different study on IP nanoparticles strongly affected the size distribution and yield of the imprinted nanoparticles [59].

Table 1-3. Chemical structure and formula of the most used cross-linkers in synthesizing IPs [52].

Cross-linker	**Chemical formula**	**Chemical structure**
Ethylene glycol dimethacrylate (EGDMA)	C10H14O4	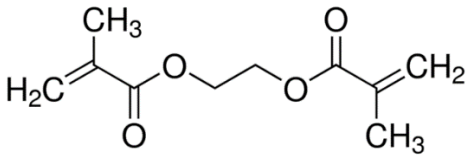
Dihydroxyethylene-bisacrylamide (DHEBA)	C8H12N2O4	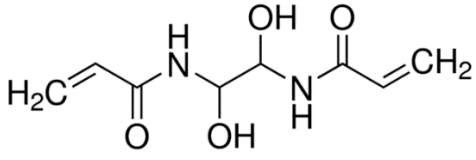

Trimethylolpropane trimethacrylate (TRIM)	C18H26O6	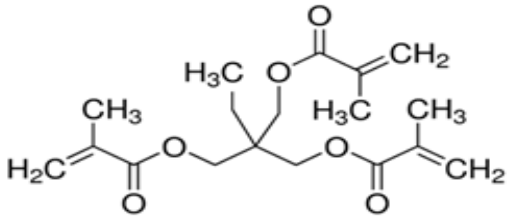
N, N-methylenebisacrylamide (MBAA)	C7H10N2O2	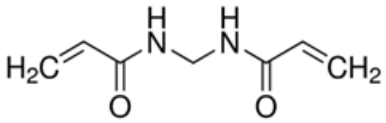

1.3.3. Solvent

As another important factor in molecular imprinting, the solvent is the chemical reagent that brings all the other components of IPs into a single phase during the synthesis process. Furthermore, in macroporous polymers, the solvent is responsible for producing pores and therefore, it is also referred to as “porogen” [40]. The type and polarity of solvent influence the complex formation between functional monomers and template molecules. This is particularly crucial in non-covalent interaction systems, where the choice of solvent affects the adsorption properties of the IP [60]. For effective non-covalent imprinting, using a non-polar or less polar organic solvent—such as toluene, acetonitrile, dimethyl sulfoxide (DMSO), or chloroform—is essential to achieve optimal printing efficiency. The specific type of solvent employed directly impacts the adsorption characteristics and morphological properties of the resulting polymer [60]. Also, it has been reported that increasing the porogen volume in pre-polymer solution leads to an increase in the polymer’s pore volume [40].

1.3.4. Initiator

Free radical polymerization is the most frequently used polymerization technique to synthesize IPs [61]. In this method, the polymerization reaction is quite fast, and it is initiated photochemically or thermally by using common azo-initiators, such as N-N'-bis isobutyronitrile (AIBN). This process is generally conducted at atmospheric pressure and low temperature (usually lower than 80 °C) in solution or bulk. Due to the mild condition requirements of reaction, this method is tolerant and suitable for most template structures and functional groups [40]. In addition to azo initiators, other initiators such as peroxides, photo initiators, and redox systems are also utilized [62]. Peroxide initiators, for example, generate more reactive oxygen-centered radicals that can lead to branching and premature chain termination, whereas photo initiators rely on light to produce radicals, allowing for rapid curing. Redox systems combine oxidizing and reducing agents to generate radicals, often at lower temperatures [63]. Each type of initiator and mechanism offers specific advantages, but azo initiators are particularly favored for their stability, controlled decomposition, and efficient polymer chain growth, making them ideal for synthesizing IPs and other complex materials [62], [64].

1.3.5. Templates used in MIPs and CIPs

As stated in the previous section, one of the advantages of MIT is being a versatile technique, i.e., different types of targets with a wide range of properties, including nano- and micro-organisms such as viruses and bacteria, can be imprinted in the polymers. Due to their reproducibility and inherent robustness, IPs can ease the production of tailor-made recognition elements for rapid detection to correspond to emerging biological infections [65]. However, despite molecular imprinting of small molecules, peptides, or even proteins that are well-innovated, the synthesis of

CIPs using whole cells as templates remains a big challenge due to their large dimensions, abundant surface chemistry and environmental chemistry adaptability. In the past decades, considerable efforts have been invested in preparing CIPs imprinted with microorganisms with successful examples such as cell-mediated lithography and microcontact stamping. Table 1-4 includes a summary of imprinted polymers with biotemplates in recent years.

Table 1-4. Summary of imprinted polymers with biological agents in recent years.

Biological Agent	**Functional monomer(s)** [a]	**Crosslinker** [b]	**Porogenic solvent** [c]	**Format** [d]	**Transducer** [e]	**Ref.**
Influenza virus	AAm, MAA, MMA, VP	DHEBA	DMSO	SI	QCM	[53], [55], [56]
Influenza virus	AAm, MAA, MMA, VP	EGDMA	Acetone	BEADS	QCM	[54], [56]
swine fever virus	AAm, MAA, MMA, VP	DHEBA	DMSO	SI	QCM	[66]
Dengue virus	AAm, AA, BAm	EGDMA	Acetonitrile, Phosphate buffer pH 4	EmI	QCM	[67], [68]
Escherichia coli, *Bacillus*	Polystyrene, AAM, Polyacrylate,	NA	NA	SI	QCM	[69], [70]

cereus bacteria	PU, VP, and Epon1002F					
Staphylococcus aureus bacteria	AAM	BisAM	Toluene	Gel beads	NA	[71]
Pseudomonas aeruginosa bacteria	AAM	N,N'-methylenebisacrylamide	DI water and hexane	Particles	Flow cytometry	[72]
N. meningitidis MC58 bacteria	MAA	EGDMA	Acetonitrile	SI	QCM	[73]
Japanese encephalitis virus	APTES	TEOS	Ultrapure water	MIPs coated Fe3O4@SiO2 microspheres	FRET	[74], [75]
Human immunodeficiency virus (HIV)	PDA	PDA	Tris-HCl buffer pH 8.5	EmI	QCM	[76]

Hepatitis A virus	PDA	PDA	Tris-HCl buffer pH 8.5	PDA-coated SiO2	RLS	[77]
Hepatitis B virus	MAT, HEMA	EGDMA	MOPS buffer pH 6	particles	SPR	[78]
Adenovirus	NIPAM, AA	MBAm, TBA, APTES	Ethanol	MIP nanoparticles	SPR	[79]
Picornavirus	PU, BPA	Phloroglucinol	Tris-HCl, THF	SI	QCM	[80]

[a] AAm: acrylamide; MAA: Methacrylic acid; MMA: methyl methacrylate; VP: vinylpyrrolidone; AA: acrylic acid; BAm: N-benzylacrylamide; APTES: 3-aminopropyl triethoxysilane; PDA: polydopamine; MAT: N-methacryloyl-L-tyrosine methyl ester; HEMA: hydroxyethyl methacrylate; NIPAM: N-isopropylacrylamide; PU: polyurethane; BPA: bisphenol A

[b] DHEBA: N,N -(1,2-dihydroxyethylene) bisacrylamide; EGDMA: ethylene glycol dimethacrylate; TEOS: tetraethoxysilicane; TBA: N-tert-butylacrylamide; MBAm: N,N'-methylenebisacrylamide

[c] DMSO: dimethylsulfoxide; THF: tetrahydrofurane.

[d] SI: stamp imprinting; EmI: epitope mediated imprinting

[e] QCM: quartz crystal microbalance; RLS: resonance light scattering; SPR: surface plasmon resonance; FRET: Förster resonance energy transfer; NA: not applicable

Vulfson and colleagues first reported the successful imprinting of bacteria using a cell-mediated lithography approach [81], [82]. A water-soluble poly(amine) was mixed with a stirred suspension of bacteria and a diacid chloride dispersion in the organic phase. In this biphasic system, bacteria tended to assemble at the water-oil interfaces. The polyamide microcapsules embedded with bacteria were generated by the covalent linkages of poly(amine) and the nucleophilic groups on the cell surface. Further photoinitiated polymerization of a diacrylate present in the organic phase

produced the solid beads imprinted with bacteria. Multilayered beads with spatially-defined imprinting cavities were finally formed by removing the bacteria template through acid hydrolysis. Inspired by this work, Harvey et al. synthesized bacterial spore-imprinted beads using Bacillus thuringiensis kurstaki spores as templates [83]. The affinity of the imprinted beads was augmented by coating imprinted cavities with lectin and concanavalin A. In another interesting study, Ye's group innovatively put forward an idea that utilized Pickering emulsion polymerization [84], [85] to synthesize polymer beads imprinted with bacteria [86]. The negatively charged bacteria was first modified with a positively charged vinyl-containing pre-polymer N-acrylchitosan, which then served as particle stabilizers to prepare a stable emulsion of the oil phase in the water phase (Fig. 1- 5A). The oil phase containing cross-linking monomers was then polymerized via free radical initiation, during which bacteria was imprinted on the surface of the polymer beads. After removing the bacterial template, the bacteria-imprinted cavities were created on the surface of polymer beads (Fig. 1- 5B). This new synthetic strategy is simple and versatile and can be extended to other microorganisms by modulating the surface-activated pre-polymers. Advantages of cell-mediated lithography include being a suitable synthesis method for large size and fragile templates; less non-specific adsorption owing to highly inert surface coating; improved reproducibility. However, it has complex operating procedures and limited applications. Furthermore, template adsorbed at the oil-water interface results in fewer imprinting cavities, and thus decreased capacity and capturing efficiency [87]–[89].

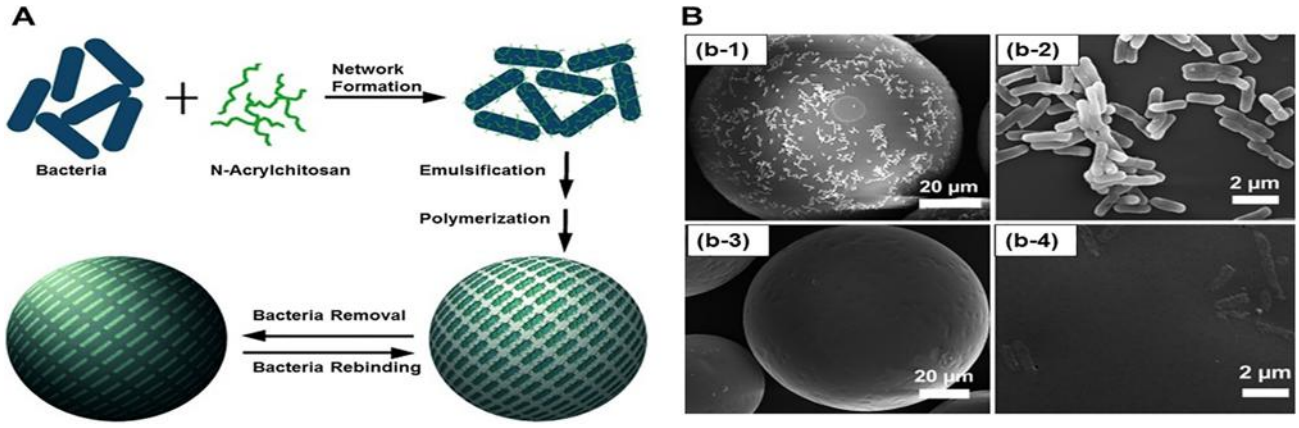

Fig. 1-5. Schematic illustration for the interfacial bacteria imprinting via Pickering emulsion polymerization, and (B) scanning electron microscopy images of the bacteria-imprinted polymer beads before (b-1, b-2) and after (b-3, b-4) the removal of the E. coli template [86]. *Reprinted with permission from John Wiley and Sons.*

Microcontact stamping is another well-established technique for preparing cell-imprinted polymer films using the whole cells as templates [90], [91]. Both organic and inorganic polymers are applicable in microcontact stamping. For example, Poller et al. selected organic polymers containing polystyrene, polyacrylamide, polyacrylate, polyurethane, polyvinylpyrrolidone, and Epon1002F (an epoxy resin derived from bisphenol A) to synthesize the imprinted surfaces targeting *Bacillus cereus* [70]. Lee et al. adopted poly(ethylene-co-vinyl alcohol) to perform the microcontact imprinting of the purple bacteria *Rhodobacter sphaeroides* [92]. With respect to the inorganic polymers, a sol-gel method was developed by Cohen et al. to produce organically modified silica thin films imprinted with whole cells of microorganisms for the concentration and specific identification of these microbes in liquids[93]. Various bacteria with diverse sizes and shapes were selected as the imprinting templates, including *Deinococcus radiodurans*, *E. coli CN13*, *S. natans*, and *B. subtilis*. The high selectivity of the imprinted films toward their corresponding template bacterium confirmed the feasibility of the synthetic approach. Most

recently, Fu et al fabricated Vibrio parahaemolyticus imprinted polydimethylsiloxane films on a microslide glass via the microcontact stamping approach [94]. The incubation of the imprinted film with the target bacterium allowed a capturing efficiency of 62.9%. This approach specifically detected 10^4 CFU/mL of *V. parahaemolyticus*, giving a linear range of 10^4-10^8 CFU/mL, ultimately paving the way in exploring novel strategies for bacterial recognition. Although the microcontact stamping method is easier to operate, has a wide range of applications and is a solvent-free system, it is not suitable for huge size and fragile templates [87], [95]. Furthermore, it is only applicable for synthesizing CIPs on the planar surfaces and can not functionalize spherical or cylindrical substrates with CIPs.

MIPs have also been successfully synthesized with virus templates. MIPs were combined with a QCM transducer to screen influenza virus subtypes in earlier work. Imprinted polymers of each template showed selective binding towards its original template. The detection limit for this sensor was reported to be 10^5 virus particles/ml [53].

The human immunodeficiency virus (HIV) is one of the main causes of death in the world. Lu et al. have developed an HIV peptide-MIP coated QCM with a specific high affinity to the template peptide. The shift in frequency of the developed QCM sensor upon injection of 100 ng/mL was 15.13 Hz, whereas this value for non-imprinted QCM was 1.8 Hz. They have also studied the selectivity of the fabricated sensor against two different peptides, and their results show that the frequency shift is much lower than for the template peptide. Moreover, their result demonstrated a linear shift in frequency in the range of 5-200 ng/mL with a 2ng/mL LOD for the HIV-1gp41, which is comparable to the ELISA method's results. The recovery performance of this sensor towards HIV-1 gp41 urine spiked sample was 86.5-94.1%, and therefore it was successfully fabricated and used for selective and sensitive monitoring of HIV-1 gp41 in urine samples [76].

Japanese encephalitis virus (JEV) recognition was performed using JEV-MIP coated silica microparticles containing pyrene-1-carboxaldehyde fluorescent dye and based on the fluorescent resonance energy transfer (FRET) [74]. Viral binding as an energy donor enhanced the FRET phenomenon, where the fluorescent dye acted as an energy acceptor. This sensor with an imprinting factor of 2.12 and a LOD of 9.6 pM at room temperature showed selective recognition of JEV over Rabies virus (RV), Leprosy virus (LV), and Hepatitis A virus (HAV). Moreover, it was applied to diluted human serum and demonstrated a recovery of almost 100%.

1.3.6. Synthesis methods and physical forms of MIPs

MIPs have mostly been synthesized in the monolith, thin-film, and microsphere forms using different polymerization methods [17], [53], [54]. The selection of synthesis method is mainly performed based on the application and employed transduction method.

The general method of synthesizing MIPs is called the molecular imprinting technique (MIT). MIT can be classified into three approaches: bulk polymerization, microcontact printing (microcontact stamping), and precipitation polymerization methods [96].

The bulk polymerization method shown in Fig. 1-6, is the simplest and preferred polymerization method for synthesizing monoliths and microbeads. In this method, the template molecule is added to the polymer solution that consists of functional monomers, cross-linker, porogenic solvent, and initiator. The initial arrangement of functional monomers around the template molecule based on chemical functionalities and the physical shape of the template forms a pre-polymerization complex. The pre-polymer solution subsequently undergoes thermal and/or UV polymerization. The imprinted sites can be obtained by removing the template molecule after

polymerization. The resulting MIP bulk can be ground to acquire the desired size of MIP particles [17].

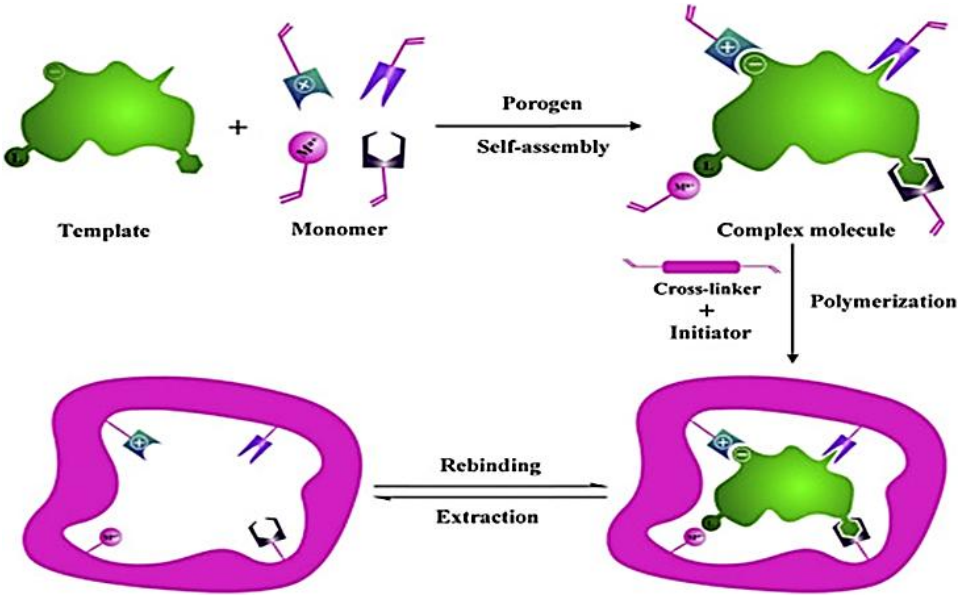

Fig. 1-6. Different steps of molecularly imprinted polymer (MI)P bulk polymerization in molecular imprinting technique (MIT) [96]. *Reprinted with permission from Elsevier.*

Microcontact printing is the most used method for synthesizing MIPs in the form of a thin layer on a flat surface (such as the surface of a QCM) [69], [97]. Fig. 1-7 demonstrates different steps of the microcontact printing method in synthesizing MIPs imprinted with BAs. In this method, first, the mixture of functional monomers, cross-linker, and the initiator is dissolved in a solvent and undergoes a subsequent pre-polymerization to reach a higher viscosity before the gel point (usually few hours in 60-70°C depending on the initiator type). Next, a stamp of the template molecule (here, Influenza virus) is prepared by sedimentation of the template on a substrate (usually glass). In parallel, the pre-polymer gel is coated onto the desired surface using a spin-coater to reach a specific thickness according to the size of the template. Immediately after, the template coated stamp is pressed onto the pre-polymer layer, followed by thermal/UV polymerization. Finally, the template removal is performed after polymerization to wash the

template molecules off the surface of the polymer, leading to the generation of cavities on the polymer's surface.

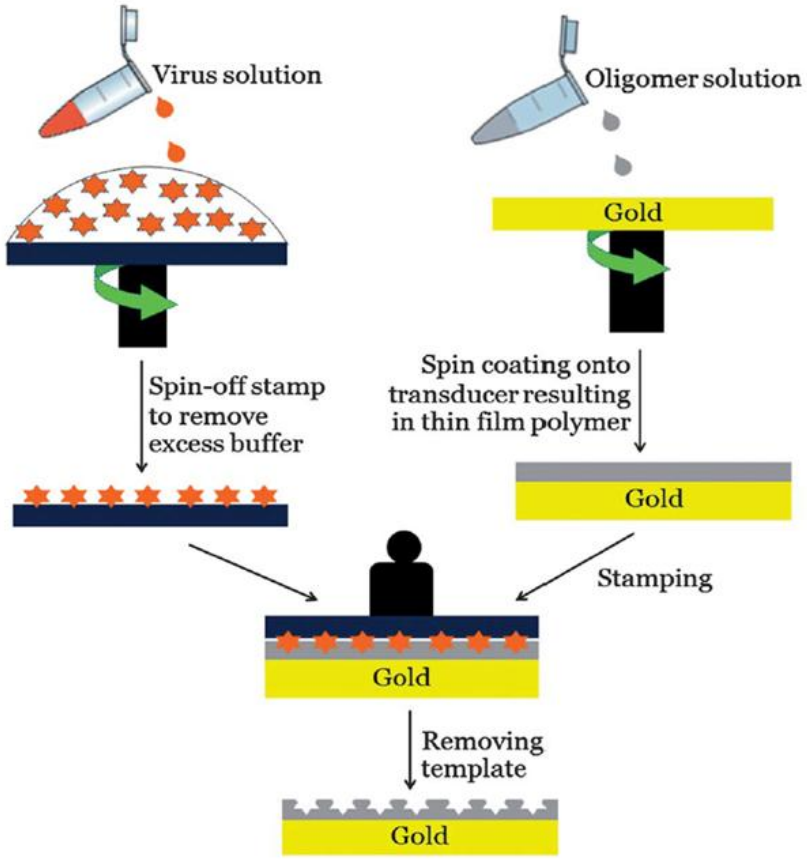

Fig. 1-7. Steps of microcontact printing method for synthesis of influenza virus-MIPs [53]. *Reprinted with permission from Royal Society of Chemistry.*

Precipitation polymerization is another method for synthesizing MIPs and producing MIP microspheres. Fig. 1-8 demonstrates different steps of the precipitation polymerization method in synthesizing MIPs [98]. In this method, all the synthesis compounds are diluted in an appropriate solvent or a mixture of different solvents. The appropriate solvent (called theta solvent) is selected based on its ability to solubilize all compounds at the polymerization temperature (called theta temperature). By reaching a certain mass of the polymer, the solvent cannot hold the polymer

chain, and therefore particles are precipitated off the solution. In this method, selecting an appropriate solvent is critical to producing discrete MIP particles [98].

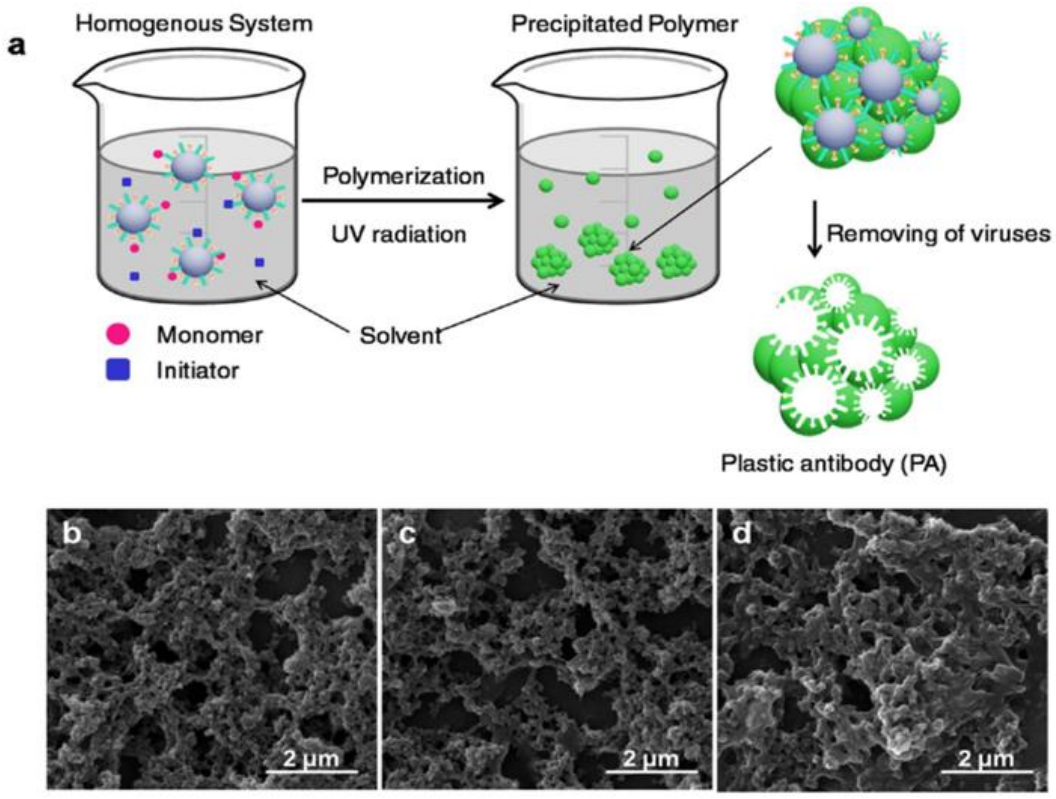

Fig. 1-8. (a) Schematic representation of precipitation polymerization method for synthesis of MIPs. Scanning electron microscopy (SEM) images of (b) H1N1, (c) H5N1, and (d) H3N2 influenza A virus as a template [54]. *Reprinted with permission from Taylor & Francis.*

1.4 MIP and CIP-based microfluidic biosensors

Imprinted polymers have exhibited notable efficacy across various applications, often surpassing conventional methodologies while providing a more cost-effective alternative [99], [100]. For instance, Takimoto et al. [101] developed submillimeter-sized MIP-based microgels for the recognition of human serum albumin through the polymerization of water-soluble monomers in

the presence of a photo initiator within water-in-oil droplets generated using a microfluidic system (Fig. 1-9). By optimizing surfactant types, concentrations, and flow rates, they were able to control the size of the microgels. Their findings indicated that these submillimeter-sized MIP-based microgels demonstrated significant selectivity and affinity for binding to human serum albumin.

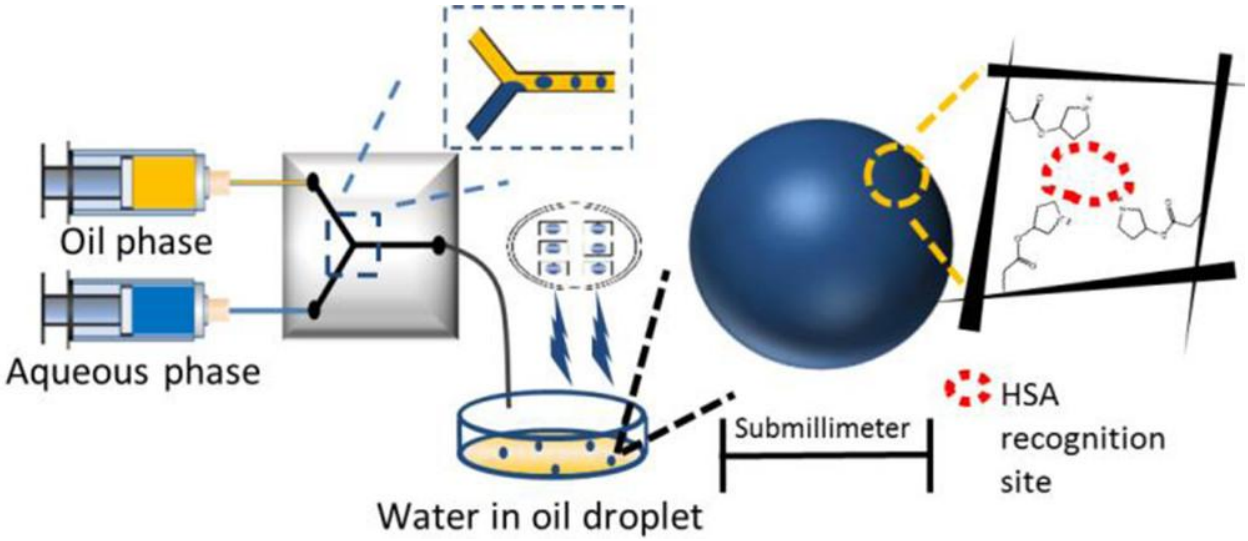

Fig. 1-9. The preparation of MIP-based microgels for the recognition of human serum albumin using a microfluidic system [101]. *Reprinted with permission from American Chemical Society*.

An immunoassay membrane based on MIPs for the separation and detection of C-reactive protein in serum samples was introduced by Hong et al [102]. They integrated the synthesized MIPs into microfluidic system for POC applications (Fig. 1-10). Their findings showed that the adhesion forces between C-reactive protein and MIPs were in the range of interaction forces observed for corresponding antibodies.

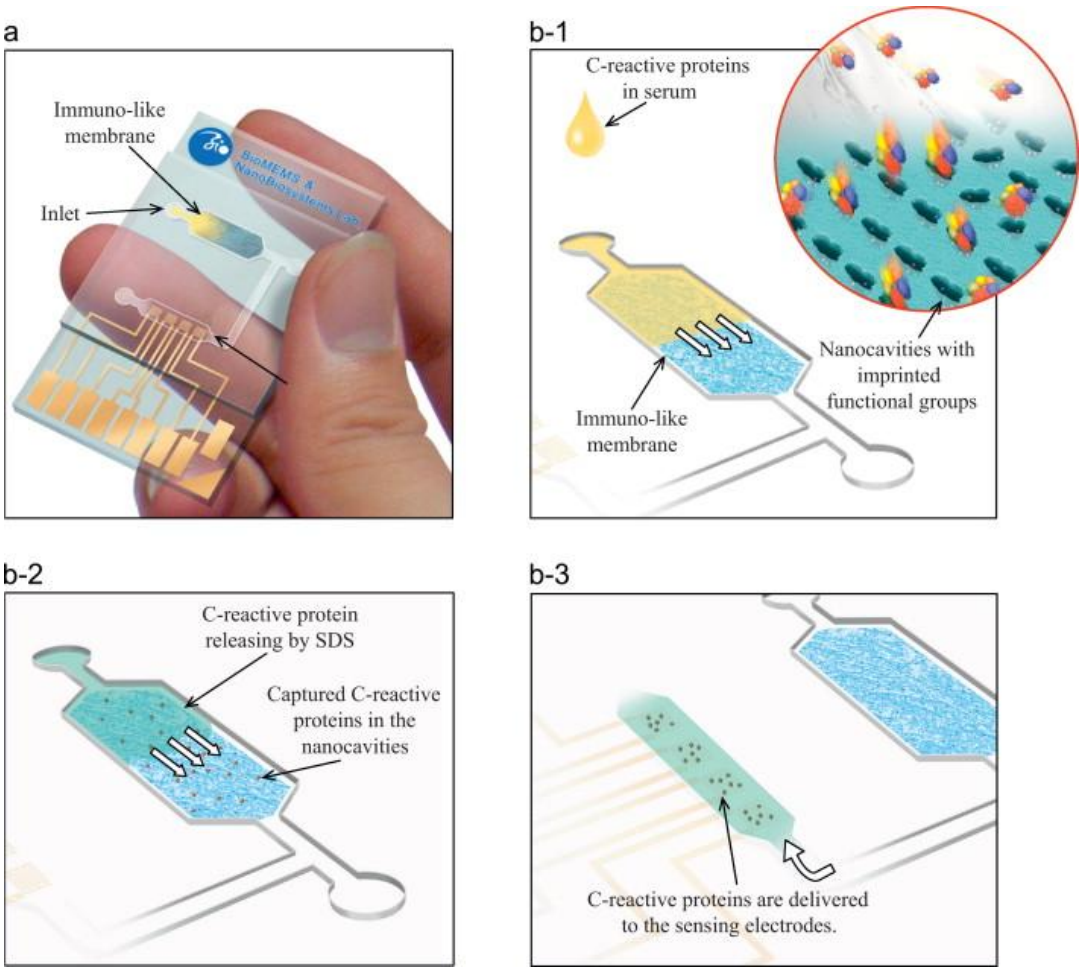

Fig. 1-10. The diagram depicts the MIP-based nanocavities integrated into a microfluidic system [102]. *(a) the microfluidic chip; (b-1) process of introducing serum samples into the system to capture C-reactive protein; (b-2) the addition of sodium dodecyl sulfate solvent (SDS) to release C-reactive protein from the immuno-like membrane; (b-3) the transfer of C-reactive protein to the electrodes. Reprinted with permission from Elsevier.*

Kellens et al. introduced a MIP-based microfluidic system utilizing functionalized diamond substrates for testosterone detection [103], highlighting its low cost, simplicity, and efficiency across urine, buffer, and saliva samples. MIPs were created on these substrates, using testosterone as the target molecule and NOBE as a bi-functional monomer. A master structure produced via e-

beam lithography facilitated the fabrication of PDMS stamps to create patterned polymer structures, which were covalently bonded to the diamond substrate. Characterization techniques, including optical microscopy and SEM, confirmed the integrity of the structures even after multiple washes. They adapted this system into a sensor employing electrochemical impedance spectroscopy, achieving a LOD of 0.5 nM. The sensor substrates demonstrated high affinity and selectivity for testosterone, with the ability to detect concentrations up to 20 nM. Notably, the polymer structures could be regenerated after use, indicating potential for reusable MIP-based sensors [103].

Another study presented a method for detecting estradiol, rhinovirus, and insulin by using a double imprinting process to replicate the selectivity of natural antibodies in a robust polymer [104]. Antibodies, including Anti estradiol, anti-rhinovirus and anti insulin antibodies, served as templates to create imprinted polymer particles, which were subsequently embedded in a secondary polymer. This resulted in a sensitive coating applied to a QCM integrated into a microfluidic chip, enabling the development of an estradiol immunosensor with significantly enhanced affinity for its target. The method was successfully used to detect viruses in plasma and allergenic proteins in bread extracts.

Harz et al. [105] investigated the use of immobilized MIPs within a microfluidic system for the fluorescence detection of dansyl-L-phenylalanine. They immobilized the MIPs onto quartz surfaces, creating uniform films for use in a spectrofluorometer. Fig. 1-11 illustrates the system, highlighting the arrangement of excitation and emission lights, the holder, and the adjustable excitation angle for ease of use. Their results demonstrated a sensitivity enhancement in the

detection of dansyl-L-phenylalanine, achieving a fiftyfold improvement compared to systems without MIPs.

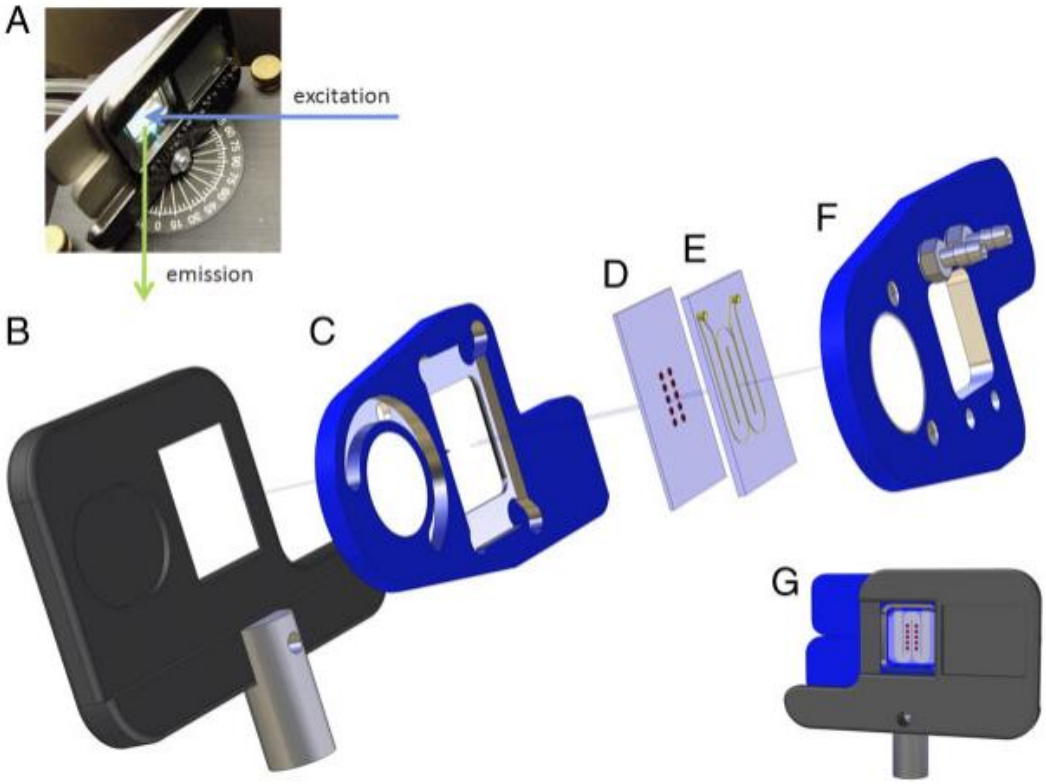

Fig. 1-11. Microfluidic setup designed for fluorescence determination of dansyl-L-phenylalanine [105]. *(A) excitation and emission light paths in a spectrofluorometer; (B) the holder for the microfluidic device; (C) and (F) magnetically attached holders with a viewing window; (D) substrate incorporating MIPs; (E) a microstructured meander for fluid flow; (G) and an overview of the complete arrangement. Reproduced with permission from Thaler et al. [52]. Reprinted with permission from John Wiley and Sons.*

Liu et al. [106] developed an innovative electrochemical detection platform that integrates MIPs with a microfluidic chip for trace measurement of therapeutic drugs. The chip as demonstrated in Fig. 1-12 featured a detection cell designed to enhance anti-interference capabilities, ensuring effective monitoring of drug concentrations in biological samples. Characterization was performed

using cyclic voltammetry and electrochemical impedance spectroscopy. The detection method by using the MIP/gate effect achieved a low detection limit of 8×10^{-12} M for warfarin sodium, suitable for clinical use. The platform successfully monitored drug concentrations in rabbit plasma. It also effectively analyzed cyclophosphamide and carbamazepine, highlighting its versatility and potential for PoC testing.

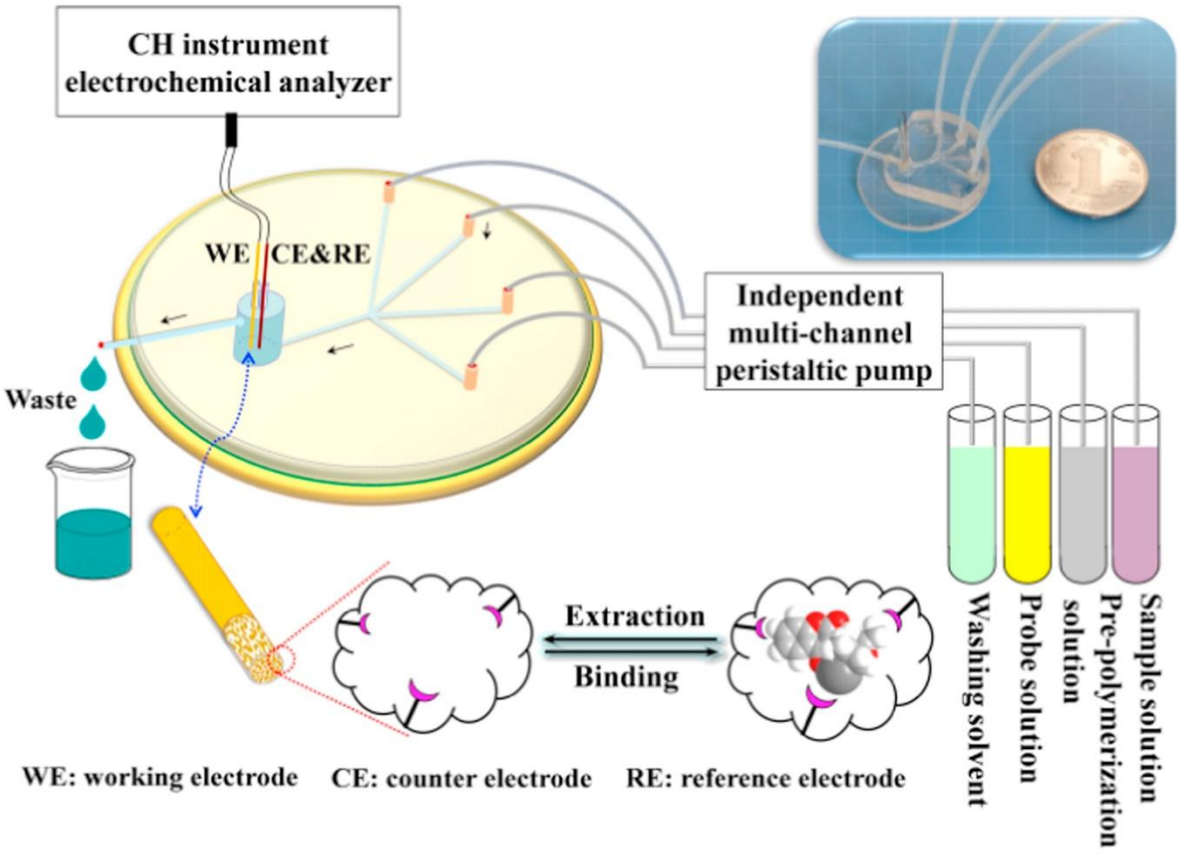

Fig. 1-12. Microfluidic chip for drug concentration monitoring, featuring four inlets for sample injection. The working electrode, a nanoporous alloy with a molecularly imprinted polymer (MIP) layer, selectively captures target molecules. Waste is discharged post-detection. The photo in the top right shows the chip, similar in size to a one-yuan coin [106]. *Reprinted with permission from Elsevier.*

Sharma et al. [107] developed MIP-based microfluidic platform as shown in Fig. 1-13 for detecting oxytocin nonapeptide, an autism biomarker. They utilized electropolymerization to deposit MIPs onto a gold electrode. Their developed sensor yielded an LOD of of 60 μM . Furthermore, they assessed the sensitivity of the microfluidic system using aqueous samples and synthetic serum, finding that the system exhibited selectivity against common interferences, including potential metabolites and various oxytocin analogs.

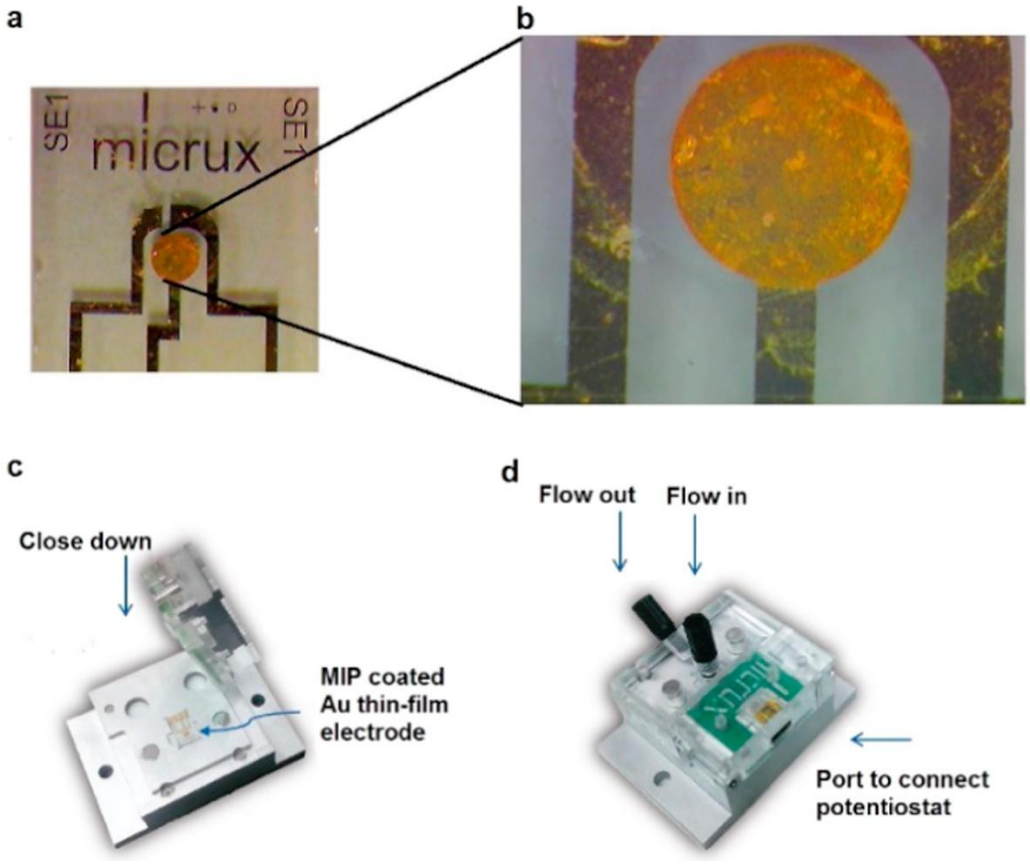

Fig. 1-13. Optical images of the gold thin-film electrode (1 mm diameter) [107]. *(a) post-polymer deposition; (b) a close-up view highlighting the uniform coverage of the electrode surface; (c) the assembly of the gold thin-film electrode within the microfluidic device; (d) the fully assembled microfluidic system. Reprinted with permission from Elsevier.*

Hong et al. [108] developed a portable analyzer featuring a single-use system for measuring propofol levels in total intravenous anesthesia, specifically targeting detection in plasma samples. Their approach utilized MIPs and electrical detection methods as shown in Fig.1-14. The design incorporated a microfluidic biochip that ensured precise sample transport to the biosensor microchambers through capillary action, featuring a three-layer structure with fluidic inlets and outlets on the top layer. Patterned double-sided stickers created microfluidic channels, while conducting MIP biosensors on the bottom layer demonstrated significantly lower impedance compared to non-conducting electrodes, enhancing sensitivity and accuracy. The imprinted nanocavities were specifically tailored for binding propofol molecules, and when propofol was captured from human plasma samples, the surface electrical properties of the sensors changed, reducing conductivity. This direct detection method monitored electrical changes, with propofol binding affecting the discharge curves' time constants, ultimately allowing the conducting MIPs to function as synthetic antibodies for isolating and sensing propofol in biological samples. This device was tested in hospitals to measure blood propofol concentrations and was compared against traditional techniques like ion mobility spectrometry and high-performance liquid chromatography. The results indicated a rapid response time of just 25 seconds and a LOD of 0.1 μg/mL.

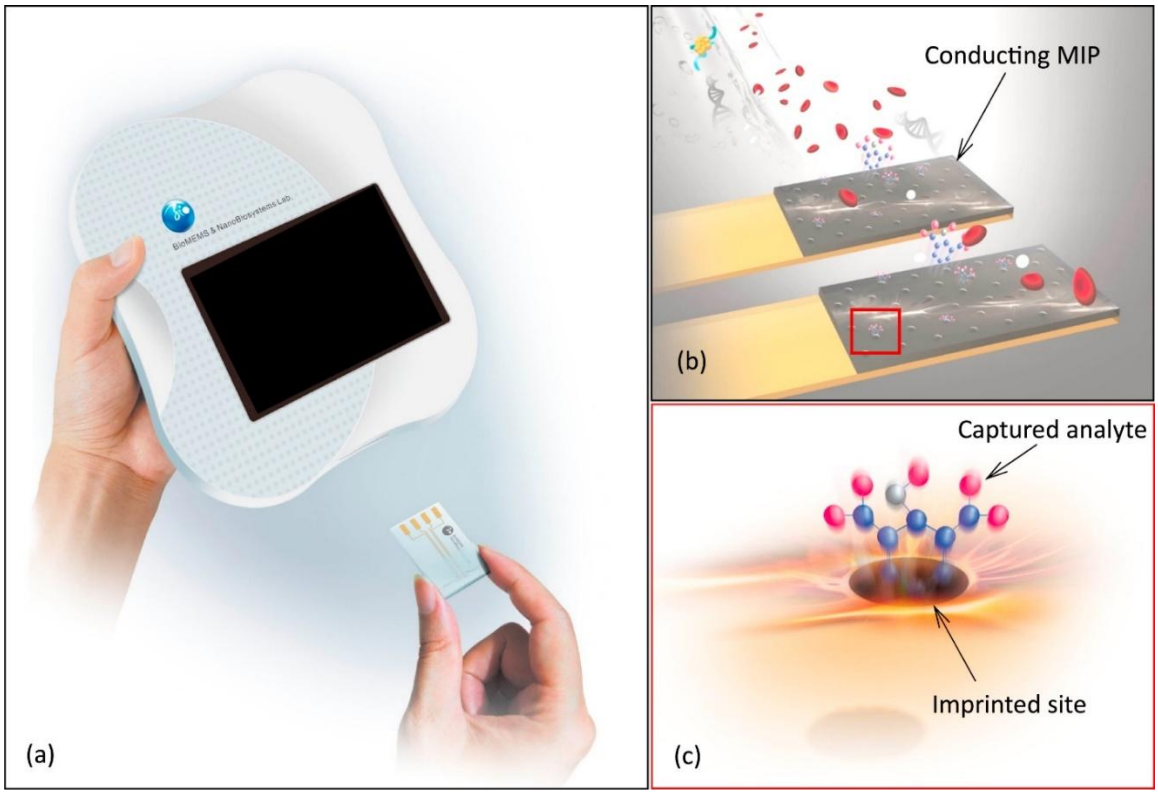

Fig. 1-14. Diagram of the propofol detection system utilizing MIP biosensor. (a) Portable analyzer; (b) process of capturing and sensing propofol with the MIP biosensor; (c) targeted interaction of propofol molecules within the MIP nanocavities [108]. *Reprinted with permission from Elsevier.*

MIPs have been incorporated into a microfluidic biochip for the detection of tobacco mosaic virus (TMV) using contact-less bioimpedance spectroscopy (Fig. 1-15) [109]. The MIP was created through surface imprinting with a virus stamp, embedded in a co-polymer of methacrylic acid and N-vinylpyrrolidone. This integration allowed for precise control of fluid dynamics, enabling researchers to investigate viral binding and dissociation kinetics, while the chip demonstrated quick response times and reusability.

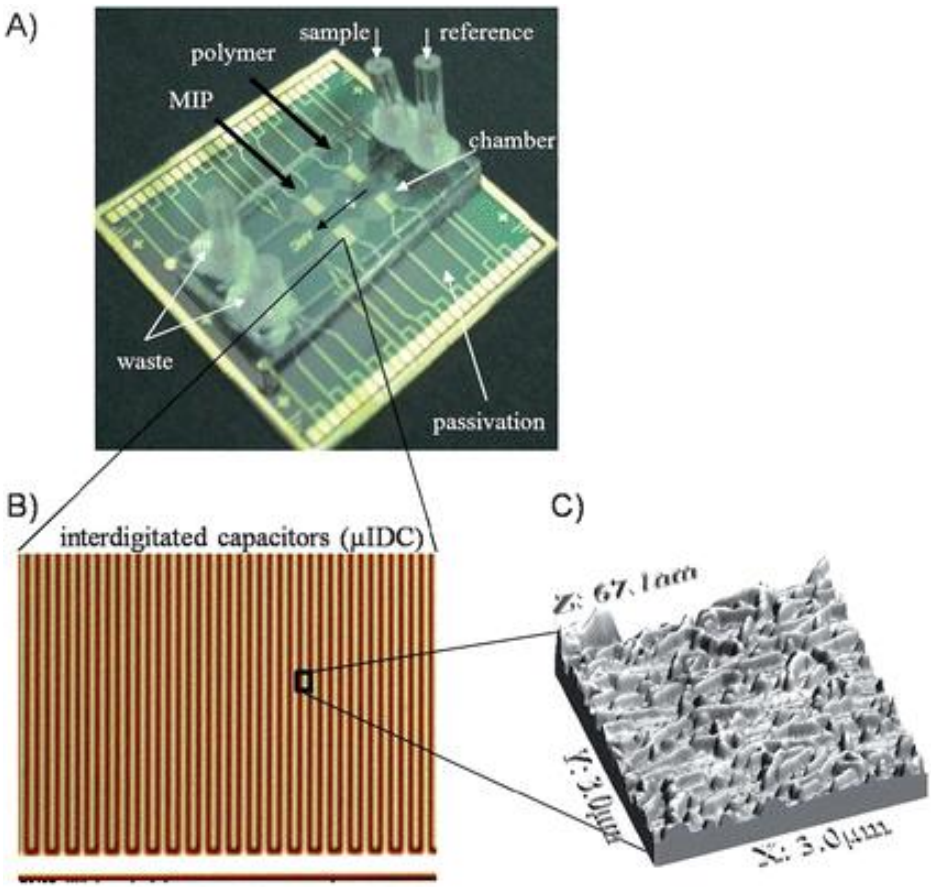

Fig. 1-15. Diagram of the MIP-based microfluidic biochip for detection of TMV virus [109]. *(A) PDMS microfluidics topped with a glass cover, a 400 nm SiNx/SiO2 layer, and contact-less dielectric sensors. (B) High-density interdigitated capacitor (μIDC). (C) AFM image of the TMV virus stamp used to imprint a poly (methacrylic acid) (PAA)/polyvinylpyrrolidone (PVP) copolymer. Reprinted with permission from Elsevier.*

The integration of CIPs with microfluidics has been limited by the challenges associated with imprinting bacteria as a large-size template and integration of CIPs with microfluidics. The large size and abundant surface functionality of bacteria complicates imprinting and makes their removal from the polymer challenging and hinders the design of specific MIPs [110], [111]. These factors has led researchers to focus on smaller, more manageable analytes in clinical and

environmental applications. However, there have been some attempts to address these challenges, which are explained below.

Ren et al. [112] utilized microcontact imprinting method by pressing of a glass slide coated with bacteria against another glass slide that was covered with partially cured PDMS. After the PDMS was fully hardened, the bacteria were removed, resulting in a textured surface with CIP cavities [112]. Microfluidic channels were used for the cell capturing experiments, where the CIP surface was covered by an array of microchannels which helped for better contact of cells with CIP surfaces. The quantification was performed using confocal microscopy and the results revealed that CIPs could selectively capture the same bacteria type when a bacterial suspension was flowed over it [112].

A CIP-based microfluidic device was developed by integrating a bacteria-imprinted polymer film into a microfluidic chip via the microcontact stamping technique (Fig. 1-16) [113]. They focused on *Synechococcus* and *Synechocystis cyanobacteria* bacteria. The novel method for creating a CIP microdevice with oriented imprints involved several key steps: they first placed a temporary PDMS mold on polylysine-coated glass and then used negative pressure to draw a cell suspension through the channels, aligning the cells with the flow. After removing the top layer of the mold to expose the glass plate with the aligned cells, they performed imprinting and subsequently extracted the cells, leaving well-defined imprints. Finally, they bonded permanent structures to complete the microchip. The efficiency of cell seperation was found to be 80–90%, which was assessed by imaging technique and flow cytometry . By adjusting factors like further imprinting orientation for alignment with bacterial flow, both capture specificity and separation efficiency could be further improved [113].

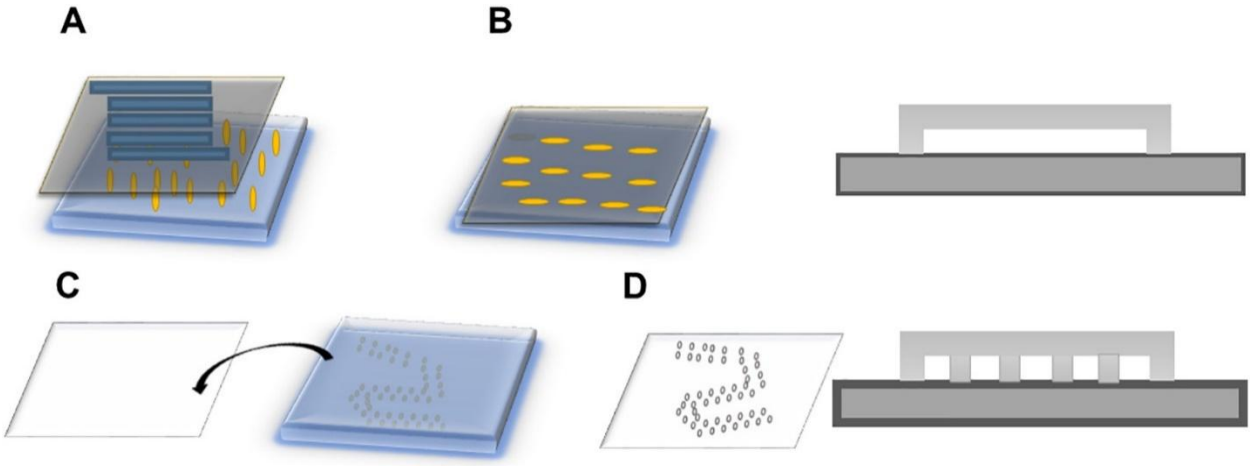

Fig. 1-16. The fabrication diagram of the CIP-based microfluidic device for bacteria separation [113]. *(a) A temporary PDMS mold is set on polylysine-coated glass. (b) Cell suspension is drawn through the channel using negative pressure, aligning cells with the flow. (c) The upper layer is removed, revealing the glass plate with aligned cells for imprinting. (d) Aligned imprints persist after cell removal, and a cross-section displays the finished chip with bonded permanent structure and 100 µm channels. Reprinted with permission from Royal Society of Chemistry.*

1.5. Scientific and technological gaps

The formulation of CIPs and synthesis parameters define the final CIPs' physical and chemical characteristics, selectivity, and binding performance. Hence, knowledge of different components' roles and synthesis conditions and their effect on the synthesized CIP's properties is essential to tune the selective binding performance of the CIPs based on the template. As mentioned earlier, the main challenge in designing CIPs is the lack of a thorough understanding of the effect of various CIP parameters on their biorecognition, target binding, and transduction. For instance, to synthesize a new class of CIP for a specific type of target, the composition of the CIP and its interactions with the transducer and the templated target need to be studied and optimized.

The most important factor in synthesizing CIPs is the choice of appropriate functional monomers, which defines the interaction between CIPs and template, and, therefore, directly affects the binding properties of the synthesized CIPs (there are more than 4000 commercially available polymerizable compounds) [114]. There are two main approaches to select the functional monomers for synthesizing CIPs with high selectivity and affinity: (i) computational method; which performs virtual monomer screening [115], and (ii) combinatorial (experimental) method; which suggests the optimal composition based on simultaneous small-scale synthesis and analysis of hundreds of CIPs [116]. Unlike small molecules whose recognition is achieved based on electrostatic interactions, recognition of cells and microorganisms relies on weaker interactions, i.e., hydrogen bonds and van der Waals interactions combined with shape complementarity. Therefore, imprinting of large molecules and cells is often effectively performed by selecting appropriate functional groups in a complex monomeric system [117]. However, due to the abundant surface functionalities of large molecules, cells and BAs, both methods get extremely complicated, and there is insufficient information from the literature to determine whether these methods could suggest the suitable functional monomers and their proportions in the case of imprinting BAs [26]. For imprinting the BAs, proteins, and large molecules, it has been shown that CIPs synthesized with multiple functional monomers with suitable sidechains could give efficient imprinting and rebinding performance [53]–[56]. Different sidechains during the preparation of CIPs allow them to have both polar and hydrophobic functionalities to interact with amino acids presented on the BA's surface. Each monomer is likely to be compatible with a set of amino acid sidechains depending on the polarity and shape of the monomer and particular amino acids. By mixing the monomers with the BA template prior to polymerization, it is assumed that a monomer will have a chance to move along the template surface until it is held by a suitable amino

sidechain. A significant gap exists in applying current CIP synthesis methods to bacterial cells, which have unique surface characteristics that differ from larger molecules and proteins. While progress has been made for proteins, viruses and large biomolecules, the specific interactions between CIPs and bacterial surfaces remain largely unaddressed. The diverse surface structures of bacteria complicate the selection of functional monomers, indicating a need for dedicated studies to develop CIPs specifically designed for bacterial targeting. Addressing this gap could enhance the efficacy of CIPs in applications like bacterial detection and treatment.

MIP coatings on planar and spherical surfaces, such as particles, have demonstrated effective binding to specific targets. However, microfluidic sensors often utilize non-planar transduction surfaces like MWs due to their advantages in enhancing fluid dynamics, increasing surface area for interactions, and facilitating the integration of multiple functionalities in compact designs. While MWs improve mass transport and enable the development of miniaturized, sensitive systems for real-time monitoring, their non-planarity poses challenges for uniform coating and functionalization, requiring tailored approaches for effective integration of complex recognition elements. Studies by Xiaogang Hu et al. [118]; Yuling Hu et al. [119], Xiaogang Hu et al. [120], Shaikh et al. [121], Tong Zhao et al. [122], Mirzajani et al. [123], Ma et al. [124], and Lu et al. [125] have successfully employed stainless steel MWs (SS-MWs) for MIP coatings focused on extracting chemical compounds using single monomer systems. However, there is a significant gap in research regarding the use of nonplanar substrates for complex CIPs targeting BAs. Changing the MIP formulation to a more complex monomer CIP composition, as required for efficient imprinting of biological targets [53], [54], affects the metallic wire and organic polymer interface and prevents obtaining an intact CIP coating. So, a statistical model for controlled coating of complex CIPs on MWs is required to be developed and validated. Using this model, optimal

recipes for synthesizing uniform CIP coatings with specific thicknesses on MWs could be achieved. Investigating the effects of CIP composition, and synthesis conditions can help obtaining reproducible uniform and controllable complex CIP coatings on metallic substrates.

There are some reports in the literature about coating the wires with MIPs to separate chemical compounds, and the detection mechanism is based on the UV-HPLC method [94], [95]. HPLC-based detection is laboratory-based and requires costly and complex equipment and trained personnel [126]. In addition, there is no report on BAs recognition using CIP coated MWs. So far, the feasibility of coating this category of CIPs on metallic MWs has not been studied. Furthermore, the electrical/electrochemical properties of CIPs and their equivalent electrical model in electrochemical sensing are unknown. Also, the electrical detection of BAs by transduction of their binding event to CIP-MWs has not been investigated.

Microfluidics has enabled the fabrication of field-deployable and low-cost sensors, which would need a small sample volume and a short time for bio detection [127]. Various MIP-based microfluidic devices to electrochemically detect target molecules have been reported to date [33], [128]. However, using CIPs in microfluidic electrochemical sensors to detect whole cells remains as a technological gap.

Overall, this thesis aimed to answer several questions in the field of CIPs and related biosensors for bacteria detection, such as:

- How can the CIPs with appropriate functional monomers for imprinting BAs be coated on metallic MWs?
- How do different CIP compositions and syntheses conditions affect the quantitative and qualitative characteristics of CIP coatings?
- Can a valid model for optimal coating of these synthetic receptors be developed?

- Can CIP-coated MWs be integrated into microfluidic devices to achieve a reliable electric read-out signal upon selective target binding?
- What are the electrical characteristics of CIPs? What is the equivalent electrical circuit model for the CIP-based electrical sensor?
- How do the electrical properties of CIPs change upon CIP-template binding?

1.6. Thesis Goals and Objectives

This research aims to help gain a fundamental understanding of CIPs in microfluidic biosensing applications by developing and optimizing a methodology for the controllable synthesis of bacteria-specific CIP coatings on the surface of conductive MWs. The prepared CIP-MWs will be integrated within a novel microfluidic biosensing platform for further electrical/electrochemical transduction of target binding to the synthesized CIPs. Fig. 1- 17 demonstrates the schematic of the research organized into three main objectives as discussed in this section.

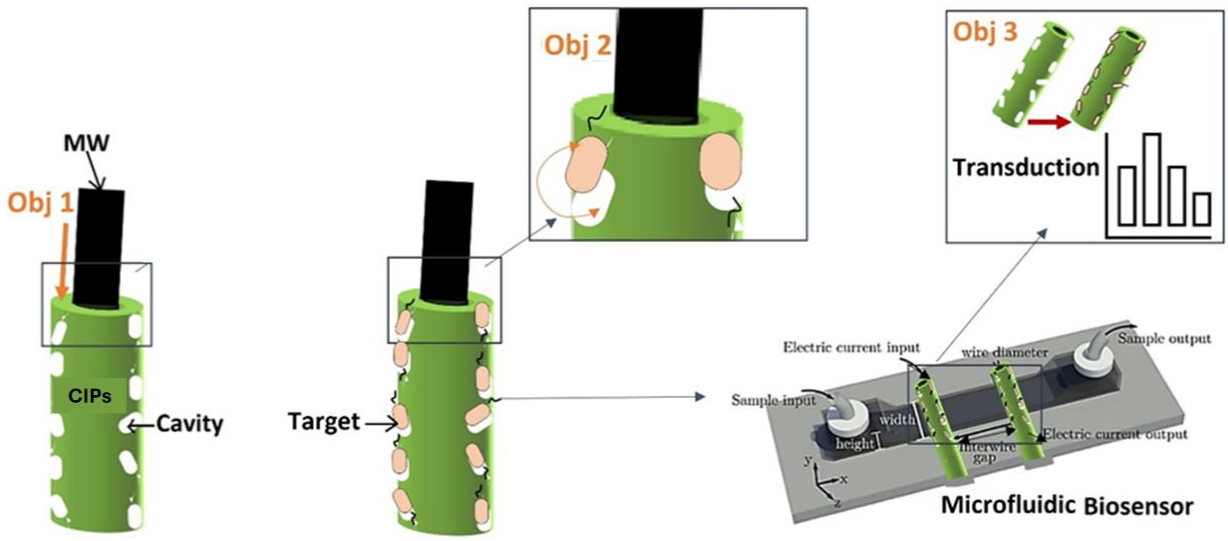

Fig. 1-17. Schematic demonstration of research objectives.

Objective 1: Investigate the effect of the CIP composition and synthesis parameters on the thickness, uniformity, and stability (retention) of CIP coatings on metallic MWs.

The first step is defining the important factors and understanding their effect on the synthesized CIP's properties. The most important components are functional monomers, cross-linkers, porogenic solvents, and initiators. Based on the gained information from the literature, the most appropriate composition of CIPs for bacteria templates will be selected. Next, different methods of coating the selected CIP compositions will be investigated, and the best method with reproducible coating results will be selected and based on that, a general procedure for the coating procedure will be developed. Then, a statistical design of investigations will be performed to study the effect of CIP composition and synthesis conditions on the final CIP coating characteristics, i.e., coating thickness, uniformity, and stability (retention).

Objective 2: Study the binding performance of the CIP-MWs in Obj. 1 to bacteria

The affinity of synthesized CIP coatings in the first objective will be evaluated by measuring their rebinding capacity to target cells in a suspension solution. NIP-MWs will also be used as control experiments to examine the effectiveness of the cavities on the CIP layers. The CIP-MWs and NIP-MWs will be incubated in target suspension with different bacteria concentrations. After incubation, MWs will be removed from the solution. The number of bound target cells to CIPs and NIPs on MWs will be determined by measuring the difference between the total number of cells in the primary solution and the residual number of cells in the solution phase after removing the MWs, using the serial dilution and culture plating method. This objective will help gain a fundamental understanding of CIP's rebinding performance based on its composition.

Objective 3: Integration of CIP-MWs within a microfluidic device and proof of concept demonstration of selective target detection based on electrical/electrochemical read-out.

In this objective, first, a microfluidic device as a platform to perform electrical/electrochemical detection will be designed, and the CIP-coated wires will be embedded inside the chip. The device will be fabricated using replica moulding of PDMS [129]. The CIP-MWs with known and optimized characteristics from the last objectives will be integrated with the device.

This objective aims to investigate the performance of the developed CIP-based microfluidic biosensor in selective capturing and detection of bacteria. NIPs will be used as a control in all the experiments. CIP affinity will be determined by exposing solutions of *E. coli* bacteria to the synthesized CIP receptors on MWs of the developed microfluidic device. We will investigate the selective binding performance of the developed biosensor to the target microorganisms using electrical/electrochemical transduction of the target binding.

1.7. Thesis Outline

This thesis consists of six chapters, starting with an introduction to the molecularly imprinted polymers (MIPs), Cell-imprinted polymers (CIPs), and microfluidic biosensors in the first chapter followed by a review of the conventional and microfluidic platforms used for biological agents' screening. Second chapter reports on the methodologies and materials utilized to synthesize CIPs and fabricate the microfluidic devices, chemicals and biological materials used in our chemical synthesis and screening assays, data and statistical analysis and tests conducted to evaluate the performance of our proposed devices. Third chapter elaborates on our CIP synthesis procedure and designs of experiments to develop uniform and stable coatings of bacteria imprinted polymers on the surface of metallic microwires (Obj. 1). In forth chapter, the binding efficiency and selectivity of developed CIPs to template and non-template bacteria are investigated using off-chip techniques (Obj. 2). In chapter five, the integration of CIPs into microfluidic devices and electrochemical transduction of bacteria binding to CIPs is investigated (Obj. 3). Finally, in chapter six, we provide a summary of the thesis with a focus on its limitations and propose the future directions of our research.

1.8. Publication Contributions

This thesis is based on the research papers co-authored by the PhD candidate as listed below. The content of chapters 1 through 5 have been drawn from these publications that were drafted by me and reviewed and revised by my supervisors, Prof. Pouya Rezai, and Pro. Satinder Kaur Brar. Both professors contributed to the conceptual design and improvements in sensor designs,

providing valuable feedback throughout my research. For all these papers, I was responsible for designing and conducting the experiments, including experimental design and data analysis. Dr. Ali Doostmohammadi, Dr. Khaled Youssef, Dr. Garrett Kraft, and Daphene-Eleni Archonta have contributed to the experimental tests, code development, and numerical analysis in different papers.

1.8.1. Contributed Journal Papers

- Shiva Akhtarian, Satinder Kaur Brar, and Pouya Rezai (2023). Electrochemical Impedance Spectroscopy-Based Microfluidic Biosensor Using Cell-Imprinted Polymers for Bacteria Detection. *Biosensors* 14, 445.
- Shiva Akhtarian, Ali Doostmohammadi, Daphne-Eleni Archonta, Garrett Kraft, Satinder Kaur Brar, and Pouya Rezai (2023). Microfluidic Sensor Based on Cell-Imprinted Polymer-Coated Microwires for Conductometric Detection of Bacteria in Water. *Biosensors* 13, 943.
- Shiva Akhtarian, Ali Doostmohammadi, Khaled Youssef, Garrett Kraft, Satinder Kaur Brar, and Pouya Rezai (2023). Metal microwires functionalized with cell-imprinted polymer for capturing bacteria in water. *ACS Applied Polymer Materials* 5, 3235-3246.
- Shiva Akhtarian, Noha Hasaneen, Rama Pulicharla, Satinder Kaur Brar, and Pouya Rezai (2023). Surface molecularly imprinted polymer-based sensors for antibiotic detection. *TrAC Trends in Analytical Chemistry*, 117389.

  .

1.8.2. Contributed Conference Papers

- Shiva Akhtarian, Satinder Kaur Brar, and Pouya Rezai (2024). Novel Impedimetric Microfluidic Biosensor Based on Cell Imprinted Polymers for Enhanced Waterborne Bacteria

Detection. The 28th International Conference On Miniaturized Systems For Chemistry And Life Sciences (μTAS). Peer reviewed

- Shiva Akhtarian, Satinder Kaur Brar, and Pouya Rezai (2024). Impedimetric Microfluidic Sensor Based on Cell Imprinted Polymers for Bacteria Detection in Water. Centre for Research and Applications in Fluidic Technologies (CRAFT) Research Symposium
- Shiva Akhtarian, Satinder Kaur Brar, and Pouya Rezai (2024). Impedimetric Microfluidic Sensor Based on Cell Imprinted Polymers for Bacteria Detection in Water. The Proceedings of the Canadian Society for Mechanical Engineering International Congress (CSME/CFD), May 26, 2024, University of Toronto, Toronto, Ontario, Canada.
- Shiva Akhtarian, Satinder Kaur Brar, Garrett Kraft, and Pouya Rezai (2023). Electrochemical Microfluidic Sensor Based on Cell Imprinted Polymer-coated Microwires for Selective Recognition of Bacteria in Water. The 27th International Conference on Miniaturized Systems for Chemistry and Life Sciences (μTAS). Peer reviewed
- Shiva Akhtarian, Satinder Kaur Brar, Garrett Kraft, and Pouya Rezai (2023). Conductometry-Based Microfluidic Bacteria Sensor with High Specificity using Molecularly Imprinted Polymer Coated Microwires. American Water Works Association (AWWA), June 14, 2023, Enercare Centre, Toronto, Canada. Peer reviewed
- Shiva Akhtarian, Ali Doostmohammadi, Garrett Kraft, Satinder Kaur Brar, and Pouya Rezai (2023). Molecularly Imprinted Polymer (MIP)-Based Microfluidic Sensor for Fluorometric Detection of Bacteria in Water. American Water Works Association (AWWA), June 14, 2023, Enercare Centre, Toronto, Canada. Peer reviewed
- Shiva Akhtarian, Ali Doostmohammadi, Khaled Youssef, Garrett Kraft, Satinder Kaur Brar, and Pouya Rezai (2022). Molecularly imprinted polymer (MIP) coatings on microscale

spherical and cylindrical substrates. The 26th International Conference on Miniaturized Systems for Chemistry and Life Sciences (μTAS). Peer reviewed

- Shiva Akhtarian, Ali Doostmohammadi, Khaled Youssef, Daphne-Eleni Archonta, Garrett Kraft, Satinder Kaur Brar, and Pouya Rezai (2022). Molecularly imprinted polymer-coated microwires for sensor applications and bacteria detection, 26th International Conference on Miniaturized Systems for Chemistry and Life Sciences (μTAS). Peer reviewed

1.8.3. Other Publications outside the Scope of the Thesis:

- Ali Doostmohammadi, Khaled Youssef, Shiva Akhtarian, Garrett Kraft, and Pouya Rezai (2024). Fluorescent bacteria detection in water using cell imprinted polymer (CIP) coated microparticles in a magnetophoretic microfluidic device. Talanta 268: 125290.
- Contributed to the conceptualization, methodology, and investigation. Also involved in the review and editing of the manuscript.Mohammad Hossein Karimi Darvanjooghi, Shiva Akhtarian, Gurpreet Kaur, Zeinab Ganji, Sara Magdouli, Satinder Kaur Brar, and Rama Pulicharla (2023). Nanomaterials: A Double-edged Sword as Pollution Busters or Pollutants?. Royal Society of Chemistry, vol. 61, ch. 2, pp. 29-62.
- Led the conceptualization, methodology, and investigation. Authored the original draft and contributed to the review and editing process.Ali Doostmohammadi, Khaled Youssef, Shiva Akhtarian, Ehsan Tabesh, Garrett Kraft, Satinder Kaur Brar, and Pouya Rezai (2022). Molecularly imprinted polymer (MIP) based core-shell microspheres for bacteria isolation.Polymer 251: 124917.
- Involved in conceptualization, methodology, and investigation. Provided critical review and editing of the manuscript.Shiva Akhtarian, Saba Miri, Ali Doostmohammadi, Satinder Kaur

Brar, and Pouya Rezai (2021). Nanopore sensors for viral particle quantification: current progress and prospects. Bioengineered 12, 9189-9215.

Contributed to methodology, investigation, and formal analysis. Led writing of the original draft and handled visualization and validation tasks.

1.8.4. Intellectual property

- "Molecularly Imprinted Polymer Coatings and Sensors for Biodetection" – US Patent Application No. 63249369 – Date of Application: Sep 28, 2021.
- "Methods for Coating Particles and Wires with Molecularly Imprinted Polymers and Integration with Microfluidic Sensors for Biodetection", Invention Disclosure- Innovation York, Invention Disclosure Reference #: 2021-014, June 3, 2021.

Chapter 2[i]

2. Materials and Methods

In this chapter, we introduce the chemicals used in our experiments and explain the common methodologies between our various experiments. The chapter will be continued with the data analysis and statistical tests performed in this thesis.

2.1. Materials

SS-MWs (125.3±0.5 µm dia., Type 304, Product No.: 40944BZ, Thermo Scientific™, USA) were used as CIP coating substrates. For the surface treatment of SS-MWs and fabrication of CIPs, methacrylic acid (MAA), acrylamide (AAM), N-vinylpyrrolidone (VP), methyl methacrylate (MMA), ethylene glycol di methacrylate (EGDMA), 2, 2′-azoisobutyronitrile (AIBN), acetonitrile, dimethyl sulfoxide (DMSO), toluene, phosphate-buffered saline (PBS), sulfuric acid, tetraethoxysilane, acetic acid, methanol, potassium ferrocyanide ($K_4[Fe(CN)_6]$), potassium ferricyanide ($K_3[Fe(CN)_6]$), potassium chloride (KCl), Ag/AgCl paste (60/40), rhodamine 110 chloride, Nile red, and trypan blue solution were purchased from Sigma-Aldrich (St. Louis, MO, USA). The Caenorhabditis Genetics Center (University of Minnesota, USA) provided the non-pathogenic bacteria microorganism *E. coli* OP50 for this study which was used as the template and

[i] Some content of this chapter has been published in:

1. Akhtarian S, Doostmohammadi A, Youssef K, Kraft G, Kaur Brar S, Rezai P. Metal microwires functionalized with cell-imprinted polymer for capturing bacteria in water. ACS Applied Polymer Materials. 2023 Jan 23;5(5):3235-46. Permissions for the use of the text has been received from American Chemical Society.
2. Akhtarian S, Doostmohammadi A, Archonta DE, Kraft G, Brar SK, Rezai P. Microfluidic Sensor Based on Cell-Imprinted Polymer-Coated Microwires for Conductometric Detection of Bacteria in Water. Biosensors. 2023 Oct 20;13(10):943.
3. Akhtarian S, Kaur Brar S, Rezai P. Electrochemical Impedance Spectroscopy-Based Microfluidic Biosensor Using Cell-Imprinted Polymers for Bacteria Detection. Biosensors. 2024 Sep;14(9):445.

target microorganism during CIP synthesis and rebinding experiments. *Sarcina lutea* (#155420) and *Listeria innocua* (#33090) microorganisms used for specificity tests were obtained from Carolina® Biological Supply Company, NC, USA and American Type Culture Collection (ATCC), respectively.

2.2. Bacteria culturing and sample preparation

All the bacterial microorganisms were cultured in LB liquid growth medium (5 g NaCl, 5 g bacto-yeast, and 10 g bacto-tryptone in 1 L distilled water) overnight inside a shaker incubator at 37°C and 150 rpm. The supernatant was removed after centrifugation at 7000 x g for 15 mins. The pellet was resuspended into fresh PBS (pH 7.0). Plate culturing and colony counting were used to determine the bacteria count when needed [130], [131].

For obtaining the bacteria sample for sensor characterization, 3 ppm NaCl in deionized water was used as a non-fatal [132] carrier electrolyte to resemble drinking waters [133] with very low salinity. For this, 3 mg of NaCl was dissolved in 1L of deionized water (DI) water. The bacterial suspension containing 10^9 CFU/mL in fresh PBS was centrifuged at 7000 x g for 15 mins, and the pellet was resuspended in the 3 ppm NaCl solution. This process was repeated three times to remove excess PBS. Serial dilution of the bacteria suspension in 3 ppm NaCl solution was performed to obtain the lower bacteria counts for dose-response investigations of the sensor. Trypan blue staining of bacteria exposed to 3ppm NaCl electrolyte for 30 mins indicated that the cells were viable after the exposure.

To examine bacteria capturing by functionalized MWs within the microfluidic device, green fluorescent protein (GFP) tagged *E. coli* cells and fluorescent microscopy were used. The mean

green intensity of the images was measured with RGB measure plus plugin of Image J software and used for comparing the fluorescent intensity.

2.3. Surface functionalization of SS-MWs

Surface functionalization of SS-MWs in this study was carried out according to literature [123], as demonstrated in Fig. 2-1. Silane coupling agents are functional silanol (≡Si-OH) compounds that can modify the metal and inorganic surfaces [134]. However, they require a high density of exposed hydroxyl groups on the surface of the substrate to form a chemical bond [135]. Therefore, the first step in the surface modification of SS-MWs was to oxidize their surface. SS-MWs were cut to a length of 4 cm and immersed in acetone. Ultrasonication was performed for 5 mins, and SS-MWs were then washed with methanol and doubly distilled (DI) water to remove the organic chemicals. After drying the wires under ambient conditions, they were immersed in a 2M sulfuric acid solution for 2 h and then washed with DI water. Among various oxidizing agents, it has been reported that sulfuric acid enhances the compactness and uniformity of surface hydroxyl groups [123] and, therefore, can provide a stronger chemical anchorage for subsequent reactions. This step also removes the organic contaminants from the surface of the wire and improves its wettability [135]. In the next step, to silanize the hydroxylated surface of the SS-MWs, they were immersed in a solution of tetraethyl orthosilicate (TEOS)-water-methanol (2:1:8, vol/vol) for 0.5 h. Furthermore, a post-silanization curing step at 150°C for 2 h was performed to cross-link the molecules of organosilanes at unreacted surface alkoxy groups to obtain a more robust silane layer with high density. Finally, the SS-MWs were rinsed with ethanol three times and dried under compressed air.

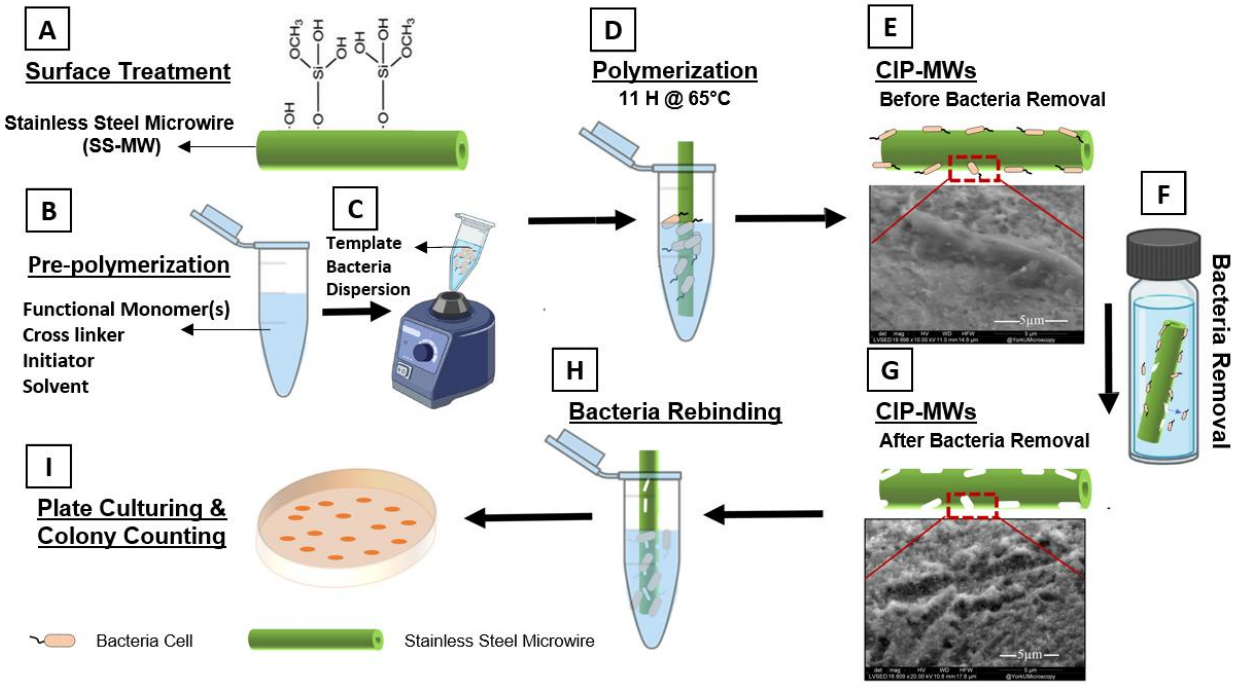

Fig. 2-1. Schematic illustration of preparing CIP-coated SS-MWs called CIP-MWs and rebinding experiment. A) Chemically modified surface of SS-MWs after subsequent oxidation and silanization; B) Pre-polymerization of polymer solution to increase cocktail viscosity; C) Dispersion of template bacteria in the pre-polymer solution; D) Polymerization at the optimized time and temperature in the presence of SS-MW and template bacteria; E) Coated surface of SS-MW with CIP before washing the template bacteria; F) Template removal from CIP coating; G) CIP-MW after washing the template bacteria. H) Immersion of CIP-MW in bacteria suspension to capture target bacteria; I) Plate culturing and colony counting to determine the remaining count of bacteria cells in the suspension after the rebinding experiment. Reprinted with permission from American Chemical Society.

2.4. Preparation of CIP-MWs

Since commonly used surface polymerization techniques for cell imprinting were difficult to be applied to non-planar MWs, single- and multi-FM CIP-MWs were prepared using bulk polymerization, according to a recipe related to single-FM MIPs [123], with some modifications (Fig. 2-1). Briefly, the FMs, cross-linker (EGDMA), and initiator (AIBN) reagents were dissolved

in a solvent with the quantities obtained from a design of experiment exercise discussed later. For observing the CIP coatings, Rhodamine 110 chloride (497 nm excitation and 520 nm emission) fluorescent dye was dissolved in the pre-polymer solutions. However, due to its poor solubility in non-polar solvents, Nile Red (530 nm excitation and 635 nm emission) was used for recipes with toluene as solvent. The solution was ultrasonicated for 2 mins to remove dissolved gases. Free radical polymerization involving azo initiators, such as AIBN, usually occurs at atmospheric pressure at moderate temperatures (usually less than 80°C). These reaction conditions are compatible with the templates and functional groups tested9. Subsequently, pre-polymerization was performed for 30 min at 65°C (Fig. 2-1B) inside an air-circulated gravity convection oven (HerathermTM, Thermo Fisher Scientific, Germany). After this step, the pre-polymer composition became thicker and lost its transparency, which indicated transition to polymerization. The pre-polymerization step was implemented to increase the cocktail viscosity to prevent template bacteria sedimentation in the subsequent steps. The bacteria must be dispersed properly in the pre-polymer solution to improve the homogeneity of CIP coatings. Subsequently, 1.5 mL of the above pre-polymerization solution was transferred into a centrifuge tube.

An *E. coli* OP50 template suspension (1:4, vol/vol to pre-polymer solution, 10^9 CFU/mL) was centrifuged at 3000 x g for 5 min, and the supernatant was removed. The pellet was resuspended into the pre-polymer solution by shaking it for 2 mins (Fig. 2-1C). Then, the surface-functionalized SS-MWs were immersed in the pre-polymer tube. The tube was sealed, and the polymerization was completed at 65◦C for 11 h (Fig. 2-1D). The first 30 mins of polymerization was done while tubes were rotating using a tube rotator inside the oven to increase the homogeneity of CIP coating along the MW surface. Trypan blue staining of bacteria exposed to the CIP pre-polymer indicated

that the cells die but do not lyse inside the pre-polymer. Therefore, they retain their geometrical properties for being imprinted in the CIP coatings as shown later in the paper.

After complete polymerization, the tubes were cut to remove the intact polymer with the MW immobilized inside, and the polymer around the MW was removed cautiously which resulted in a repeatable CIP coating process with controlled thicknesses. The details have been provided in Appendix A (Fig. A1-1). The wires were conditioned for an additional 2 h at 65◦C (Fig. 2-1E). The CIP-MWs were consequently soaked in methanol: acetic acid (9:1 v/v), methanol, and DI water for 20 s (called template removal solution) to remove bacteria templates from the CIP coatings (Fig. 2-1F) and generate associated cavities for rebinding (Fig. 2-1G). As a control group, NIP-MWs were prepared simultaneously using an identical synthesis procedure, except for adding *E. coli* templates.

2.5. CIP-MWs characterization

The morphology of the CIP- and NIP-MWs was observed using scanning electron microscopy (SEM) (Quanta 3D FEG, Thermofisher, USA). An inverted fluorescent microscope (DMIL LED Inverted Routine Fluorescence Microscope, Leica, Germany) equipped with a color camera (MC170 HD, Leica, Germany) was used for optical and fluorescent imaging of CIP- and NIP-MWs.

The coating thicknesses of the imprinted polymers were quantified using the image processing software ImageJ with a custom-developed macro that detected the edges of the MW in the optical image to calculate the mean ($\bar{x}$) and standard deviation (SD) of the MW diameter from 100

measurements along its length (Fig. A1-2). Coating uniformity was determined using Equation 2-1.

$$\text{Uniformity} = (1\text{-}SD/(\bar{x})) \quad (2\text{-}1)$$

The stability of the coatings was assessed by statistical comparison of the MW diameters before and after exposure to the template removal solution. A significant difference in the diameters (Mann-Whitney U test, p-value<0.05) was assessed as non-stable (labelled F for fail), while a non-significant difference (p-value>0.05) was considered as a stable CIP coating (labelled P for pass).

2.6. Design of experiments (DOE) and statistical analysis

Minitab 16 statistical software was used to develop DOE and statistical data analysis. A level of significance of 0.05 was adopted. Equality of variances was examined using Levene's test, and Welch's ANOVA was conducted instead of conventional one-way ANOVA when the assumption of homogeneous variances was not met ($p<0.05$). When ANOVA resulted in a significant difference between the means, a post hoc pair-wise analysis was conducted to identify which pairs of means were significantly different. Tukey HSD and Games-Howell post hoc tests were performed for datasets with homogenous and inhomogeneous variances, respectively [136].

A uniform CIP coating on the SS-MWs with ~2 μm thickness was required for bacteria imprinting. However, the coating characteristics depend on the polymer composition and polymerization conditions (temperature and time). Here, we utilized a statistical DOE to control the NIP coating uniformity and thickness on the SS-MWs and optimize the coating compositions with single and complex monomer combinations of most used FMs for imprinting biological templates, i.e., MAA, AAM, MMA and VP. We first developed a screening DOE based on the

Taguchi method to evaluate the selected factors' significance and variation levels. The factors in this study were defined as the type of FM, molar ratio of FM to cross-linker, type of solvent, and polymerization variables, i.e., polymerization time and temperature, as presented in Table 2-1. In terms of solvent, acetonitrile, toluene, PBS, and DMSO were selected to optimize CIP's formulation. PBS is included since it provides a condition similar to the natural environment of the biological templates. Levels for the other factors were defined based on preliminary experiments.

Table 2-1. Important factors and their levels in CIP composition and polymerization on MWs. Reprinted with permission from American Chemical Society.

Important Factors	**FMs**	**FM: Cross-linker Ratio**	**Solvent**	**Polymerization Time (h)**	**Polymerization Temperature (˚C)**
Levels	MAA	1:1	Acetonitrile	7	60
	AAM	1:2	DMSO	12	70
	VP	1:4	PBS		
	MMA	1:6	Toluene		

FMs: Functional monomers; MAA: Methacrylic acid; AAM: Acrylamide; VP: N-vinylpyrrolidone; MMA: Methyl methacrylate; DMSO: Dimethyl sulfoxide; PBS: Phosphate-buffered saline

The developed DOE using Taguchi L16 orthogonal array indicated that 16 experiments were required for this procedure, according to Table 2-2, performed with three replicates for each composition. Next, to better understand the effect of different parameters on the response factors, we used the response surface methodology (RSM). RSM also provides an optimization module for predicting the optimal levels of these parameters. Finally, a mixture DOE was performed to

optimize the FM ratios to immobilize complex CIPs on SS-MWs. A simple centroid mixture design augmented with axial points with 19 runs and three replicates was performed in this thesis (see Appendix A).

Table 2-2. Screening design of experiment runs generated using Taguchi method. Reprinted with permission from American Chemical Society.

Experiment Number	**FM**	**FM: Cross-linker Ratio**	**Solvent**	**Polymerization Time (h)**	**Polymerization Temperature (◦C)**
1	MAA	1:1	Acetonitrile	7	60
2	MAA	1:2	DMSO	7	60
3	MAA	1:4	PBS	12	70
4	MAA	1:6	Toluene	12	70
5	AAM	1:1	DMSO	12	70
6	AAM	1:2	Acetonitrile	12	70
7	AAM	1:4	Toluene	7	60
8	AAM	1:6	PBS	7	60
9	VP	1:1	PBS	7	70
10	VP	1:2	Toluene	7	70
11	VP	1:4	Acetonitrile	12	60
12	VP	1:6	DMSO	12	60
13	MMA	1:1	Toluene	12	60
14	MMA	1:2	PBS	12	60
15	MMA	1:4	DMSO	7	70
16	MMA	1:6	Acetonitrile	7	70

2.7. CIP-MWs rebinding performance to bacteria

To evaluate the rebinding performance of the optimized CIP compositions consisting of single, two, three, and four FMs, to *E. coli* OP50 cells, the corresponding NIP-MWs and CIP-MWs were prepared and tested, along with SS-MWs, with bacterial solutions at an initial count of 10^4 CFU/mL. In each bacteria rebinding experiment, a 3 cm long CIP-MW was immersed in 1 mL of *E. coli* OP50 suspension (10^4 CFU/mL) and incubated for 30 mins at room temperature (Fig. 2-1H). The CIP-MW was then removed from the suspension. Using serial dilution and culture plating methods (Fig. 2-1I), the number of bacteria bound to CIP-MW was determined by comparing the total bacteria count in the primary suspension to the residual bacteria count following the removal of CIP-MW. The total number of colonies was counted after incubation at 37°C for 20 h. Control experiments were conducted with bare and NIP-MWs. All the experiments were carried out in five replicates. The bacterial capturing efficiency was then calculated using Eq. 2.

$$\text{Bacterial Capturing Efficiency (\%)} = \left(\frac{\text{Initial bacteria count} - \text{Residual bacteria count}}{\text{Initial bacteria count}}\right) \times 100 \qquad (2)$$

2.8. Specificity test

The specificity of CIP-MWs was investigated by exposing the CIP-MWs imprinted with *E. coli* OP50 as the template to suspensions of three different bacteria microorganisms, including *E. coli* OP50, *Sarcina* and *Listeria innocua*. The experiments and analyses were conducted based on the bacteria rebinding procedures mentioned above.

2.9. Microfluidic device

2.9.1. Microfluidic device for conductometric measurements

The microfluidic sensor comprised two mirrored polydimethylsiloxane (PDMS, Sylgard 184 silicone elastomer kit, Dow Corning Co., USA) layers containing the design of a microchannel (500 µm ×900 µm), the network of inlet-outlet, and two MW channels (130 µm ×130 µm) with an inter-wire distance of 1.5 mm (Fig. 2-2A). Each layer was 5mm in thickness. The master molds for replica molding of PDMS were designed using CAD Solidworks software and fabricated using 3D printing (Proto3000, Toronto, Canada).

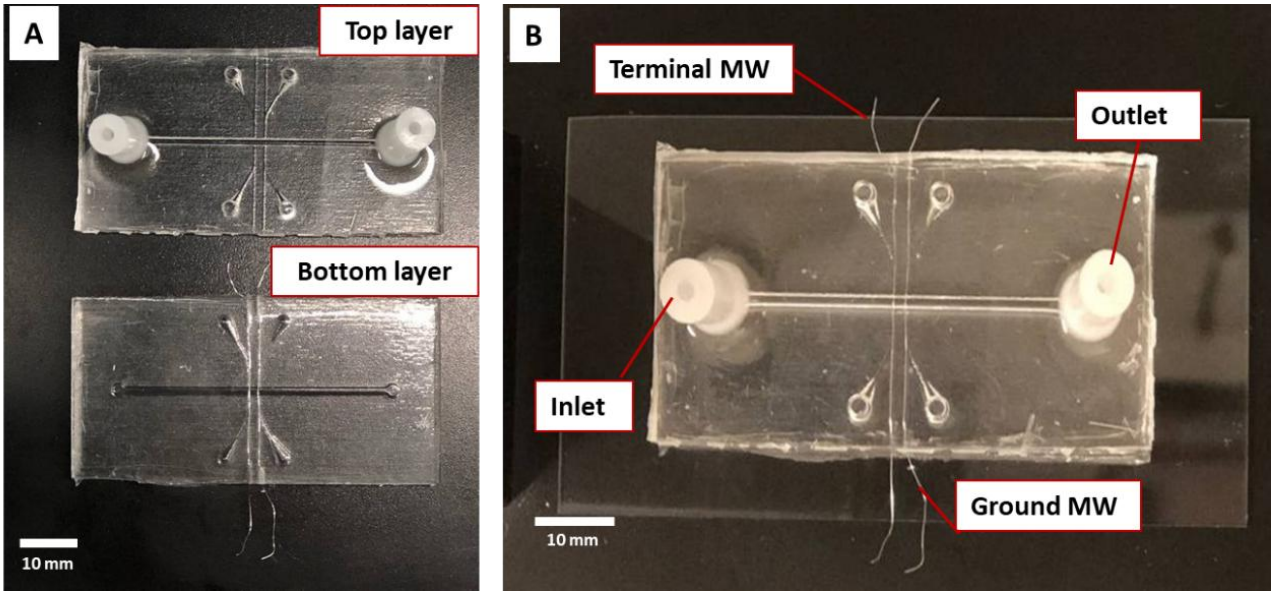

Fig. 2-2. Conductometric microfluidic bacteria sensor design. A) Top and bottom PDMS layers with installed MWs for fabrication of microfluidic device, B) Final microfluidic device after plasma bonding of two PDMS layers [137], *Open Access.*

The pre-polymer of PDMS was prepared by mixing PDMS base with its curing agent (weight ratio of 10:1), followed by degassing in a vacuum desiccator for 15 mins. The pre-polymer was poured over the master molds, followed by curing on a hot plate at 75 °C for 2 h. After curing, the

PDMS layers were peeled off, and CIP-MWs were installed in MW channels on one layer. Using Oxygen plasma, the two PDMS layers were bonded together and then bonded to a glass slide (Fig. 2-2B). In control experiments, not-coated MWs referred to as SS-MWs and NIP-MWs were also integrated into microfluidic devices. Three replicates of each sensor were fabricated and tested.

2.9.2. Microfluidic device for impedimetric measurements

The microfluidic device was fabricated with two identical layers of PDMS, incorporating the modified sensor design. It featured two parallel microchannels with three perpendicular MW channels for integrating three electrodes essential for electrochemical measurements, along with inlet–outlet networks (Fig. 2-3A). A CIP-MW served as the working electrode within the test microchannel, positioned in the central MW channel. Adjacent to the working electrode, an uncoated MW (SS-MW) was utilized as the counter electrode, maintained at a distance of 1.5 mm. Additionally, an MW with an Ag/AgCl coating functioned as the reference electrode and was positioned 3 mm away from the working electrode, to reduce interference with reactions at the working electrode. In the parallel microchannel, a similar arrangement was adopted, except for the working electrodes, where NIP-MWs were utilized.

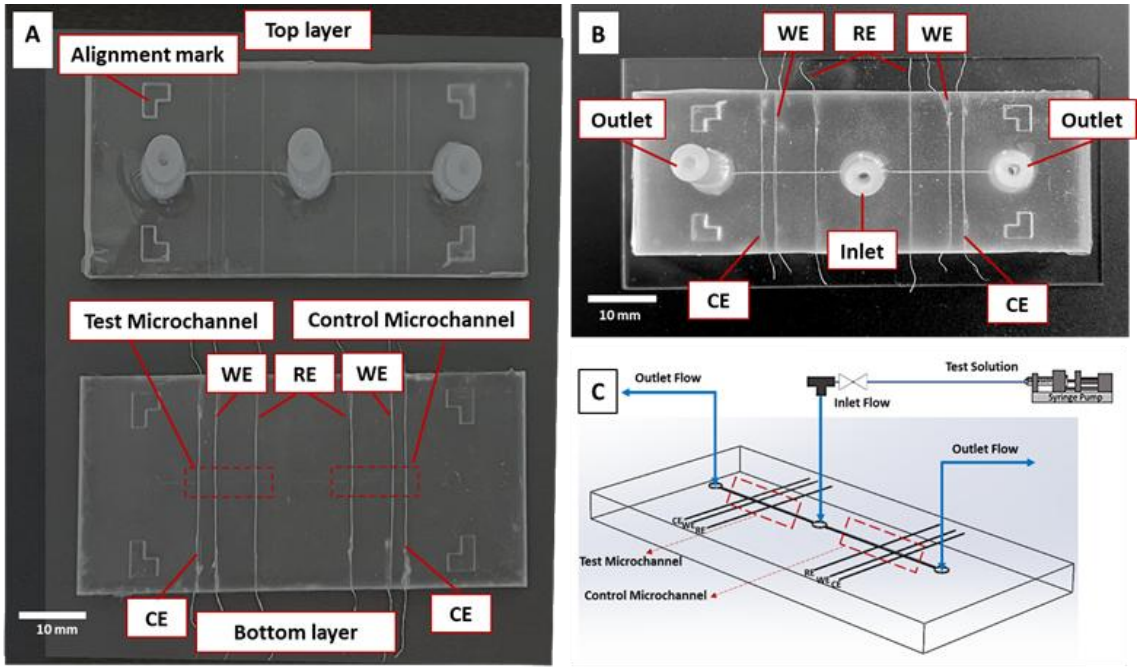

Fig. 2-2. Impedimetric microfluidic bacteria sensor design and fabrication. (A) Upper and lower PDMS layers with integrated MWs. (B) Final microfluidic device post-plasma bonding of PDMS layers onto a glass slide. (C) Schematic of the sensor design illustrating flow directions and concurrent test and control measurement microchannels with CIP-MW and NIP-MW working electrodes (WEs), respectively. For reference electrodes (REs) and contour electrodes (CEs), Ag-MWs and SS-MWs were used, respectively [138], *Open Access.*

2.10. Experimental Setup for Electrochemical Measurements

2.10.1. Experimental Setup and procedures for conductometric measurements

Fig. 2-4 demonstrates the experimental setup for conductometric measurements. A syringe pump (Legato 110, KD Scientific Inc., USA) was used to infuse the sample through the microfluidic channel with a flow rate of 0.2 mL/min. A DC electrical source meter (Model 2410, Keithley Instruments Inc., USA) and its interface software Kickstart installed on a PC were used to measure the electrical resistance across the CIP-MWs. The terminal and ground MWs were

connected to the source meter. A current sweep between 10nA-1μA with a step size of 10nA was applied for 110 s during each experiment, and the corresponding voltage across the CIP-MWs was recorded. Using Ohm's law, the electrical resistance for 100 data points was calculated by dividing the voltage by the applied current values (R = V/I). A DMIL LED conventional inverted fluorescence microscope (Leica, Germany) was used to monitor the micro-channel during experiments.

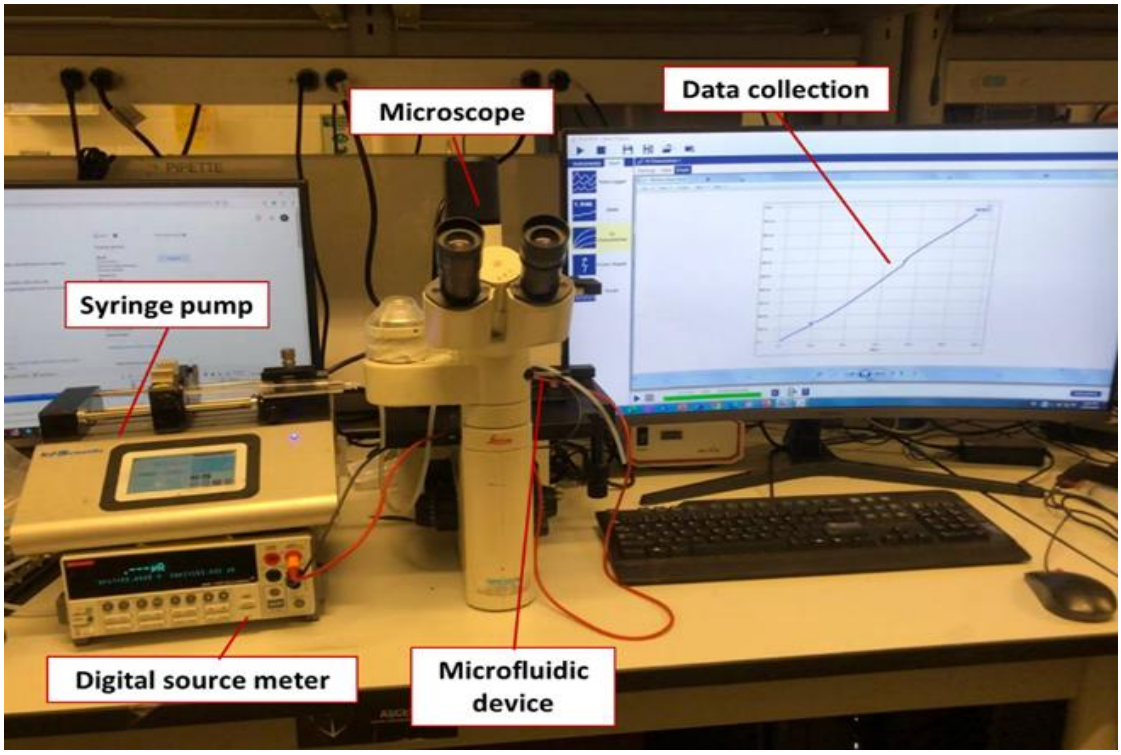

Fig. 2-4. Experimental setup used to test conductometric microfluidic bacteria sensor, showing the instruments required for the sensor characterization [137], *Open Access.*

The electrical resistance measurement was performed in three stages. In the first stage referred to as pre-incubation electrolyte 1 wash, 3ppm NaCl solution as a blank electrolyte was infused through the microchannel, and the measurement was performed. The resistance value obtained at this stage (R_0) was used as the baseline resistance of the sensor. Next, the bacteria suspension at a known concentration was run through the microchannel for 30 mins to allow incubation and

conjugation of bacteria with CIP cavities. Subsequently, the second electrical resistance measurement, R_1, was performed. The last resistance measurement, R_2, was done after running a blank electrolyte for the second time (post-incubation electrolyte 2 wash) through the microchannel for 10 mins. Measurements were repeated five times at each step and for replicate devices.

2.10.2. Experimental Setup and procedures for impedimetric measurements

Fig. 2-5 demonstrates the experimental setup for impedimetric measurements. A DMIL LED standard inverted fluorescence microscope (Leica, Wetzlar, Germany) was employed to observe the microchannels and MWs throughout the measurements. EIS measurements were carried out with an Interface 1010E Potentiostat (Gamry Instruments, Warminster, PA, USA), with a standard three-electrode system, using a 0.1 M KCl solution containing 5 mM $K_3[Fe(CN)_6]$ over a frequency range of 0.1–100 kHz, at room temperature, with a 10 mV perturbation amplitude. The sample was infused into the inlet microchannel at a 0.2 mL/min flow rate using a syringe pump (Legato 110, KD Scientific Inc., Holliston, MA, USA). Electrochemical spectra were fitted with an equivalent electrical circuit, and the charge transfer resistance (R_{CT}) was measured pre- and post-bacteria exposure. Data acquisition and analysis were accomplished using Gamry Framework software Version 7.10.

The EIS measurement consisted of two stages where the charge transfer resistance of both device cells (microchannels with 3 electrodes) was measured before and after exposure to bacteria. In the initial stage, the electrolyte solution was infused through the microchannel, and measurements were taken. The resulting charge transfer resistance value ($R_{CT,1}$) served as the baseline resistance. Following this, a bacteria suspension of specified count was introduced into

the microchannels and allowed to incubate for 30 min to facilitate the bacteria binding to the CIP. The second EIS measurement ($R_{CT,2}$) was conducted after flushing the microchannels with a blank electrolyte solution for 10 min to remove the unbonded bacteria from the device. The measurements were repeated for the replicate devices.

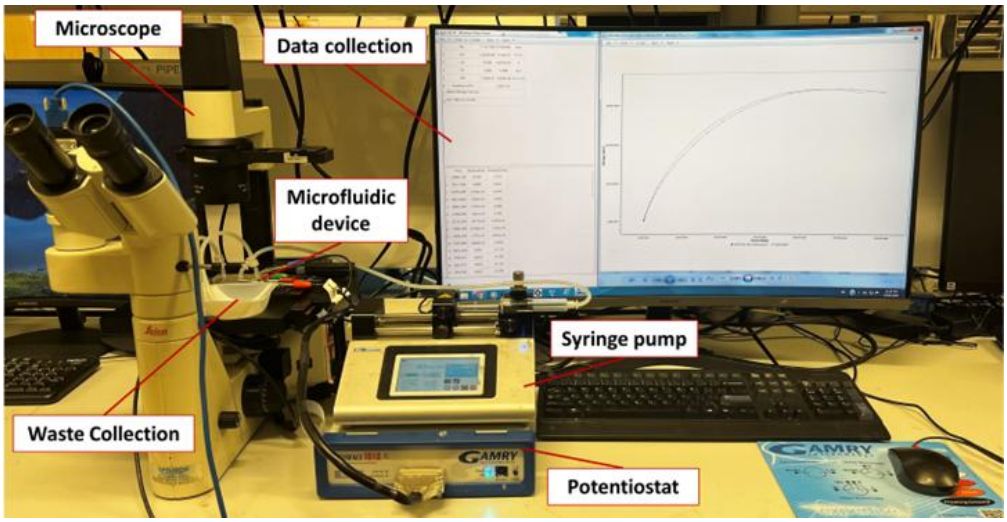

Fig. 2-5. Experimental setup used to test the impedimetric microfluidic bacteria sensor [138], *Open Access.*

2.11. Data analysis for sensor characterization

Minitab 16 statistical software was used for statistical data analysis. A significance level of 0.05 was adopted. The Mann-Whitney U test, also known as the Wilcoxon rank sum test as the nonparametric version of the parametric t-test, was utilized to identify if any two pairs of means were significantly different [139].

The dynamic range of the sensor was identified based on statistical difference of normalized resistance responses between adjacent bacteria counts (p-value<0.05). The linearity of the sensor

was determined by line fitting into the dynamic range of the dose-response curve and analyzing the R_2 values. The limit of detection (LOD) and limit of quantification (LOQ) were determined as bacteria counts with $\Delta R/R_0$ equal to that of the blank NaCl solution plus 3 and 10 times its standard deviation (SD), respectively. The sensitivity of the sensor in the linear range of the dose-response curve was found based on the slope of the linear range response.

2.11.1. Data analysis for conductometric sensor characterization

The obtained R_1 and R_2 resistances were normalized by the measured baseline resistance using the fold change method (R_i/R_0, i=1 or 2) to eliminate the variability among devices. The sensor dose-response curve was generated based on the normalized resistance difference method ($\Delta R/R_0=(R_0-R_2)/R_0$). Here, R_1 was not used as this resistance includes the effect of bacteria attached to the wire but not necessarily captured by the CIP cavities. Experiments at various bacterial counts were performed and the sensor dose-response curve of $\Delta R/R_0$ versus bacteria count was plotted.

2.11.2. Data analysis for impedimetric sensor characterization

The change in the collected R_{CT} values was normalized by dividing the change in R_{CT} by the baseline R_{CT} of each experiment (before bacteria incubation) to standardize performance across devices [140]. The dose–response curve of the sensor was established using the normalized charge transfer resistance difference method according to Equation 2-2. Different bacterial counts were tested, and the resulting dose–response curve of $\Delta R/R_{CT,1}$ against the bacteria count was generated.

$$\Delta R/R_{CT,1} = (R_{CT,2} - R_{CT,1})/R_{CT,1} \quad (2\text{-}2)$$

Chapter 3[i]

3. Development of CIP-MWs

This chapter elaborates on our CIP synthesis procedure and designs of experiments to develop uniform and stable coatings of bacteria imprinted polymers on the surface of metallic microwires (CIP—MWs) (Obj. 1 of the thesis).

3.1. Introduction

The choice of appropriate functional monomers (FMs) is the most critical factor in synthesizing MIPs and CIPs since it defines the interaction between polymers and templates and, therefore, directly affects the binding properties of the formed recognition sites [40]. Generally, there are three distinct ways for MIPs and CIPs to interact with templates and, consequently, the targets, i.e., through covalent, non-covalent, and semi-covalent bonds.

In the covalent imprinting approach, covalent bonds are formed between the template molecules and FMs before polymerization by chemical modification of template molecules with FMs. After polymerization, the template is removed from the imprinted polymer by cleavage of this covalent bond, and the target rebinding is achieved via the reformation of these covalent bonds. The

[i] Some content of this chapter has been published in:

1. Akhtarian S, Doostmohammadi A, Youssef K, Kraft G, Kaur Brar S, Rezai P. Metal microwires functionalized with cell-imprinted polymer for capturing bacteria in water. ACS Applied Polymer Materials. 2023 Jan 23;5(5):3235-46. Permissions for the use of the text has been received from American Chemical Society.
2. Akhtarian S, Doostmohammadi A, Archonta DE, Kraft G, Brar SK, Rezai P. Microfluidic Sensor Based on Cell-Imprinted Polymer-Coated Microwires for Conductometric Detection of Bacteria in Water. Biosensors. 2023 Oct 20;13(10):943.
3. Akhtarian S, Kaur Brar S, Rezai P. Electrochemical Impedance Spectroscopy-Based Microfluidic Biosensor Using Cell-Imprinted Polymers for Bacteria Detection. Biosensors. 2024 Sep;14(9):445.

establishment of acetal bonds, ketals, boronic ester bonds, and Shiff base bonds are some examples of covalent interactions in molecular imprinting [141]. In non-covalent imprinting, the weaker non-covalent bonds, such as hydrophobic interactions, π–π bonding, hydrogen bonding, and electrostatic interactions, are formed between the FMs and templates. In the semi-covalent approach, the template is covalently bonded to FMs during polymerization, while only non-covalent interactions are exploited during rebinding [142].

Unlike smaller molecule templates, proteins and biological cells are complexes containing a large variety of biopolymers and molecules. Thus, the design of specific covalent bindings for these templates is challenging. Furthermore, covalent interactions have a longer response time due to the requirement of precise binding and association of the target. Hence, for imprinting cells, non-covalent interactions such as van der Waals forces, π–π interactions, hydrophobic interactions, ionic and electrostatic affinity, and hydrogen bonds are preferred to achieve easier binding and dissociation between CIPs and cells. Since these chemical interactions occur between functional groups of FMs and molecules on the cell surface, the selection of appropriate monomers that can form non-covalent bonds with the template is of great importance in imprinting large molecules and cells [117], [143], [144]. During the last few years, CIPs synthesized by combinations of multiple FMs, including methacrylic acid (MAA), acrylamide (AAM), methyl methacrylate (MMA) and N-vinylpyrrolidone (VP), have been reported to have enhanced selectivity toward biological templates like viruses by providing additional side chains during non-covalent imprinting [53]–[55], [66]. According to the shape and polarity of the monomer and the particular amino acid, each monomer may be compatible with a set of amino acid sidechains present abundantly on the surface of biological cells.

Multi-FM CIP thin films have been reported to capture microorganisms on quartz crystal microbalances (QCM) surfaces or microparticles for concentration-based optical or piezoelectric transductions, respectively [70], [143], [145]. MIPs with a single FM (mostly MAA) have also been synthesized on stainless steel microwires (SS-MWs) to separate chemical compounds in solid-phase microextraction (SPME) applications [123]–[125]. To date, the effects of CIP composition, especially incorporating additional FMs, and the polymerization time and temperature, on forming a uniform and durable CIP coating on MWs, and the application of these CIP-MWs for bacterial capturing have not been investigated. We hypothesize that immobilizing bacteria-specific CIPs on metallic MWs can enable future electrical detection of target bacteria, while MWs can enhance sensor performance by providing increased surface area. Compared to planar microelectrodes, CIP-MWs can be immersed in the solution to increase the chance of analyte-CIP interaction for enhanced bio-detection.

In this chapter, we report the functionalization of the surface of SS-MWs with *E. coli*-imprinted CIP coatings, consisting of single to quadruple FMs and compared their rebinding performance to bacteria targets. Parametric study and statistical designs of the experiment (DOE) were performed to optimize the synthesis parameters for obtaining uniform and stable CIP coatings with specific thicknesses, which were experimentally validated. Obtaining a specific coating thickness is beneficial for tailoring the recognition sites and efficient removal of targets based on the shape and size of the desired analytes, i.e., bacteria size ranges from 0.5-10 μm [146]. The developed CIP-MWs will be installed within a portable microfluidic sensor to perform electrical transduction of bacteria binding to CIPs, which we report in the next chapters.

3.2. Results

3.2.1. Optimization of single-FM NIP coatings on SS-MWs

The diameter of bare SS-MWs was measured to be 125.3±0.5 µm. The effects of solvent and FM type and ratio to cross-linker, as well as polymerization time and temperature (Table 2-1) on the thickness, uniformity, and stability of the NIP coatings on SS-MWs were investigated. Fig. 3-1 shows the fluorescent images of Rhodamine or Nile Red dyed NIP layers coated on SS-MWs after performing the sixteen Taguchi DOE-based recipes listed in Table 2-2 and before exposing them to the template removal solution for stability test.

Overall, the uniformity of the synthesized NIP coatings for all monomers using acetonitrile as solvent (Fig. 3-1, recipes 1, 6, 11 and 16) was acceptable. Among these recipes, the coatings performed with MAA and AAM FMs (Fig. 3-1, recipes 1 and 6) show better uniformity and consistency on the silanized surfaces of SS-MWs. This could be attributed to the hydrophilicity and higher polarity of these monomers compared to MMA and VP [147], [148]. As opposed to acetonitrile, using PBS, DMSO, and toluene as a solvent negatively affected the coating formation and its uniformity. For example, recipes 3 and 9 showed a bubbling effect in the resultant coating that reveals the non-compatibility of PBS as a solvent. Recipes 8 and 14 with PBS solvent had no bubbling, potentially due to the better compatibilities of AAM and MMA FMs, but still showed poor uniformities. The coating from recipes 2, 5, 12, and 15 with DMSO as the solvent and recipes 4, 7, 10 and 13 with toluene solvent resulted in poor dotted coatings.

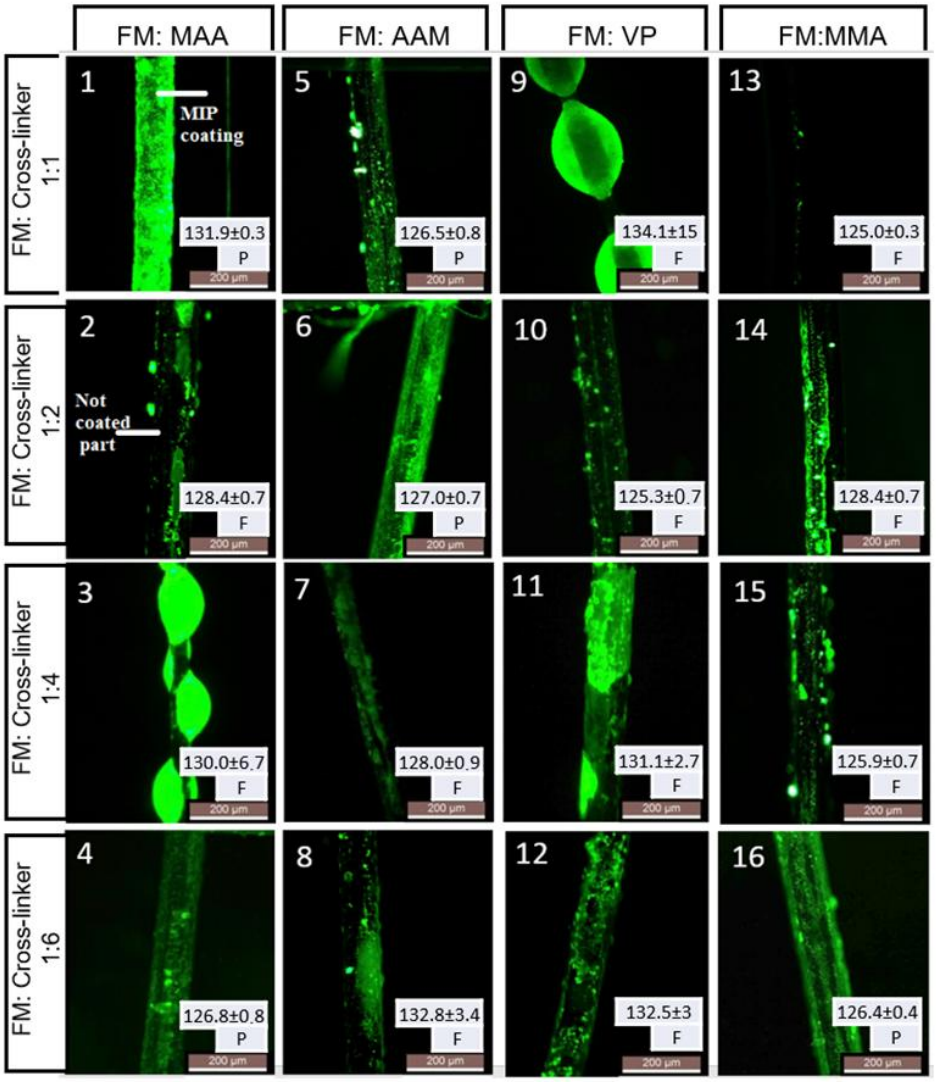

Fig. 3-1. Fluorescent images of 16 recipes (top left numbers) based on the screening DOE generated using the Taguchi method in Table 2-2. Images were acquired before the stability test (i.e., exposure to template removal chemical), and all recipes had Rhodamine 110 with a green fluorescent protein (GFP) as a fluorescent dye. Columns from left to right show the fluorescent NIP layers coated on SS-MWs synthesized from monomers MAA, AAM, VP, and MMA, respectively, with different levels for the other four design factors. Rows from top to bottom show different FM:cross-linker ratios of 1:1, 1:2, 1:4, and 1:6, respectively. The mean and standard deviation of thickness measurements and the stability test results (P for pass and F for fail) are given for each sample in the bottom right corner of each figure [149]. *Reprinted with permission from American Chemical Society.*

The average thicknesses of the NIP layers and the results from exposing the coated layers to the template removal solution (i.e., stability test: P as pass and F as fail) are also shown in the bottom right corner of each panel in Fig. 3-1. From the successful recipes 1, 6, 11 and 16, only the VP-based NIP layer failed the stability test, while the other three NIP layers adhered well to the SS-MWs after treatment with the template removal solution containing methanol and acetic acid. The obtained main effect plots of the response surfaces for the thickness, uniformity, and stability of the NIP Coatings on SS-MWs are demonstrated in Fig. 3-2. While coatings with VP as FM can reach higher thicknesses than the other three FMs, these coatings pose the lowest uniformity and stability. The thickness and stability of coatings with MMA as the functional monomer were very low, which was not desired considering the size of bacteria templates.

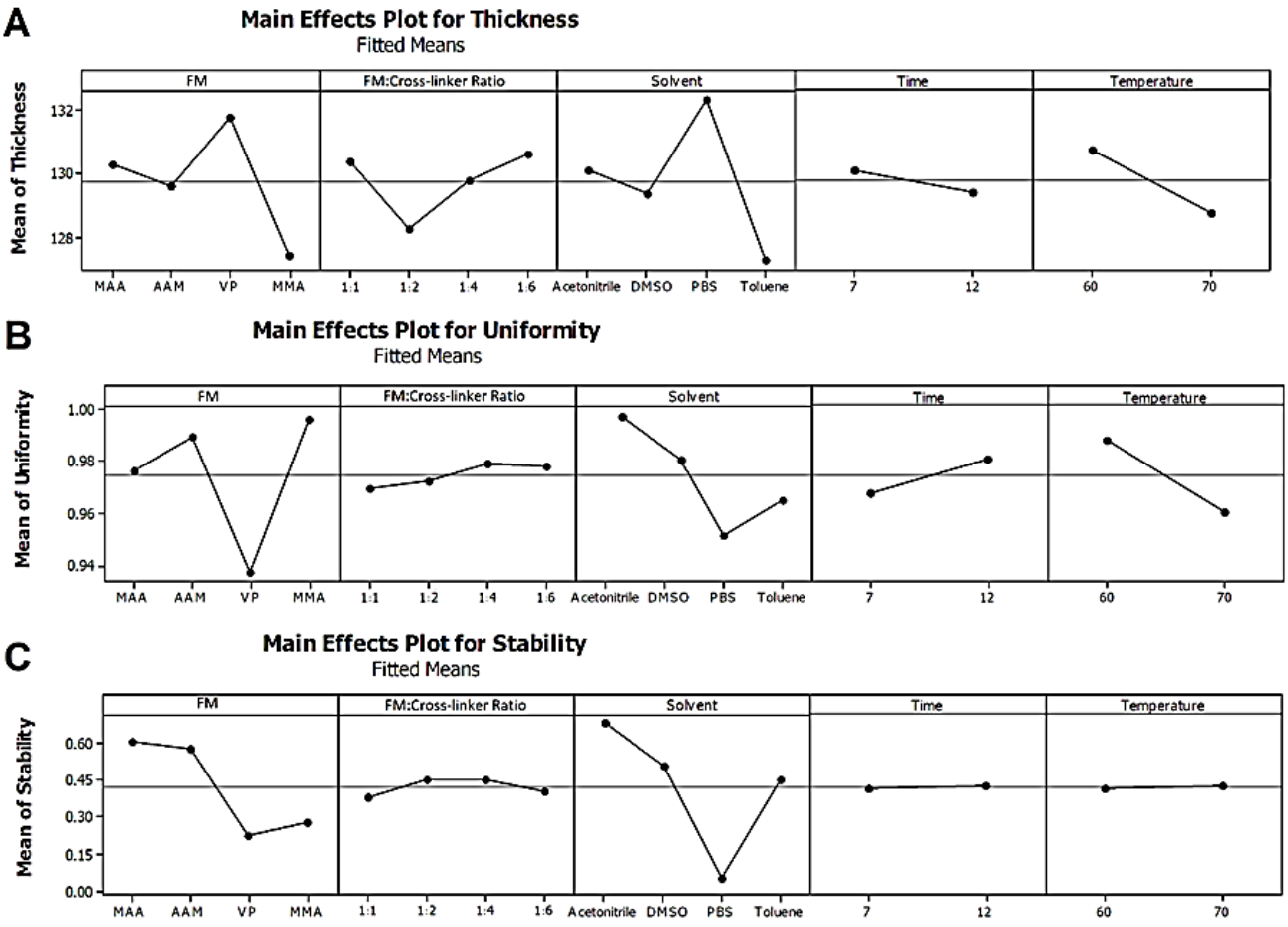

Fig. 3-2. Main effect plots from analyzing the results of Taguchi DOE (Table 2) demonstrate the effects of factor levels on the A) thickness, B) uniformity, and C) stability of the obtained NIP coatings on SS-MWs [149]. *Reprinted with permission from American Chemical Society.*

Our findings on the effect of FM are in agreement with the results observed by Xiaogang Hu [119], [150], [151] using MAA, AAM and VP as FMs for coating silanized surfaces of Silica fibers. Their results showed a more homogeneous coating in the thickness range of 2.3-2.7 µm using AAM and MAA. Likewise, Yuling Hu [119] reported a better homogeneity and morphological structure using MAA and 4-VP during a monomer optimization study.

Increasing the cross-linker ratio to FM from 1:1 to 2:1 decreased the coating thickness while having a small positive effect on the uniformity and stability of the coatings. Further increase in the cross-linker ratio to 4:1, however, increased the thickness and enhanced the uniformity marginally while having almost no effect on the stability of the coating. The maximum FM: cross-linker ratio of 1:6 increased the thickness of the NIP coating, while the effects on the uniformity and stability were insignificant. The cross-linker to FM ratio of 4:1 has been reported previously to provide the highest uniformity and morphological coating characteristics in different tested ranges from 1:1 to 1:16 [150]–[152].

Compared to other solvents like DMSO, acetonitrile provided the most durable coating with high uniformity and a close-to-target thickness value of 2 µm. This result is in agreement with the previous reports by Xiaogang Hu et al. [150], [151], where acetonitrile provided more uniform and reproducible coatings with higher thicknesses than DMSO. Our coatings with the lowest uniformity and stability were observed when PBS and toluene were used as solvents.

The results in Fig. 3 2. show that, while increasing the time and temperature could decrease the thickness of the NIP coatings, higher uniformities could be obtained at lower temperatures and longer polymerization times. It is reported in the literature [150] that a shorter polymerization time would lead to decreased uniformity and cannot increase the coating thickness [118], which is in accordance with our findings. Furthermore, prolonged polymerization times could result in cross-linker degree enhancement, impacting the capacity to remove the wire from the polymer bulk[150]. It was shown that multiple polymerization steps by repeating the same coating procedure would increase the coating thickness to about 1.2 µm [118], while we could achieve uniform coatings of 2 µm thickness in a single step.

NIP coating investigations on SS-MWs indicated that all the defined factors had a significant effect (p-value <0.05) on the coating thickness with the following order of importance from high to low: i) solvent type, ii) FM type, iii) FM: cross-linker ratio, iv) temperature, and v) time. On the other hand, the polymerization time and temperature did not show a significant effect (p-values >0.05) on the stability response.

To fabricate uniform NIP coatings based on each of the FMs used in our studies, we conducted RSM optimization as described in the Materials and Methods section. Table A1-1 shows the optimized values for each recipe for synthesizing NIP-MWs based on each FMs, and Fig. A1-3 shows the coated NIP-MWs using these optimized recipes. For example, the optimal single-monomer composition with MAA as FM (the first recipe in Table A1-1) can be obtained by using acetonitrile as the solvent, with an optimal FM: cross-linker ratio of 1:4.76. While acetonitrile was the most compatible solvent for MAA, AAM and MMA, it was not optimal for VP. This could be due to the low polarity of this FM, which resulted in better compatibility with toluene, a non-polar solvent.

3.2.2. Optimization of multi-FM NIP coatings on SS-MWs

CIPs consisting of multiple FMs have been reported to offer enhanced selectivity toward microorganisms compared to single-monomer CIPs [53], [55]. However, immobilization of these complex CIPs on MWs has not been reported, while highly needed for the development of biomimetic sensors based on wires and CIPs. Accordingly, the coating of multi-monomer NIPs on SS-MWs was optimized in this section using a mixture DOE. A simple centroid mixture design augmented with axial points with 19 runs and three replicates was performed in this thesis (Table 3-1).

Table 3-1. Experimental runs generated using the mixture DOE.

Experiment	**Functional Monomer Proportion**			
Number	MAA	AAM	VP	MMA
1	0.07	0	0	0
2	0	0.07	0	0
3	0	0	0.07	0
4	0	0	0	0.07
5	0.035	0.035	0	0
6	0.035	0	0.035	0
7	0.035	0	0	0.035
8	0	0.035	0.035	0
9	0	0.035	0	0.035
10	0	0	0.035	0.035
11	0.023333	0.023333	0.023333	0
12	0.023333	0.023333	0	0.023333
13	0.023333	0	0.023333	0.023333
14	0	0.023333	0.023333	0.023333
15	0.0175	0.0175	0.0175	0.0175
16	0.04375	0.00875	0.00875	0.00875
17	0.00875	0.04375	0.00875	0.00875
18	0.00875	0.00875	0.04375	0.00875
19	0.00875	0.00875	0.00875	0.04375

Based on the single-monomer studies in Fig. 3-2 and for simplicity, the FM: cross-linker ratio, polymerization time, polymerization temperature, and the solvent type were held constant at 1:4, 11h, 65°C, and acetonitrile, respectively. Therefore, the thickness, uniformity and stability responses were only affected by the types and compositions of the four FMs. Fig. A1-4 demonstrates the contour plots from analyzing the results of mixture DOE for the thickness and uniformity responses. Using the optimization module of the mixture DOE, the optimal compositions for uniform and stable immobilization of different combinations of FMs on the surface of SS-MWs were obtained, as included in Table 3-2.

Table 3-2. Optimal recipes for single to four-monomer NIPs on SS-MWs. Reprinted with permission from American Chemical Society.

NIP Composition	**FM**				**Cross-Linker**	**Solvent**	**Initiator**
	MAA (µl)	AAM (mg)	VP (µl)	MMA (µl)	EGDMA (µl)	Acetonitrile (mL)	AIBN (mg)
1-Monomer	84	0	0	0	900	3.9	12.8
2-Monomer	179	31.5	0	0	570	2.2	30
3-Monomer	179	21	0	10.5	570	2.2	30
4-Monomer	180	21	4.2	5.2	570	2.2	30

The results showed that a higher ratio of MAA and AAM could lead to more uniform coatings. This can be related to the strong polarity of these monomers with carboxylic and amide sidechains, respectively, compared to MMA with ester and non-polar VP monomers [56]. Optimization of FM ratios suggests that to achieve a uniform and stable coating of NIPs with ~2 µm thickness on SS-

MWs using a combination of selected four FMs, the proportion of MAA in the monomer blend should be around 85%.

The mixture analysis was further validated by using the response optimization approach to predict the proportions of FMs required for NIP coatings with not only the maximum but also the minimum coating qualities and uniformities. The predicted compositions were tested in three replicates each, as shown in Fig. A1-5. The results of multiplexed NIP coating experiments were in good agreement with the predictions. Uniform duplex, triplex and quadruplex monomer NIP coatings were successfully achieved on SS-MWs (Fig. A1-5, top row). Under conditions where the model predicted the least coating qualities, the experiments followed the model and resulted in no NIP coatings on the MWs (Fig. A1-5, bottom row). Higher proportions of MAA and AAM in the FM composition resulted in the maximum uniformity of coatings, while the compositions consisting of higher proportions of MMA and VP resulted in non-uniform or no coating on SS-MWs. The coefficient of determination (R^2) criterion is used in statistical analysis to assess how well a model explains and predicts future outcomes [153]. R^2 values obtained from the mixture analysis were 98.41 for thickness, 99.12 for uniformity, and 99.7 for stability, presenting a good mixture model fit to the experimental data.

3.2.3. Preparation of multi-FM CIP coatings on SS-MWs

The scanning electron microscopy (SEM) images in Figure 4 show a bare SS-MW (Fig. 3-3A-C), the optimized 4-monomer NIP-MW (Fig. 3-3D-F), and the equivalent CIP-MW after polymerization (Fig. 3-3G-H) and after the removal of bacterial cell templates (Fig. 3-3I). The NIP-MW and CIP-MW samples were prepared with the same exact recipe (Table 3-1, 4-monomer recipe), but the CIP-MW included the bacterial templates during the fabrication process. The bare

SS-MW had a smooth surface compared to the NIP-MW, showing the successful coverage of the NIP on the surface of the MW.

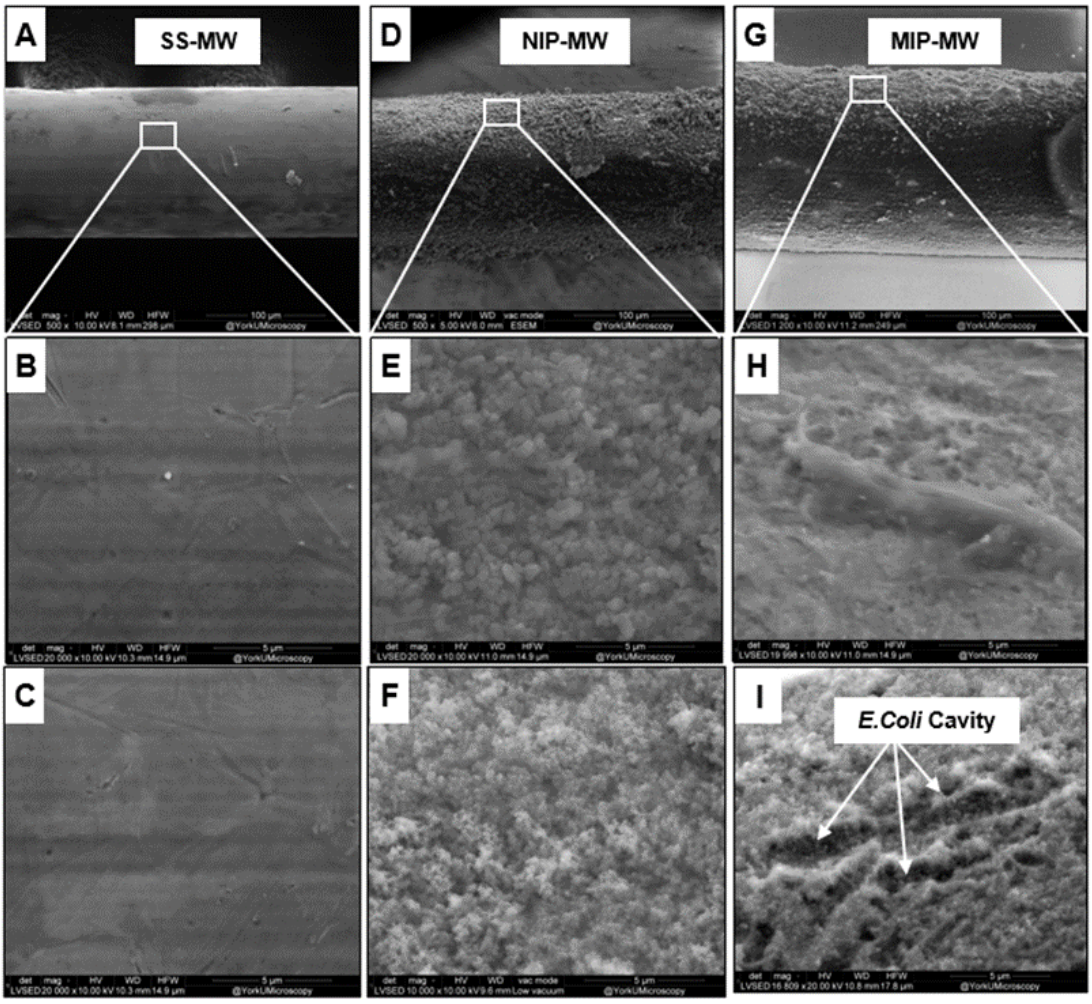

Fig. 3-3. SEM images of (A-C) a bare SS-MW, (D-F) a NIP-coated microwire (NIP-MW), and (G-I) a CIP-coated microwire (CIP-MW). NIP-MW and CIP-MW were prepared based on the optimal 4-monomer recipe in Table 3. Images in the second and third rows were taken before and after washing the samples with bacteria removal solutions, respectively [149]. *Reprinted with permission from American Chemical Society.*

Several studies have reported that over-oxidizing MIPs in highly acidic or basic solutions can efficiently remove bacterial cell templates [154], [155]. Accordingly, the template removal process

was examined on our NIP-MW and CIP-MW samples, and the resultant cavities from the bacterial cell templates were evaluated in SEM images. As shown in Fig. 3-3F, in comparison to Fig. 3-3E, exposure of the NIP-MW to the template removal solution did not alter its morphology. However, the high-magnification SEM image of the CIP-MW in Fig. 3-3H shows that a bacterium cell was entrapped within the CIP coating. The extraction reaction was effective in removing template cells from the CIP coatings, exposing bacilli-like surfaces complementary to *E. coli*. As can be seen in Fig. 3-3I, matching cavities with comparable size and shape to those of *E. coli* OP50 cells were obtained after bacteria templates were removed [146]. Lower magnification SEM images of the CIP-MWs before and after bacteria template removal are shown in Fig. A1-6, demonstrating the distribution of bacterial cavities on a larger area. It is worth mentioning that Trypan blue staining was used to examine the viability of bacterial cells after exposure to our CIP preparation recipe which revealed that the bacteria die during this process but do not lyse (Fig. A1-7).

Compared to classical bulk imprinting, thin surface-imprinted CIP films can form imprinted cavities with a high surface density, low heterogeneity, and fewer geometrical constrictions. This approach enables effective template removal and rebinding of the target analyte to CIP coatings by providing high control over the imprinting procedure [20], [155]–[157]. The results in this section exhibit the efficiency and applicability of our method for imprinting bacterial cell-based CIPs on MWs that can be used for isolating and capturing target bacteria on cylindrical transducer surfaces in biomimetic sensors in the future.

3.3. Conclusion

In conclusion, we developed a facile and general approach for synthesizing bacteria-imprinted polymer coatings on SS-MWs, utilizing chemical bonding between functional monomers and the surface functional groups of silanized SS-MWs. This strategy successfully produced stable and

uniformly coated MWs with CIP configurations ranging from single to quadruple functional monomers. Through systematic studies, we optimized the synthesis parameters to achieve specific coating thicknesses, which enhance the capture efficiency and template removal for bacteria template. Moving forward, we will investigate the rebinding performance and specificity of these coatings, crucial for assessing their effectiveness in selectively targeting bacterial organisms and advancing their application in biosensing technologies.

Chapter 4[i]

4. Investigating binding efficiency and selectivity of CIP-MWs to bacteria

In this chapter, we investigate the binding efficiency and selectivity of the developed bacteria-imprinted polymer coatings on CIP-MWs (Obj. 2 of the thesis). Building on the functionalization detailed in previous chapters, we aim to understand how effectively these coatings can target and capture both template and non-template bacteria. The importance of this investigation lies in the practical applications of CIP-MWs in biosensing and microbial detection, where the ability to selectively bind specific bacterial microorganisms is essential for accurate diagnostics and environmental monitoring.

4.1. Introduction

To investigate the binding efficiency and selectivity of the developed CIP-MWs, we employ off-chip techniques that allow for a detailed analysis of the interactions between the CIP-MWs and various bacterial targets. These techniques facilitate controlled experimental conditions and enable

[i] Some content of this chapter has been published in:

1. Akhtarian S, Doostmohammadi A, Youssef K, Kraft G, Kaur Brar S, Rezai P. Metal microwires functionalized with cell-imprinted polymer for capturing bacteria in water. ACS Applied Polymer Materials. 2023 Jan 23;5(5):3235-46. Permissions for the use of the text has been received from American Chemical Society.
2. Akhtarian S, Doostmohammadi A, Archonta DE, Kraft G, Brar SK, Rezai P. Microfluidic Sensor Based on Cell-Imprinted Polymer-Coated Microwires for Conductometric Detection of Bacteria in Water. Biosensors. 2023 Oct 20;13(10):943.
3. Akhtarian S, Kaur Brar S, Rezai P. Electrochemical Impedance Spectroscopy-Based Microfluidic Biosensor Using Cell-Imprinted Polymers for Bacteria Detection. Biosensors. 2024 Sep;14(9):445.

us to measure binding efficiency quantitatively. By comparing the binding performance of CIP-MWs against the intended template bacteria and a range of non-template bacteria, we will assess the specificity of the coatings and their potential for reducing cross-reactivity in complex samples.

Through systematic experimentation and analysis, this chapter will provide insights into the mechanisms that underpin binding interactions, contributing to the optimization of CIP-MWs for future applications.

4.2. Rebinding performance of CIP-MWs to bacteria

The *E. coli* OP50 bacterial capturing efficiencies of the SS-MWs, NIP-MWs and CIP-MWs prepared based on the optimized compositions in Table 3-1 are shown in Fig. 4-1 for single- to four-FM compositions. The concentration of bacteria in all experiments was fixed at 10^4 CFU/mL.

According to Fig. 4-1A, the bacterial capturing efficiency of optimal single-monomer CIP (1-CIP-MW) was approximately 30% and did not show a significant difference (p-value >0.05) compared to the bacterial capturing efficiency of uncoated SS-MWs and NIP-MWs. The similarity in capturing efficiency can be attributed to non-specific bacterial adsorption on the surfaces of bare MWs and single plex NIPs and CIPs. In single monomer composition using MAA as FM, the carboxylic groups may be deprotonated and cannot form hydrogen bonds with the bacterial template. Likewise, due to the negative charge of the bacterial membrane and MW's surface, the possibility of bacteria attraction towards the coating may have been very low.

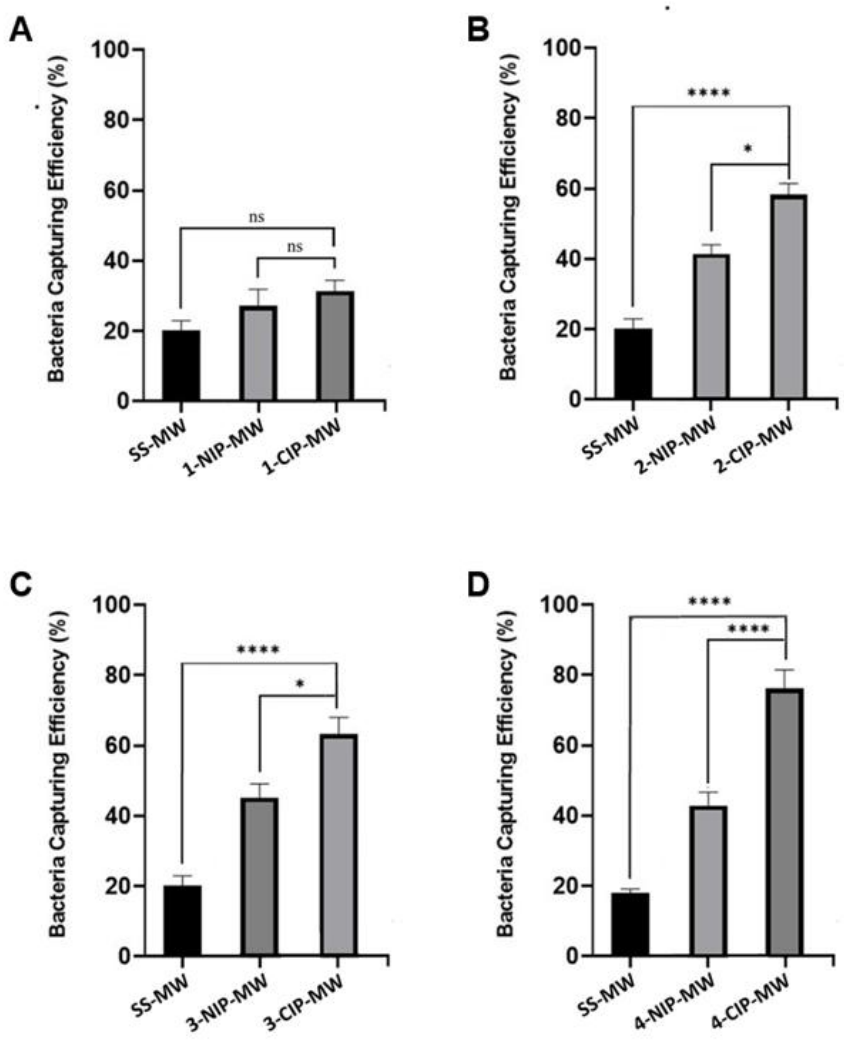

*Fig. 4-1. Bacterial capturing efficiency of bare SS-MWs, NIP-MWs and CIP-MWs in removing bacteria from suspensions containing 10^4 CFU/mL of E. coli OP50. Results are shown for A) single-FM, B) two-FM, C) three-FM, and D) four-FM compositions. Numbers on the x-axis represent the corresponding FM compositions. Error bars are standard deviations (SD) and ns: non-significant, *: p-value <0.05, **: p-value <0.01, ****: p-value <0.0001* [149]. *Reprinted with permission from American Chemical Society.*

By adding AAM to the CIP composition (i.e., 2-CIP-MW), higher bacterial capturing efficiencies in NIP-MWs and CIP-MWs were achieved (Fig. 4-1B). The improved bacterial capturing results in Fig. 4-1B may have been obtained from adding amide functional groups into

the polymer, which can interact via hydrogen bonds with the bacterial membrane. Furthermore, electron delocalization and resonance can form partial charges on nitrogen and oxygen chemical species in AAM, which can electrostatically interact with the functional groups of the bacterial surface. The main functional groups on the *E. coli* membrane include carboxyl and amino groups, as well as carboxyl and phosphate groups associated with extracellular polymeric substances and Lipopolysaccharides (LPS). Based on the pKa value (5 for carboxylic acid and 2.12 for phosphate), the dominant ionic species exposed on the bacteria membrane arise from the negatively charged carboxylic groups associated with polysaccharides and proteins as well as from the phosphate groups associated with the LPS [158]. This supports the interactions of CIP and bacterial templates that significantly increases bacterial capturing efficiency.

The addition of MMA as the third monomer did not improve the interactions with the bacterial template and, consequently, did not show an effect on the bacterial capturing efficiency for 3-CIP-MW compared to 2-CIP-MW (Fig. 4-1C). Although MMA can introduce hydrogen bonds similar to AAM, since the amount of AAM is decreased in this recipe, the bacterial capturing efficiency did not change significantly.

The addition of the fourth FM (VP) has resulted in a dramatic increase in the binding performance of 4-CIP-MWs (Fig. 4-1D). The bacterial capturing efficiency was calculated to be 76±10%, an increase of 11% in capturing efficiency compared to the conventional CIPs reported in the literature [83,159]. The increase could be attributed to VP's large molecular structure featuring a steric hindrance effect, which helps to synthesize a stable complex. Incorporating VP into the polymer provides hydrophilic and hydrophobic interactions with the bacterial template. Similar to AAM, the possibility of resonance and electron delocalization in VP can form partial charges adding electrostatic interactions with the functional groups of the bacterial surface.

Likewise, a partial positive charge enhances the interactions with the negative charge present in the bacterial membrane, which helps to increase the bacterial capturing efficiency. The difference in the capturing efficiency of CIPs and NIPs of the same FM composition could be attributed to the specific capturing behavior of CIPs. The results suggest that this specific capturing is improved in the sample with four types of FMs (Fig. 4-1D) which could be because of the increased bacterial affinity of imprinted cavities on this 4-CIP-MW, resulting in enhanced uptake of the *E. coli* cells. By defining the cell binding ratio (CBR) as the count of bacteria bound to CIP-MWs divided by the bacteria count bound to NIP-MWs (BCE_{CIP}/ BCE_{NIP}), a CBR of ~1.7 was obtained for the 4-CIP-MWs.

It can be seen that the addition of various proper functional side chains can help to provide a more stable template-polymer complex during self-assembly and imprinting of relatively large *E. coli* OP50 bacterial cell surfaces with various functionalities. It is assumed that by mixing the template with monomers before polymerization, the monomers will move along the template's surface until being held by a suitable amino sidechain, creating a partially optimized MIP network after the cross-linking and polymerization [40]. For instance, a recent study used AAM, MAA, and MMA copolymers as FMs [53]. However, the resulting MIPs could not differentiate between five different virus subtypes. This led to the modification of the monomer system by including VP as an additional monomer resulting in a dramatic increase in the selectivity displayed by the MIP for the influenza A virus subtypes [53]. It is worth mentioning that the amount of VP in the copolymer system of CIP-MWs is limited, and an increase in its ratio in the CIP composition will decrease the uniformity of NIP/CIP coatings on SS-MWs based on the coating optimization results.

4.3. Effect of initial bacteria count on rebinding to CIP-MWs

The affinity of the optimized 4-FM NIP and CIP coatings on SS-MWs to different concentrations of bacteria was evaluated by measuring their rebinding capacity to *E. coli* OP50 cells in aqueous suspensions. Bacterial samples with initial counts of 10^2, 10^3 and 10^4 CFU/mL were used to examine if rebinding is concentration dependent. Since the number of colonies in samples with 10^2 CFU/mL bacteria after the rebinding experiment was too few to count, the results from these samples were inconclusive and not reported in Fig. 4-2. The results for 10^3 and 10^4 CFU/mL bacteria counts are shown in Fig. 4-2A and Fig. 4-2B, respectively.

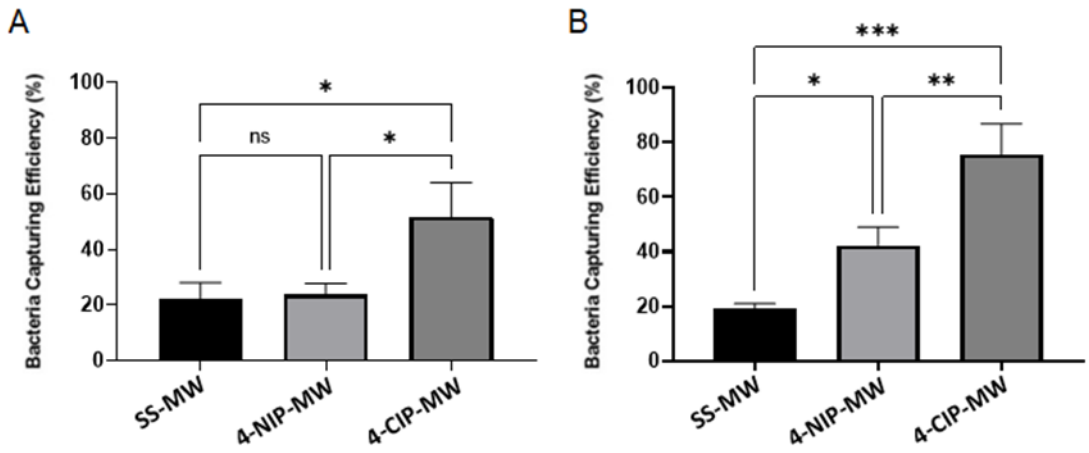

*Fig. 4-2. Bacterial rebinding performance of not coated SS-MWs, 4-NIP-MWs and 4-CIP-MWs in terms of removing bacteria from solutions containing (A) 10^3 and (B) 10^4 CFU/mL of E. coli OP50. Error bars are standard deviations (SD) and ns: non-significant, *: p-value <0.05, **: p-value <0.01, ***: p-value <0.001* [149]. *Reprinted with permission from American Chemical Society.*

As shown in Fig. 4-2, a trace of non-specific bacteria rebinding was noticed for SS-MWs and 4-NIP-MWs, which were not statistically different (P-value > 0.1) from each other in the samples

with an initial bacterial count of 10^3 CFU/mL (Fig. 3-5A). The capturing efficiency of 4-NIP-MWs increased and became slightly different from SS-MWs (P-value < 0.05) at the higher initial bacterial count of 10^4 CFU/mL (Fig. 3-5B). This incremental increase in binding is due to the higher numbers of bacteria available in the sample and their more frequent interactions with the NIP coating which is favorable to the cells. The 4-CIP-MWs always exhibited a significantly higher capturing efficiency than the SS-MWs and the 4-NIP-MWs, which became more significant at higher bacterial count levels. For instance, the average bacteria capturing efficiency in the sample with 10^3 CFU/mL cells was 52% which increased to 76% at 10^4 CFU/mL. These results were mainly due to the bacterial affinity of imprinted cavity sites on the 4-CIP-MWs and more opportunities for bacteria cells to interact with them at higher concentrations, leading to superior uptake of the *E. coli* cells.

4.4. Specificity of 4-CIP-MWs

Fig. 4-3 shows the results of our specificity experiments using the 4-CIP-MWs, while SS-MWs and 4-NIP-MWs were used as control experiments. The results show that while CIP-MWs imprinted with *E. coli* OP5O cells could capture a significant number of *E. coli* compared to SS-MWs and NIP-MWs, their bacteria-capturing performance did not significantly differ from the NIP-MWs (p-values >0.05) when exposed to other non-specific bacteria targets, i.e., *Sarcina* and *Listeria*. This reveals the specific capturing behavior of our CIP-MWs towards the *E. coli* template cells used in the imprinting process. In all cases, a significant difference was observed between the capturing efficiency of SS-MWs and NIP-MWs, which can be attributed to the non-specific adsorption of bacteria to polymeric coatings.

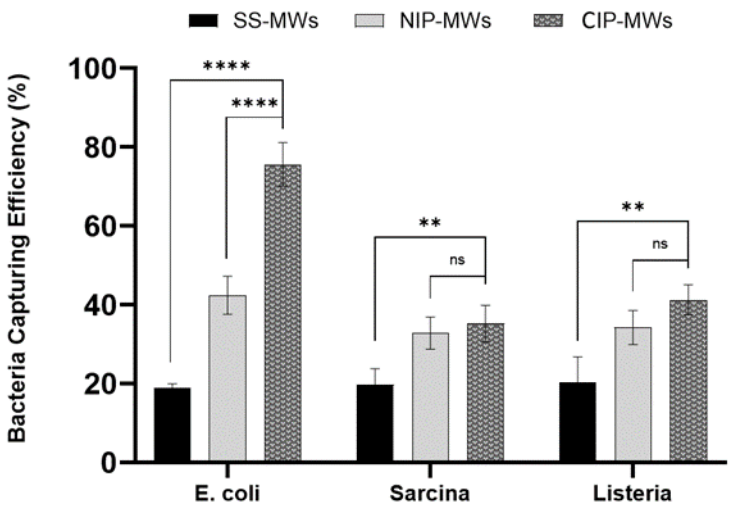

*Fig. 4-3. Bacterial capturing efficiency of E. coli-imprinted 4-CIP-MWs in removing three different bacteria microorganisms of E. coli, Sarcina and Listeria from singleplex suspensions with initial concentrations of 10^4 CFU/mL. Error bars are standard deviations (SD) and ns: non-significant, **: p-value <0.01, ****: p-value <0.0001* [149]. *Reprinted with permission from American Chemical Society.*

4.5. Investigating the effect of bacteria gram type on imprinting efficiency

In order to investigate the influence of bacteria gram type on imprinting efficacy, gram-positive bacteria (*Sarcina*) were used as templates during imprinting, and the rebinding experiments were performed by exposing the resulted CIP-MWs to same target as imprinted bacteria. The results of these tests are shown in Fig. 4-4A. As compared to the rebinding performance previously obtained by gram-negative bacteria (*E. coli* OP50) in Fig. 4-3, bacteria capturing efficiency had dropped significantly in the case of using *Sarcina* cells. Also, the specific binding, which can be considered the difference in bacteria capturing efficiency of NIP-MWs and CIP-MWs, became less significant for the *Sarcina*-imprinted polymers. The reason for the lower binding capacity to Sarcina bacteria could be due to the larger size of this bacteria (1.8-3 microns in diameter). Also, according to

literature, *Sarcina* bacteria has cuboid shape. Because of the cuboidal shape, *Sarcina* tends to form packets often in tetrads but occasionally in cubes of eight cells, which increases the size of colonies. As a result of increased size of colonies, more surface area of the wire could be occupied with fewer bacteria cells. Consequently, we explored the potential influence of the number of cavities. For this, instead of using a single MW, two MWs were implemented in the rebinding experiments. The BCE was enhanced when two MWs were used in rebinding assays (Fig. 4-4B), showing the important role of the cavity numbers. Also, due to the pocketed morphology and agglomeration, the capturing on wire can be less stable and, by consequence, a lower BCE could be achieved.

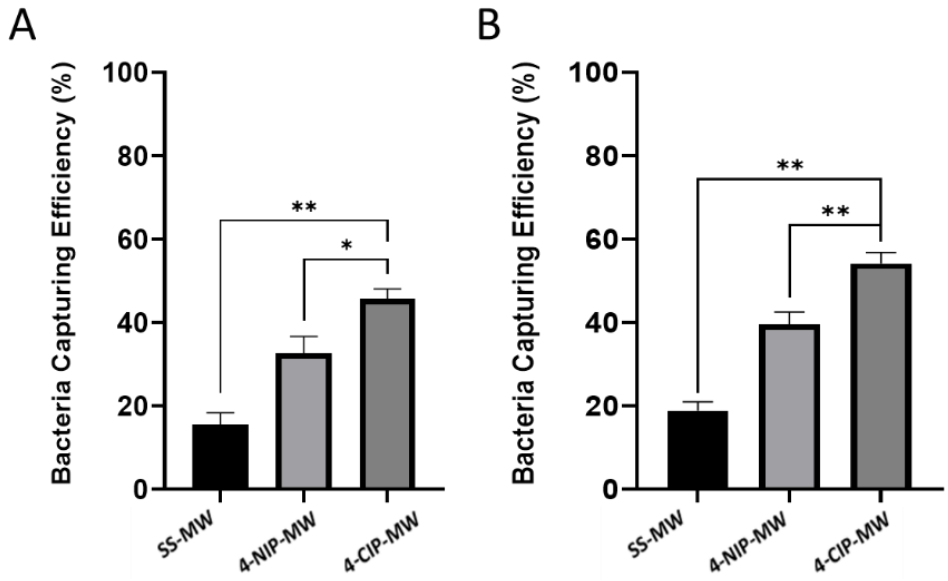

*Fig. 4-4. Bacterial capturing efficiency of Sarcina-imprinted 4-CIP-MWs in removing Sarcina bacteria from suspensions with initial concentrations of 10^4 CFU/mL. (A)Using one MW, (B) Using two MW. Error bars are standard deviations (SD) and *: p-value <0.05, **: p-value <0.01.*

Another possibility for decreased BCE when using *Sarcina* bacteria could be due to changing bacterium types from gram-negative to gram-positive. This change in bacteria type results in their different cell walls and proteins (Fig. 4-5). So, one reason for lower bacteria capturing efficiency

with *Sarcina* could be its different cell wall chemistry that could introduce different interactions with polymer/MW and reduce the number of imprinted cavities. Gram-positive bacteria have a greater volume of peptidoglycan (a polymer of amino acids and sugars that create the cell wall of all bacteria in their cell membranes), which is what makes the thick outer covering. This thick outer covering, or membrane, can absorb a lot of foreign material [160]. To gain a better understanding of the CIP-MWs morphology imprinted with *Sarcina*, SEM imaging was performed as shown in Fig. 4-6. As seen, the morphology of CIP-MWs imprinted with Sarcina cells differs from the previously fabricated CIP-MWs with *E. coli*-OP50 cells. The surface of CIP-MWs was bubble-shape coatings, which did not change significantly after washing with template removal solutions. So, a reason for decrease BCE could be not efficient removal of entrapped bacteria, therefore less number of cavities for rebinding assays.

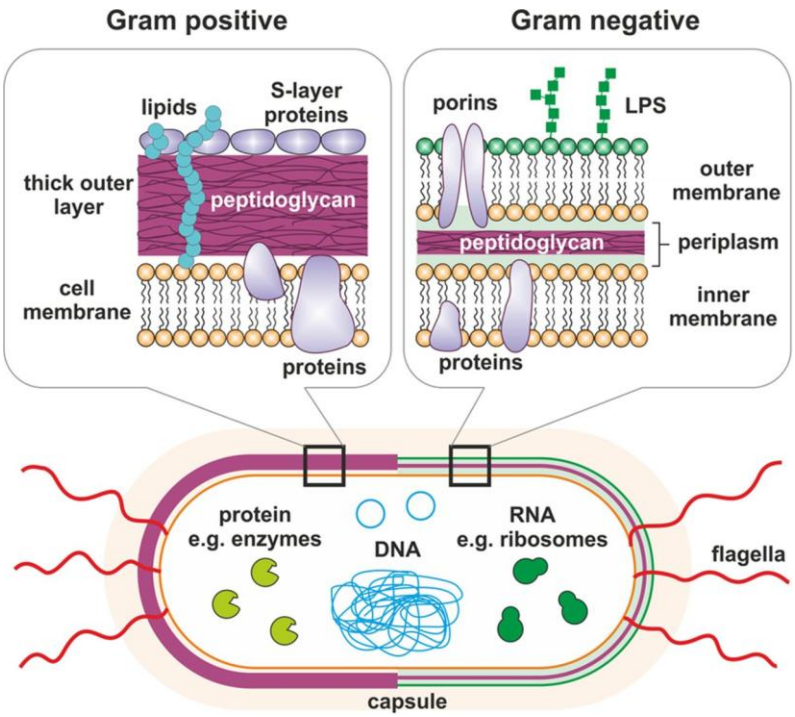

Fig. 4-5. Difference in the cell wall composition of gram-negative and gram-positive bacteria [161]. *Reprinted with permission from American Society for Microbiology.*

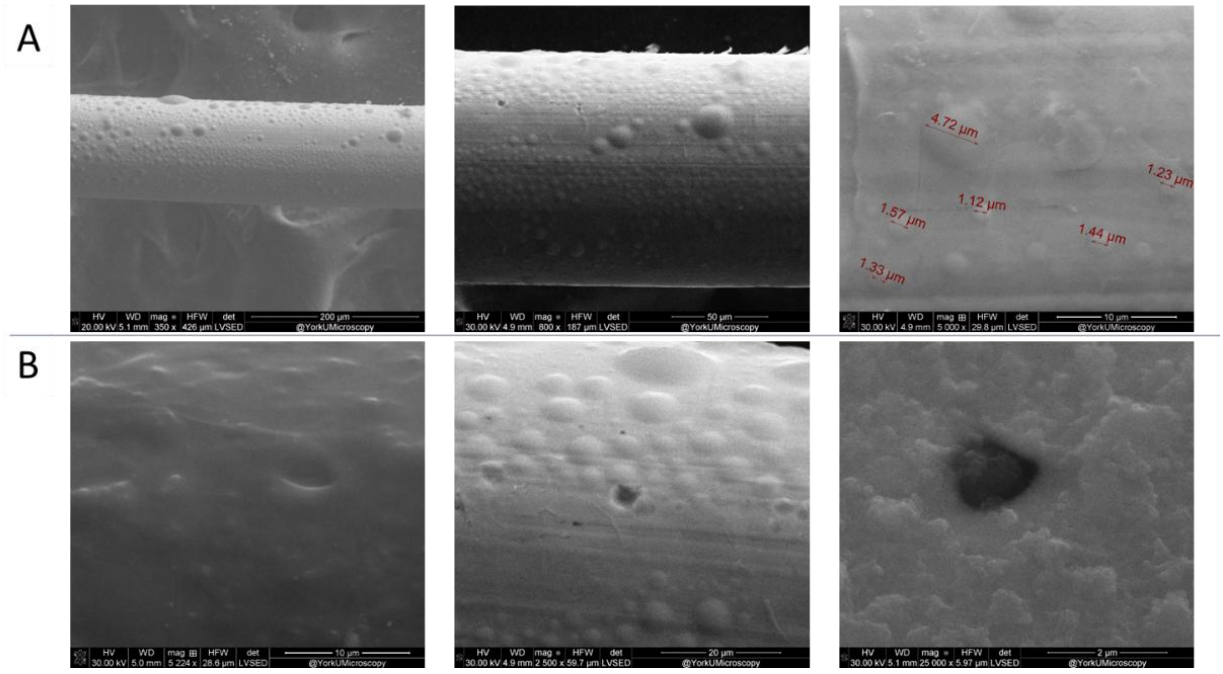

Fig. 4-6. Sarcina MIPs (A) before and (B) after washing with template removal solution, there were some semi-sphere-shaped cavities but not many of them. The red dimensions at A 3rd raw panel represent diameter of these spheres. The red dimensions at A 3rd raw panel represent diameter of these spheres.

To investigate further, we hypothesized that different gram-types of bacteria could play an important role in imprinting and capturing efficiency. We tested this hypothesis by using another gram-negative bacterium, *Salmonella*, for imprinting. Results of rebinding assays obtained with this experiment (Fig. 4-7C) were in good agreement with the results obtained for *E. coli* OP50 (Fig. 4-7A), which confirms the validity of our hypothesis. Furthermore, selectivity tests were performed to investigate the specificity of CIP-MWs when imprinted with *E. coli* and *Salmonella* bacteria and exposed to different microorganisms than their template. Although the two microorganisms are structurally similar [162], the cross selectivity tests were promising. When target bacteria were the same as the template (Fig. 4-7A, C) there was a statistically significant difference between the BCE of NIP-MWs and CIP-MWs, which can be attributed to specific capturing of target bacteria by cavities of same microorganism. However, when non-template

bacteria were used as the target **(**Fig. 4-7B, D**)**, there was less significance in the BCE of NIP-MWs and CIP-MWs.

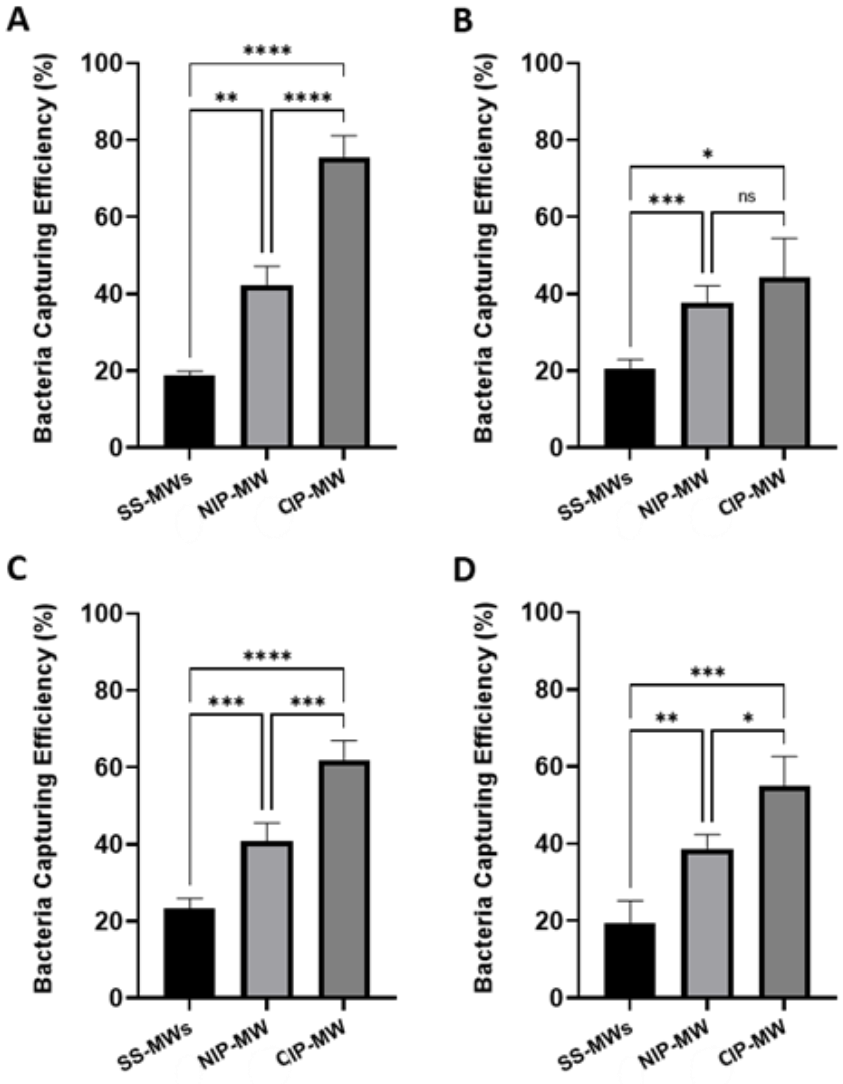

*Fig. 4-7. Results of the off-chip selective rebinding experiments. Bacterial capturing efficiency of synthesised CIP-MWs with (A) Template: E. Coli, Target: E. Coli, (B) Template: E. Coli, Target: Salmonella, (C) Template: Salmonella, Target: Salmonella, (D) Template: Salmonella, Target: E. Coli. Error bars are standard deviations (SD) and *: p < 0.1, **: p < 0.01, ***: p<0.001, ****: p<0.0001.*

4.6. Conclusion

In conclusion, this chapter has provided a comprehensive analysis of the binding efficiency and selectivity of bacteria-imprinted polymer coatings on MWs through off-chip techniques. The rebinding assays revealed that bacteria capturing efficiency strongly depended on the composition of FMs used for CIP synthesis. While the bacteria capturing efficiency for the CIP-MWs synthesized using a single FM (MAA) was not significant, our four-FM *E. coli* OP50 imprinted CIP-MWs exhibited a high rebinding capacity toward target bacteria cells, with a bacterial capturing efficiency of 76±10%. By controllable synthesis of complex CIPs on metallic MWs, electrical probes with selectivity to bacteria templates on the surface of metallic MWs can be achieved and used for isolating biological cells and direct electrical transduction through substrate electrodes. The CIP-MWs will be implemented within microfluidic sensors as working electrodes for sensing biological targets in POC and PON sensing applications. The approach reported herein can find applications in developing inexpensive, rapid, and reliable biomimetic sensors and open a window of interest for exploring biomimetic recognition systems.

Chapter 5[i]

5. Integration of CIP-MWs into microfluidic devices and electrochemical transduction of bacteria binding to CIP-MWs

5.1. Introduction

In the rapidly evolving field of biosensors, various transduction techniques have been employed, including optical [11–15], mass-based [163], and electrochemical methods [16]. Among these, electrochemical detection is particularly advantageous due to its high sensitivity, fast measurements, low cost, and ease of miniaturization, which make it suitable for on-site applications [19,20]. While numerous electrochemical biosensors have been developed using bio-recognition materials such as bacteriophages, aptamers, and antibodies [23,24], their practical deployment is often hindered by high cost and the instability of bio-receptors under variable environmental conditions.

As detailed in the previous chapter, CIPs offer a promising alternative, with competitive affinity to target cells similar to biological recognition materials but with lower costs and greater stability across various environmental conditions [95].

[i] Some content of this chapter has been published in:

1. Akhtarian S, Doostmohammadi A, Youssef K, Kraft G, Kaur Brar S, Rezai P. Metal microwires functionalized with cell-imprinted polymer for capturing bacteria in water. ACS Applied Polymer Materials. 2023 Jan 23;5(5):3235-46. Permissions for the use of the text has been received from American Chemical Society.
2. Akhtarian S, Doostmohammadi A, Archonta DE, Kraft G, Brar SK, Rezai P. Microfluidic Sensor Based on Cell-Imprinted Polymer-Coated Microwires for Conductometric Detection of Bacteria in Water. Biosensors. 2023 Oct 20;13(10):943.
3. Akhtarian S, Kaur Brar S, Rezai P. Electrochemical Impedance Spectroscopy-Based Microfluidic Biosensor Using Cell-Imprinted Polymers for Bacteria Detection. Biosensors. 2024 Sep;14(9):445.

In previous chapter, whole bacteria cells were used to create CIP-coated microwires (CIP-MWs), which showed strong binding efficiency to *E. coli*.

Microfluidics further advances this field by enabling the creation of field-deployable, low-cost sensors that require minimal sample volumes and facilitate rapid bio-detection [127]. Various MIP-based microfluidic devices to electrochemically detect target molecules have been reported to date [33], [128]. However, using CIPs in microfluidic electrochemical sensors to detect whole cells remains as a technological gap.

Electrochemical sensors have been successfully integrated with MIPs and used with various readout methods including field-effect transistors, conductometry, electrochemical impedance spectroscopy (EIS), voltammetry, and amperometry. These platforms convert the interaction between MIPs and target molecules on an electrode surface into various electrical signals [32].

In this chapter, we report the integration of CIP-MWs into low-cost microfluidic electrochemical sensors to transform the binding of CIP cavities to target *E. coli* bacteria into a quantitative signal. By incorporating CIP-MWs into a microfluidic device, we create sensors that promise field deployability, minimal sample volume requirements, and reduced analysis times.

In section 5.2. CIP-MWs were integrated into a conductometric-based microfluidic device, creating a miniaturized, cost-effective sensor based on electrical resistance, requiring minimal sample volumes and providing quick analysis [19]. However, the sensor's limits of detection (LOD) and quantification (LOQ) were relatively high, at 2.1×10^5 CFU/mL and 7.3×10^5 CFU/mL, respectively, along with low sensitivity within a narrow dynamic range of 10^4 to 10^7 CFU/mL. These factors required significant improvement to meet performance benchmarks for bacterial detection in practical applications.

In section 5.3., we present the incorporation of CIP-MWs into an impedimetric electrochemical microfluidic device with a novel design that converts the interaction between CIP cavities and target *E. coli* bacteria into a measurable electrical readout. The developed sensing platform demonstrated enhanced performance with a lower detection limit compared with conductometric detection and holds promise for future integration into handheld devices, enabling sensitive, on-site, and affordable pathogen monitoring.

5.2. Conductometric-based CIP-MW Microfluidic Biosensor

We first utilize Conductometric measurement by monitoring the resistance of bacteria suspensions with various cell counts in a microchannel between two suspended CIP-MWs and investigate the effect of captured cells by the CIP coatings on the conductance signal.

Conductometric measurement involves monitoring the change in conductivity of the MIP receptor layer over time in response to MIP binding to its complementary analyte, which changes the concentration of ionic species at the interface of liquid-solid [164]. This approach employs direct current (DC) and has the potential to be advantageous in the creation of fast, compact, and portable and simple biosensors. Furthermore, the DC approach does not require a reference electrode and does not have the complications associated with selecting an appropriate equivalent circuit models for analyzing the frequency-dependent impedance. Additionally, DC measurements usually require shorter times and a lower volume of solution [165]. However, electrolysis could affect the resistance measurements in DC methods by generating bubbles on electrodes or changing the ion concentration of the liquid. Thus, this method can only be applied to liquids with low ion concentrations (low-conductivity) [166] such as drinking water [167].

In this section, we report the integration of CIP-MWs into a low-cost conductometric microfluidic sensor. By monitoring the resistance of bacteria suspensions with various cell counts in a microchannel between two suspended CIP-MWs, the effect of captured cells by the CIP coatings on the conductance signal was studied. The developed sensing platform can be integrated into a hand-held device in the future, enabling on-field and low-cost monitoring of pathogens.

5.2.1. Bacteria Capturing by various microwires inside the microfluidic device

To examine bacteria capturing by functionalized MWs within the microfluidic device, green fluorescent protein (GFP) tagged *E. coli* cells and fluorescent microscopy were used. Fig. 5-1 demonstrates the optical and fluorescent microscopy images (10x magnification) of the uncoated SS-MWs, NIP-MWs, and CIP-MWs within the microfluidic device at three stages of the experiment, i.e., pre-incubation electrolyte 1 wash, bacteria incubation at 10^8 CFU/mL for 30 mins, and post-incubation electrolyte 2 wash. Preliminary experiments to study the effect of incubation time on the bacteria capturing of CIP-MWs revealed an optimum incubation time of 30 mins as discussed in section 1 of the Appendix B.

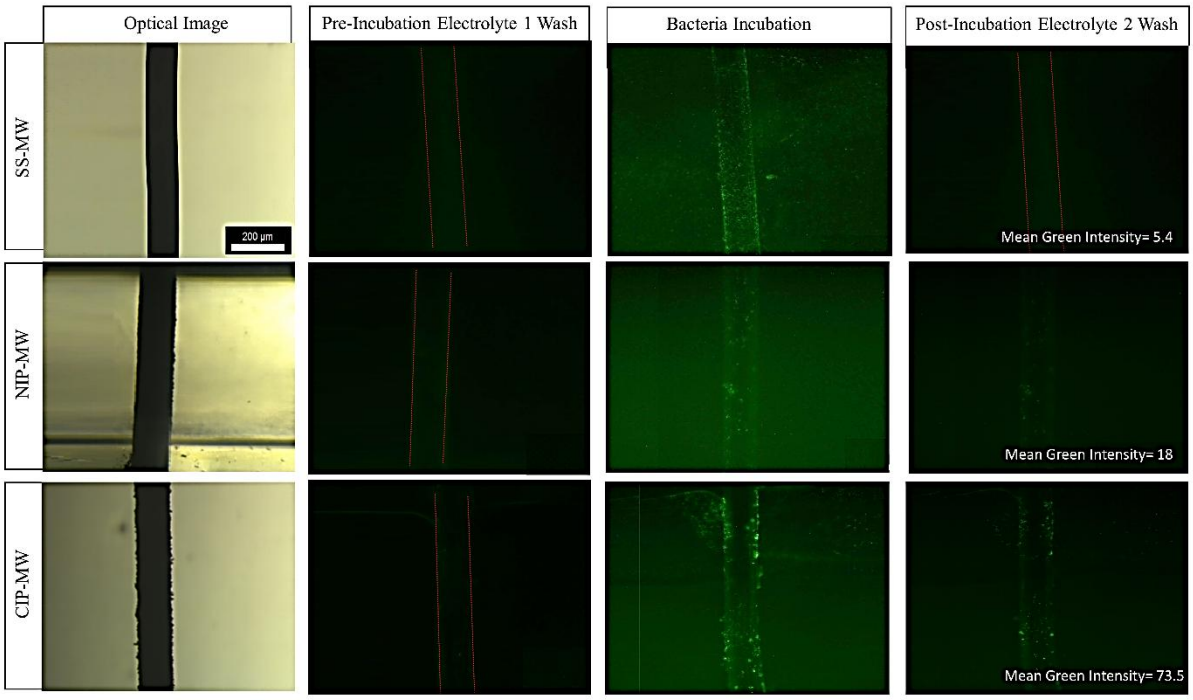

Fig. 5-1. Optical images of the SS-MW, NIP-MW, and CIP-MW (rows) along with their fluorescent images in the microfluidic channel during pre-incubation electrolyte 1 wash, bacteria incubation at 108 CFU/mL for 30 min, and post-incubation electrolyte 2 wash (columns). E. coli bacteria were tagged with green fluorescent protein (GFP), hence resulting in a green hue in the channel during the incubation phase and GFP expression spots around the CIP-MW post-incubation. RGB analysis was done using Image J and post-incubation green intensities of 5.4, 18, and 73.5 were obtained for SS-MW, NIP-MW and CIP-MW, respectively [137], *Open Access.*

When uncoated SS-MWs were installed in the microfluidic device (Fig. 5-1, top row), there was no significant fluorescent signal during the pre-incubation wash. The fluorescent signal increased during the incubation with bacteria, as the GFP expressing bacteria were infused into the microchannel. However, during the post-incubation wash, the fluorescent signal decreased to near blank (mean green intensity=5.4) as the GFP bacteria were washed out of the microchannel.

When a microfluidic device with a pair of NIP-MW electrodes was used (Fig. 5-1, middle row), there was a more intense green light signal after the post-incubation wash (mean green intensity=18). This reveals that there were still some GFP bacteria present in the region of interest within the device. Comparing with the SS-MWs, these bacteria were observed to be attached to the surface of NIP-MWs due to their non-specific adsorption to the NIP coatings [168].

Conducting this experiment with the microfluidic device that had the CIP-MWs installed as electrodes (Fig. 5-1, bottom row) resulted in a very high intensity fluorescent signal after the post-incubation wash with a mean green intensity of 73.5. This higher signal observed for CIP-MWs can be attributed to the enhanced bacteria capturing of the CIP coating related to its imprinted cavities.

The results of this section visually confirmed a considerable capturing of bacteria on CIP-MWs and enticed us to investigate the detectability of the bacteria using the electrical resistance readout method.

5.2.2. Conductometric analysis of the microfluidic device

After observing the bacteria capturing characteristics of the SS-MWs, NIP-MWs and CIP-MWs, we aimed to understand the response time of our sensor in terms of reading a constant electrical resistance upon applying a sweep current in the range of 10nA-1μA with a step size of 10 nA. Accordingly, the timelapse resistances of a SS-MW based microfluidic sensor at three stages of pre-incubation wash (R_0), bacteria incubation at 10^6 CFU/mL (R_1), and post-incubation wash (R_2) are presented in Fig. 5-2.

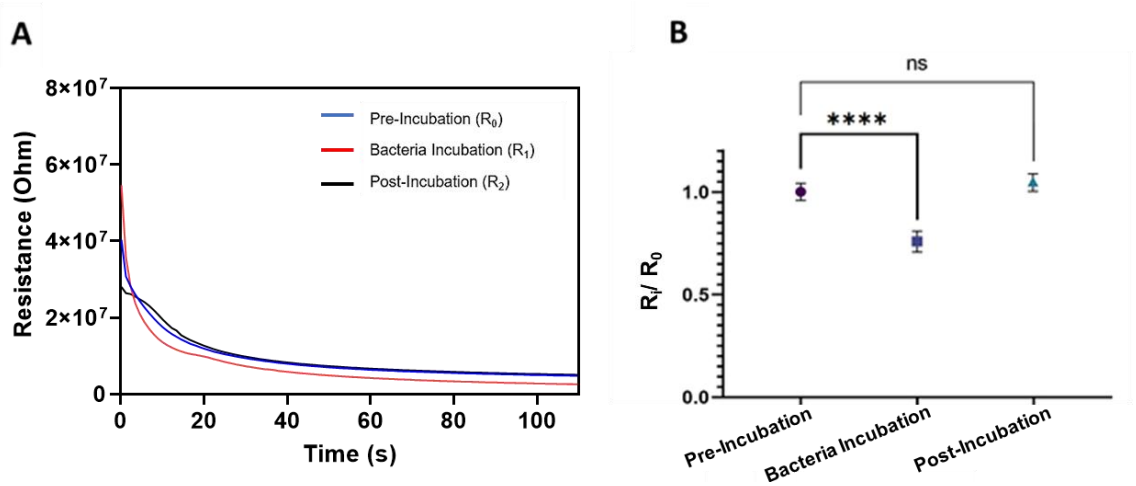

Fig. 5-2. Electrical resistance characterization of SS-MW based microfluidic sensors [137], *Open Access. A) Timelapse resistances of one sensor at three stages of pre-incubation wash (R0), bacteria incubation at 106 CFU/mL (R1), and post-incubation wash (R2). B) Averaged normalized resistances (Ri/R0, i=0, 1 or 2) of three SS-MW based sensors during three stages of operation. Each measurement was repeated 5 times. Error bars are standard deviations (SD) and ns: non-significant, ****: P-Value <0.0001.*

As shown in Fig. 5-2A, the sensor had a transient state at the beginning of the measurement, which is due to the sudden application of an external electric field intrinsic to the measurement system [132]. It also could be due to a sudden change in the ion concentration around the SS-MWs by applying the current [30]. This transient state lasts for approximately 50-sec after which the resistance between the wires stabilizes.

To obtain the steady-state values of R at each stage of the experiment, the moving average technique [170] was performed to obtain the plateau start point of the resistance curves (see Section 2 of the Appendix B). A combination of conventional and verified methods was used in the declaration of this plateau. Specifically, the six sigma statistics [167], and the moving average method [2] were combined to arrive at the optimized code for this application. The code can be found in Fig. B3, below. This code determines the presence of a plateau in the dataset using a

forward moving average function. Using a user-defined threshold, in this case, <1% of the neighboring averages, we are able to determine the initial points of the plateau for our dataset.

Lastly, we calculated the representative value of the plateau. Based on this analysis, the data points from 55-100 corresponding to 0.55-1 μA current sweep range were stable and satisfied the plateau criteria in all experiments. Therefore, these data points were used for obtaining the mean and standard deviations (SD) of resistance measurements for further normalization and analysis.

Repeat experiments for three SS-MW based sensors were performed and the average normalized resistances before, during, and after bacteria incubation were plotted in Fig. 5-2B. As shown, the normalized resistance during bacteria incubation is significantly lower (p-value <0.0001) than the baseline resistance. This decrease can be attributed to the presence of suspended bacteria cells between SS-MWs within the microchannel that facilitate the charge transfer between the electrodes. However, the resistance increases to the baseline resistance (R_2/R_0 ~1) after post-incubation wash, confirming that all the bacteria cells have been washed away with the second electrolyte, expectedly.

Fig. 5-3 illustrates the normalized electrical resistance measurements from the sensors fabricated using NIP-MWs and CIP-MWs. As opposed to the results obtained from the uncoated SS-MWs in Fig. 5-2B, when NIP-MWs were used (Fig. 5-3A), the resistance after post-incubation wash was slightly lower than the baseline resistance (R_2/R_0 <1, p-value= 0.012). This decrease in the resistance after washing the bacteria from the microchannel could be due to non-specific absorption and attachment of bacteria to the surface of NIP-MWs which is demonstrated in Fig. 5-1. Interestingly, when CIP-MWs were used in the sensor (5-3B), the post-incubation resistance drop became a lot more significant (p-value= 0.0008) than the NIP-MWs. The increased normalized resistance drop resulted from the strong attachment of bacteria cells to the CIP-MW

cavities that could not be washed away during the post-incubation wash. The results in Fig. 5-2 and Fig. 5-3 clearly show the significant capturing ability of the CIP-MWs and successful transduction of this binding event to measurable electrical signals.

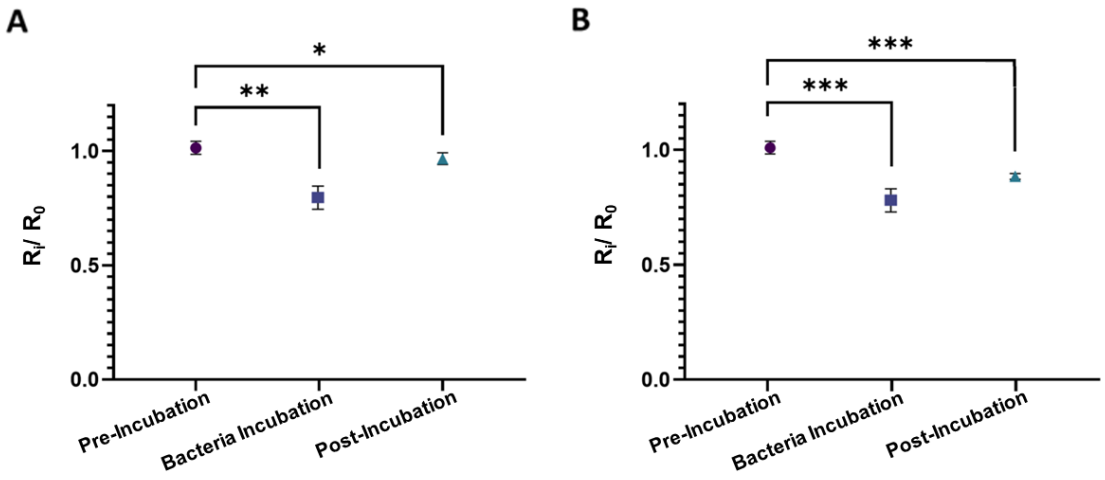

*Fig. 5-3. Normalized electrical resistance measurements from the sensors fabricated using A) NIP-MWs and B) CIP-MWs, each in triplicates and five measurements per condition. Bacteria count during 30min incubation was 106 CFU/mL. Error bars are standard deviations (SD) and ns: non-significant, *: P-Value <0.05, **: P-Value <0.01, ***: P-Value <0.001* [137], *Open Access.*

5.2.3. Characterization of the CIP-MW based microfluidic sensor

To further characterize the performance of the CIP-MW based sensor, the effect of bacteria count on the normalized inter-wire resistance shift of the sensor was studied. *E. coli* bacteria suspensions with cell counts between 0 to 10^9 CFU/mL were prepared with serial dilution and used in these experiments. Fig. 5-4 shows the normalized post-incubation wash resistance (R_2/R_0) of the CIP-MW based sensor along with the responses obtained from two parallel control experiments, i.e., uncoated SS-MWs and NIP-MWs. It was observed that for the bacteria counts between 0 and 10^5 CFU/mL, the CIP sensor did not have a significantly different response than the control

experiments (p-value> 0.05). However, the difference became more significant by further increasing the bacteria count to 10^6-10^9 CFU/mL, demonstrating the dominant effect of CIP coating as compared to NIP coatings or no coating at all. As shown in Fig. 5-4A**,** the difference between the post-incubation normalized resistance of the CIP sensor with NIP sensor was always less significant (*P-Value <0.01)* than the sensor with uncoated SS-MWs (*P-Value <0.0001).* This can be because of non-specific adsorption of bacteria to the NIP coatings [48] that can affect the resistance measurement as shown before.

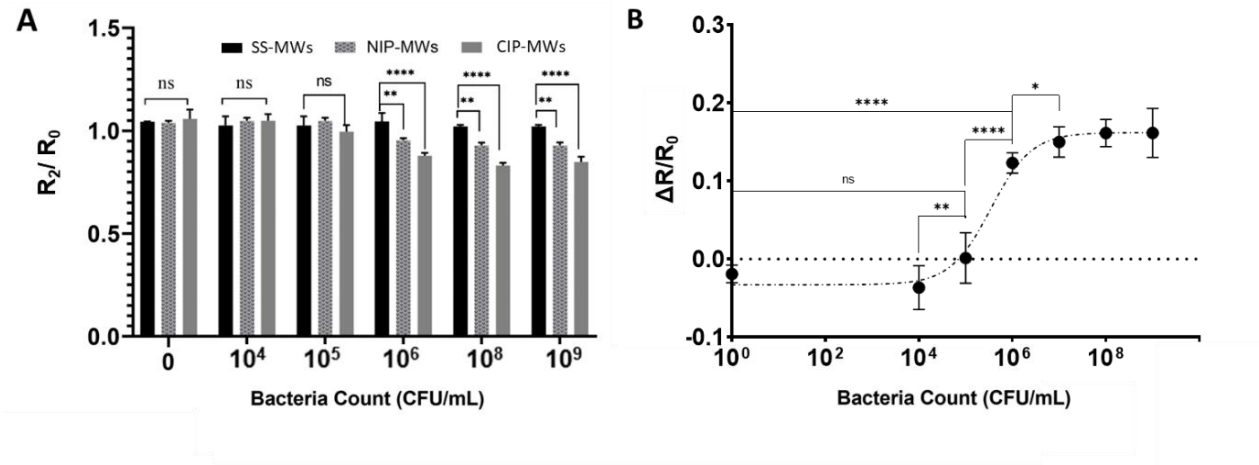

Fig. 5-4. Microfluidic bacteria sensor characterization [137]*, Open Access. A) Normalized post-incubation wash resistance (R2/R0) response of the microfluidic sensor fabricated with uncoated SS-MWs, NIP-MWs, and CIP-MWs, when exposed to different bacteria counts. B) The dose-response ΔR/R0 curve established for the CIP-MWs based sensor. Error bars are standard deviations (SD) and ns: non-significant, *: P-Value <0.05, **: P-Value <0.01, and ****: P-Value <0.0001.*

Fig. 5-4B shows the dose-response $\Delta R/R_0$ curve established for the CIP-MW based microfluidics sensor for bacteria counts from 0 to 10^9 CFU/mL. As can be seen, the dose-response curve of the sensor is non-linear; there is an insignificant response at bacteria concentrations below 10^4 CFU/mL and a saturation in the normalized resistance shift for bacteria counts higher than 10^7

CFU/mL. The former effect may be due to the sensor insensitivity and the latter effect is due to the high number of bacteria cells surpassing the CIP cavities [48]. The dynamic range of the sensor was determined to be 10^4-10^7 CFU/mL due to the significant statistical difference between the subsequent readout signals of the sensor in this range. A linear fit in this range with a goodness of R^2=0.93 resulted in a sensitivity of 7.35 μS per CFU/mL, which is in the range of sensitivities achieved in similar works for conductometric detection of *E. coli* bacteria using antibodies [49] and aptamers [50]. Based on the 3-sigma and 10-sigma methods, the LOD and LOQ of the CIP sensor were calculated as 2.1×10^5 CFU/mL and 7.3×10^5 CFU/mL, respectively.

The achieved detection range and limit with our established conductometric CIP-MWs based sensor is comparable with other electrochemical methods for detection of bacteria using CIPs [51]. However, our proposed sensor has the advantage of the conductometric method's simplicity and low-cost over other electrochemical methods, such as need for complex instruments as well as a reference electrode [52]. The performance of the developed sensor is also comparable to the performance achieved by coupling other transduction methods with CIPs such as frequency-based sensing techniques using Quartz Crystal Microbalance (QCM) [48,53]. However, conductometric sensing does not have the complexity associated with measuring the frequency change below curtain amounts of bacteria, which is shown to limit the measurable concentration range in related works [48]. The developed sensor can potentially be employed in detection of bacteria in surface waters which typically contain bacterial cell counts in the range of 10^5–10^6 cells/ML [54]. Nevertheless, the detection limit achieved by the developed sensor can be improved by increasing the active surface area of electrodes by using a microelectrode array to maximize the total surface area and imprinted cavity density available for bacteria binding and detection. Furthermore, a pre-

enrichment process can also be integrated to increase the target bacterial concentration for detecting bacteria at lower initial counts, which are going to be investigated in the future works.

5.2.4. Specificity of the CIP-MW based microfluidic sensor

To investigate the specificity of the CIP-MWs in the developed sensor, *Listeria* and *Sarcina* cells were used as the target microorganism, while the template for CIP preparation was *E. coli*. Fig. 5-5 shows the results performed in triplicates with five repetitions per experiment. As seen in Fig. 5-5A, using *E. coli* as the target microorganism results in a significant (P-Value <0.0001) drop in the normalized resistance of the sensor after washing the microchannel with electrolyte 2. However, in the case of using non-template microorganisms as the target, i.e., *Listeria (*Fig. 5-5B) and *Sarcina (*Fig. 5-5C) cells, the difference in the sensor's pre- and post-bacteria resistance is less significant (P-Value <0.05) and insignificant (P-Value >0.05), respectively. Considering the size and shape of these two microorganisms, where *Listeria* cells are rod-shaped with approximately 0.5 μm diameter and 0.5–2.0 μm length, and *Sarcina* cells are spherical with 1.8-3 μm diameter [55], the small level of significance obtained using *Listeria* cells could be attributed to scarce capturing of these cells by *E. coli* cavities, which are similar in shape and size to the *Listeria* cells rather than the *Sarcina* bacteria. In conclusion, we concluded that our sensor is specific to the bacteria microorganism, even if cells with similar shapes and morphologies are used in the sensor.

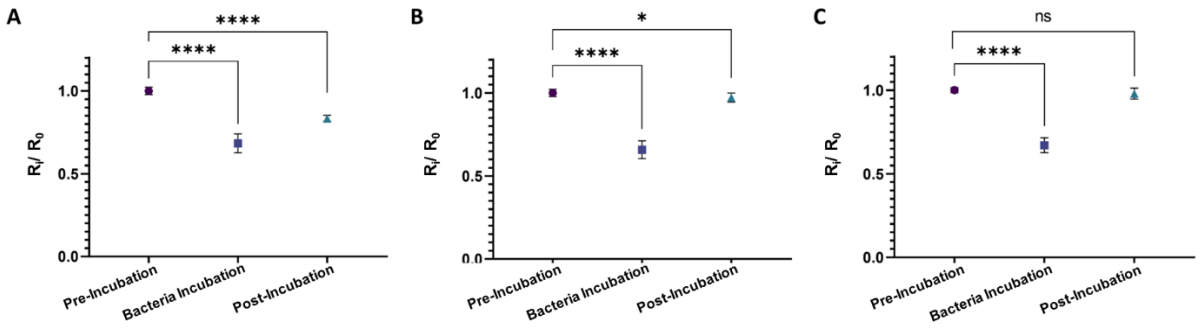

*Fig. 5-5. Results of the developed CIP-MWs based sensor's specificity test where different microorganisms were used as the target, while the template for CIP preparation was E. coli. The target cells are A) E. coli, B) Listeria, and C) Sarcina cells with count of 10^8 CFU/mL. Measurements were performed in three devices and five measurements per device. Error bars are standard deviations (SD) and ns: non-significant, *: P-Value <0.05, **: P-Value <0.01, ***: P-Value <0.001, and ****: P-Value <0.0001* [137], *Open Access.*

5.2.5. Conclusion

A low-cost and miniaturized CIP-based microfluidic sensor for conductometric detection of bacteria in water was designed and fabricated, and its sensing capacity toward target and non-target bacteria was assessed. The reported sensor detects whole bacteria cells and does not have the complications associated with sample preparation and nucleic acid isolation as required for nucleic acid-based pathogen detection methods. Another advantage is using low-cost and stable CIPs as artificial receptors compared to biological receptors such as enzymes, antibodies, aptamers, bacteriophages which are expensive and non-stable in different environmental conditions, resulting in poor reproducibility and false results. The sensor comprised a pair of CIP-MWs installed perpendicular to a microchannel. The interwire DC electrical resistance of the device was shown to significantly decrease after running bacteria suspensions for 30 mins through the microchannel in comparison to the corresponding NIP-based sensor. Using bacteria suspensions with counts in the range of 0 to 10^9 CFU/mL, the dose-response curve of the sensor

was established. The LOD and LOQ of 2.1× 10^5 CFU/mL and 7.3× 10^5 CFU/mL were obtained within the dynamic range of 10^4 to 10^7 CFU/mL, respectively. A linear fit in this range resulted in a sensitivity of 7.35 μS per CFU/mL. Furthermore, the sensor showed specificity towards the imprinted cells when exposed to other bacteria microorganisms, i.e., *Listeria* and *Sarcina*. The sensor described herein can provide a solution for simple, inexpensive, stable, selective, and real-time sensing of bacteria in water at the PON. The developed sensing platform can be integrated into a hand-held device in the future, enabling on-field and low-cost monitoring of pathogens. However, the performance of the conductometric measurement-based sensor for detecting whole bacterial cells requires enhancement.

5.3. Impedimetric-based CIP-MW Microfluidic Biosensor

The impedimetric sensing technique based on EIS measurements is an effective and reliable method for investigating antibody–antigen interactions on electrode surfaces [20,21]. This powerful electrochemical method is capable of detecting subtle changes occurring at the solution–electrode interface, making it suitable for enhancing the performance of CIP-MW-based biosensors. It has been widely employed for characterizing materials, surface modification procedures, and monitoring analyte binding to receptors [22]. Furthermore, the compact nature of the equipment required for EIS facilitates its miniaturization, making it readily amenable to PoN biosensors. Additionally, impedance provides a rapid response, low detection limit, cost-effectiveness, and the ability to conduct real-time sample monitoring.

EIS has been commonly employed to study the interfacial characteristics of sensors [179]. Since in our CIP-MWs based sensor, the capturing of target occurs on the electrode's surface, these techniques could provide useful information regarding presence/absence of target and its concentration. Generally, the measurement technique used is determined by the electrochemical

characteristics of the target molecule. The current generated can be used to quantify electroactive targets. Targets that are not electroactive may cause a shift in the conductivity and/or porosity of the MIP film. An external redox probe can be used along with EIS to monitor this shift indirectly [179]. The most common redox probes for indirect detection in combination with MIPs are ferrocene, hexamine ruthenium chloride, and Ferri/ferrocyanide [180], because of their rapid charge transfer with a variety of modified and unmodified transducers. The binding of a non-electroactive target analyte to an MIP at various concentrations reduces the porosity of the MIP film and the permeability of the redox probes to the electroactive sites, in turn causing the current intensity to drop/the sensor impedance to rise. This method can therefore determine the amount of the analyte indirectly. Furthermore, the polymer's morphology may transform due to a particular reaction, causing a change in the diffusion rate of the redox probe, which can be observed as a difference in the faradic current [179].

To further improve the sensor performance, the sensor design was next changed to a three-electrode configuration (Fig. 2-3) and impedimetric measurements were conducted to evaluate the AC characteristics of the electrochemical cell with CIP-MWs as working electrodes. Impedimetric biosensors operate based on the interaction between analytes and bioreceptors, resulting in alterations in capacitance and electron transfer resistance across the surface of a working electrode (refer to Fig. 5-6). As the concentration of analytes rises, the impedance across the electrode surface fluctuates, a phenomenon detected by a transducer. The direction of impedance change, whether an increase or decrease, depends on the specific analyte. Bioreceptors typically consist of antibodies, although they can encompass other molecules capable of detecting a broad spectrum of analytes ranging from proteins to entire bacteria and viruses.

Impedimetric detection of an analyte can be accomplished either with or without the presence of an additional electron/redox mediator. When electron mediators like $Fe(CN_6)^{3-/4-}$ (ferricyanide/ferrocyanide) are present, the impedance is referred to as Faradaic impedance. In contrast, in the absence of such mediators, the observed impedance is termed non-Faradaic impedance. The utilization of electron mediators ensures an ample supply of redox species, thereby preventing impedance limitation. When the target analyte binds to an MIP at various concentrations, it decreases the porosity of the MIP film and restricts the passage of redox probes to the electroactive sites. Consequently, this leads to a reduction in current intensity or an increase in sensor impedance. Utilizing this method enables the indirect quantification of the analyte.

In this section, by monitoring the charge transfer resistance of CIP-MWs in a microchannel, we studied the effect of captured bacteria by the CIP-MWs. The developed sensing platform demonstrates enhanced performance with a lower detection limit compared with conductometric detection and holds promise for future integration into handheld devices, enabling sensitive, on-site, and affordable pathogen monitoring.

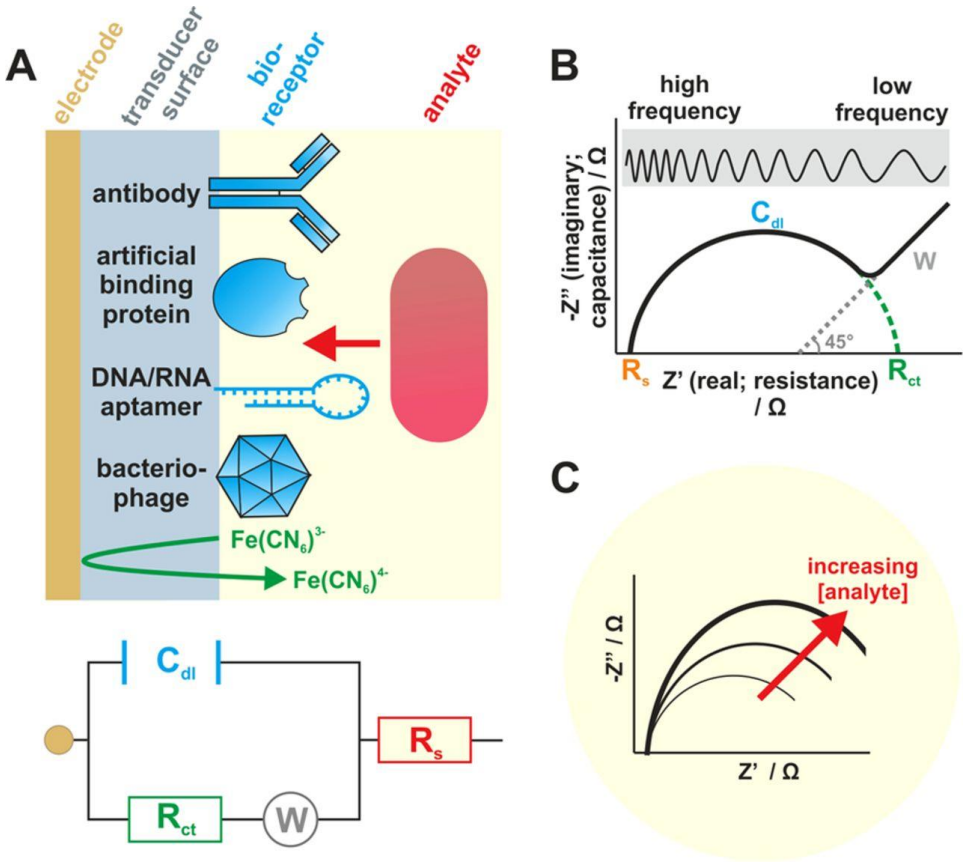

Fig. 5-6. A) The structure and function of impedimetric biosensors for bacterial detection [161], *showcasing electrode surface modification and the attachment of various bioreceptors. Electron mediators like ferri/ferrocyanide Fe(CN6)3−/4− monitor charge transfer resistance. The Randles circuit components are labeled. B) A Nyquist plot depicting the Randles circuit. (C) Impedance changes proportional to analyte concentration. Reprinted with permission from American Society for Microbiology.*

5.3.1. EIS Analysis of the Microfluidic Device and Equivalent Electrical Circuit Fitting

Electrochemical systems are often represented and analyzed through an equivalent circuit, which simulates the complex interplay of electrolyte/interface dynamics and redox reactions using electrical components such as resistors, capacitors, and sometimes inductors [181]. This approach enables a detailed investigation and evaluation of components within the system. By constructing and implementing these equivalent circuits, researchers gain insights into the underlying

electrochemical processes, facilitating a deeper understanding of how these systems respond to changes in conditions like bacterial binding in microfluidic sensing platforms. In this section, we aimed to investigate the impedimetric characteristics of CIP-MWs upon binding with whole bacteria within our integrated microfluidic sensor. To explore this, we measured the Faradaic impedance of the sensor in the presence of the $K_3[Fe(CN)_6]/K_4[Fe(CN)_6]$ redox couple as a probe. The changes in the electrochemical properties of the redox probe were analyzed by subsequent fitting of this spectra to the standard Randles circuit, as depicted in Fig. 5-7A. This equivalent circuit model helped explain the system's behavior, incorporating the ohmic resistance of the electrolyte (R_s), the Warburg impedance resulting from ion diffusion (Z_w), the double layer capacitance (C_{dl}), and the interfacial electron transfer resistance (R_{CT}). However, fitting the resulting spectra with the standard Randles circuit yielded a poor goodness of fit with an error value of 0.29. This discrepancy was attributed to the presence of a constant phase element (CPE) in the system, which accounted for non-ideal behavior of a capacitor in a real system. To address this limitation, the model was refined by incorporating a modified Randles circuit with a CPE element, as shown in Fig. 5-7B. This modification resulted in a significant improvement in the fitting quality with an acceptable goodness of fit and error value of 4.6×10^{-4}, indicative of a better representation of the electrochemical processes occurring within the system. The observed enhancement underscores the importance of accounting for the non-ideal capacitive behavior inherent in the system's response. These findings align with previous studies that highlight the necessity of CPE elements in impedance modeling of real systems as it defines nonhomogeneous charge distribution and surfaces in EIS experiments [177,178].

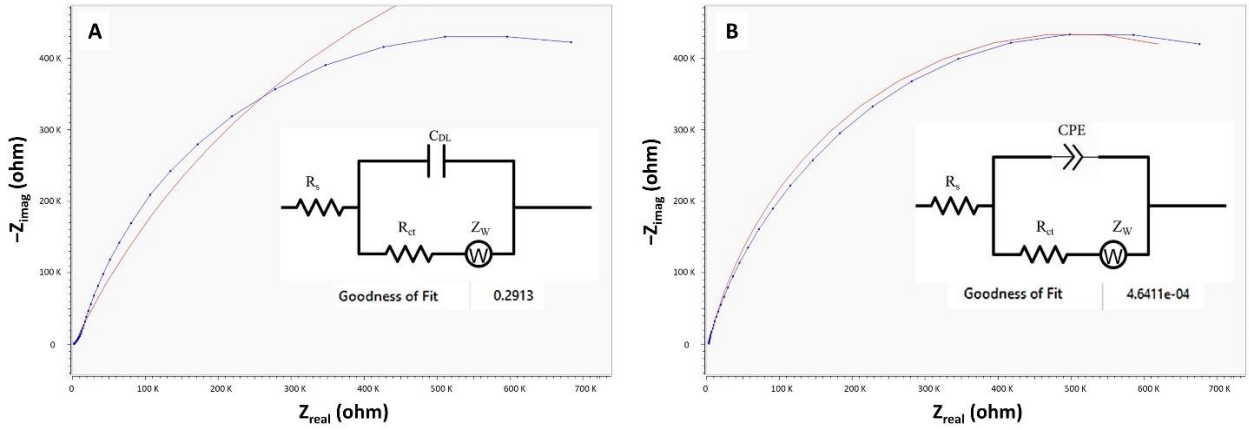

Fig.5-7. Electrochemical impedance spectroscopy (EIS) measurements and equivalent electrical circuits of the microfluidic sensor with CIP-MWs as the working electrode (WE) in the presence of K3[Fe(CN)6]/K4[Fe(CN)6] as the redox probe. (A) Standard Randles circuit diagram fit. (B) Modified Randles circuit diagram fit. Insets show the goodness of fit values. The blue lines represent the experimental data, while the red lines correspond to the fitted curves from the circuit models [138], *Open Access.*

5.3.2. EIS Characterization of Bacteria Binding to CIP-MWs

As bacteria bind to the surfaces of CIP-MWs, which serve as the WE in our sensor design, they may disrupt the charge transfer between the electrode surface and the electrolyte. This interaction can alter the interfacial properties of the WE. For EIS characterization of bacteria binding to CIP-MWs, parallel EIS measurements were conducted for microfluidic devices with NIP-MWs and CIP-MWs serving as WEs. Each test measurement was performed in two stages: before and after bacteria incubation (bacteria count 10^5 CFU/mL). The resulting Nyquist plot spectra are depicted in Fig.5-8.

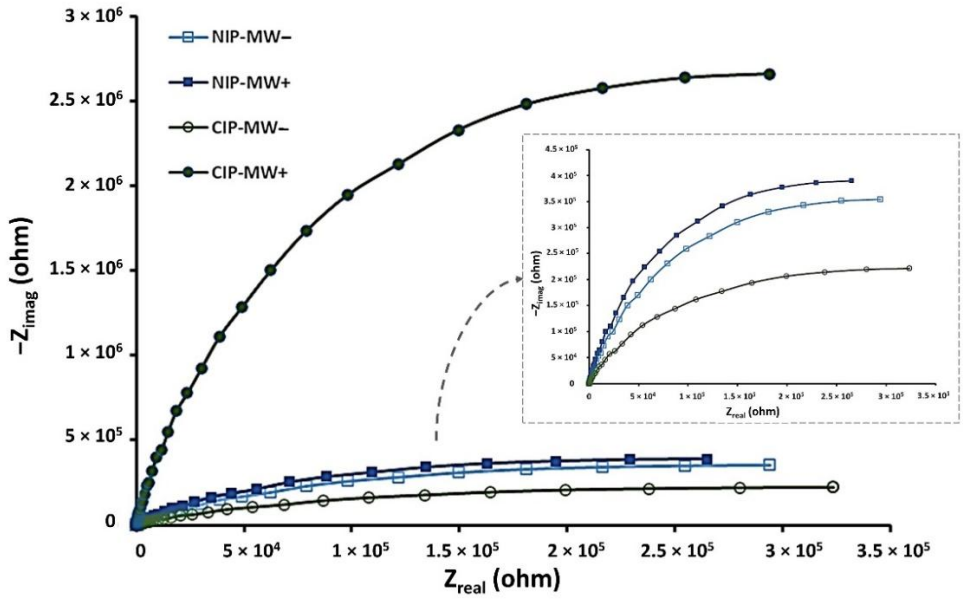

Fig.5-8. Electrochemical impedance spectroscopy (EIS) curves of microfluidic devices in 0.1 M KCl containing 5 mM $K_3[Fe(CN)_6]$ with NIP-MWs and CIP-MWs serving as working electrodes. Minus and plus signs in the legend denote measurements obtained pre-and post-bacteria incubation, respectively. The inset shows an enlarged view of the NIP-MW (− and +) and CIP-MW data [138], *Open Access.*

In a Nyquist plot, the semi-circle portion at high frequencies represents faradaic transfer of electrons at the surface of the WEs, while the low-frequency spectrum provides insights into the diffusion process of redox species between the electrolyte and the electrode surface. To understand the underlying mechanism of the observed response, the data were simulated using the modified Randles equivalent circuit model shown in Fig.5-7B. The R_s and Z_w impedance characterized the bulk properties and diffusion dynamics of the redox probe in the electrolyte solution, respectively, which remained unaffected by physicochemical transformations at the electrode surface [184] and, thus, were unaltered by CIP–bacteria binding. Conversely, parameters like R_{CT} and the capacitance of the double layer were contingent upon the dielectric and insulating characteristics at the electrode–electrolyte interface [185]. As mentioned earlier, a CPE was introduced into the circuit

to better fit the impedance spectrum, reflecting defects and inhomogeneities of the layer [186]. Notably, R_{CT} was highly sensitive to electrode modifications resulting from *E. coli* bacteria binding to the CIP biorecognition layer. This binding process slowed interfacial electron transfer kinetics and elevated electron transfer resistance [187]. Consequently, the number of captured bacteria on the electrode surface could be inferred from the concentration-dependent electron transfer resistance of the redox probe, even at low analyte concentrations [184].

It can be seen from Fig.5-8 that the diameter of the semi-circle in Nyquist plot, indicating charge transfer resistance, was smaller for CIP-MWs than that for NIP-MWs. This difference may be due to the bacteria cavities and porosity in the CIPs, which facilitated ion transfer compared with the intact NIP coating. The semi-circle diameter for CIP-MWs after incubation with bacteria (CIP-MW+) increased significantly, directly indicating enhanced charge transfer resistance. This was likely due to the presence of captured bacteria by CIP-MWs, which hindered the transfer of redox ions between the electrode and the solution. For the control experiment performed in parallel with NIPs, there was a slight increase in the diameter of the semi-circle post-bacteria incubation (NIP-MW+). This could be due to small non-specific adsorption and bacterial attachment to NIP-MWs, which hindered ion transfer [188]. These results were consistent with prior studies, where the presence of bacteria was shown to significantly increase the charge transfer resistance due to hindrance in ion transfer pathways [189]. For instance, similar behavior has been observed in the work of Piskin et al. [190], where bacterial capture on bacteriophage-modified electrodes surfaces led to substantial R_{CT} changes. Our findings further demonstrate the robustness and superior sensitivity of CIPs compared with biological recognition agents like bacteriophages, particularly in comparison with NIP-MWs, highlighting the effectiveness of CIPs in creating selective cavities that facilitate targeted bacteria capture.

Fig.5-9A presents the results for the measured R_{CT} values pre- and post-incubation with bacteria, for five replicates. While there was a slight increase in the R_{CT} values post-bacteria incubation for devices using NIP-MWs as WEs (*p*-value = 0.032), this increase in R_{CT} became a lot more significant for CIP-MWs (*p*-value = 0.0008). The normalized $\Delta R/R_{CT,1}$ result shown in Fig.5-9B reveals a 10-fold rise in the normalized charge transfer resistance change in CIP-MWs, confirming the bacteria cell attachment to selective cavities on CIP coatings, hindering redox ion transfer between the solution and the electrode surface. The *p*-values obtained from the Mann–Whitney U test demonstrated the statistical significance of the observed differences. Specifically, the significant increase in R_{CT} values for CIP-MWs (*p*-value = 0.0008) underscores the strong impact of bacteria capture on charge transfer resistance, in contrast to the more modest changes observed with NIP-MWs. This statistical analysis supports the conclusion that CIP-MWs offer a more effective and selective bacterial detection method, as evidenced by the highly significant difference in R_{CT} post-incubation.

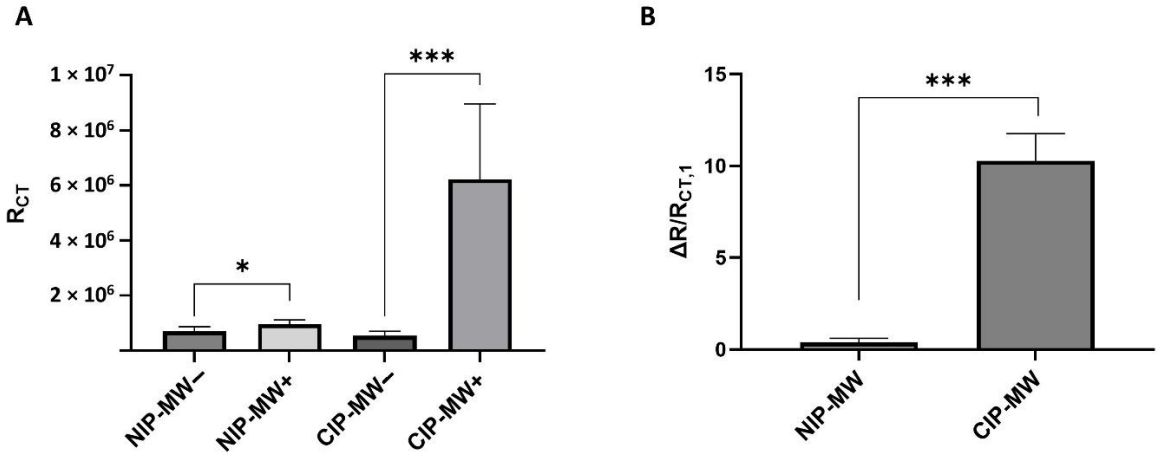

*Fig.5-9. Charge transfer resistance (R_{CT}) values for microfluidic devices in 0.1 M KCl containing 5 mM $K_3[Fe(CN)_6]$ with NIP-MWs and CIP-MWs serving as working electrodes. (**A**) R_{CT} values obtained before normalization and (**B**). normalized R_{CT} change values. The minus and plus signs in the x axis indicate*

*pre-and post-bacteria incubation measurements, respectively. The error bars are standard deviations (SD). *: p-value < 0.05; ***: p-value < 0.001* [138], *Open Access.*

5.3.3. Quantitative *E. coli* Bacteria Detection by EIS

The target bacteria detection in this study relied on measuring Faradaic impedance in the presence of the redox couple. It was hypothesized that the number of bacteria captured by CIP-MWs on the electrode surface would affect the transfer of redox ions between electrode and solution. Thus, the number of captured bacteria on the electrode could be determined by looking at how the redox probe's electron transfer resistance changed, which could be measured using EIS. Following the examination of bacteria capturing properties exhibited by SS-MWs, NIP-MWs, and CIP-MWs and their impacts on the relevant concentration dependent parameter, R_{CT}, the effect of bacteria counts on the sensor's normalized change in charge transfer resistance was investigated. Using serial dilution, suspensions of *E. coli* bacteria with cell counts between 0 and 10^7 CFU/mL were prepared. Fig.5-10A illustrates the normalized shift in charge transfer resistance of the sensor based on CIP-MW, alongside responses obtained from parallel control experiments utilizing NIP-MWs.

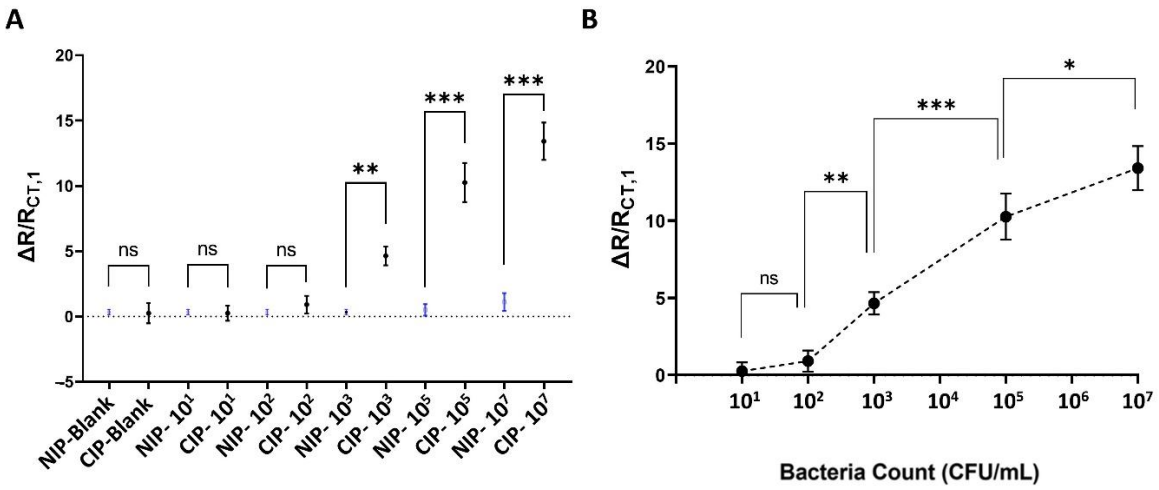

*Fig.5-10. EIS-based microfluidic bacteria sensor characterization. (**A**) Normalized post-incubation charge transfer resistance shift of the microfluidic sensor with CIP-MWs and parallel control experiments utilizing NIP-MWs, when exposed to different bacteria counts. (**B**) The dose–response $\Delta R/R_{CT,1}$ curve established for the CIP-MW-based sensor. Error bars are standard deviations (SD). ns: non-significant; *: p-value < 0.05; **: p-value < 0.01; ***: p-value < 0.001* [138], *Open Access.*

Fig.5-10A reveals that at bacterial counts ranging from 0 to 10^2 CFU/mL, the response of the CIP sensor was not significantly different from the control experiments (*p*-value > 0.05). However, the difference became more significant by further increasing the bacteria count to 10^3–10^7 CFU/mL, demonstrating the dominant effect of the CIP coating as compared with NIP coatings with no significant responses. This behavior aligned with findings from previous works [137,186], where the sensitivity of CIP-based sensors significantly increased at higher bacterial concentrations, reinforcing the effectiveness of CIP-MWs in selective bacterial detection. The results also indicated that the detection capability of CIP-MWs at higher concentrations surpassed that of NIP-MWs, highlighting the advantages of using CIPs for enhanced sensitivity in pathogen detection applications.

Fig.5-10B illustrates the sensor's dose–response curve generated from CIP-MWs across bacterial concentrations ranging from 0 to 10^7 CFU/mL. The curve demonstrated negligible response at bacterial levels below 10^2 CFI/mL, indicating the sensor's lack was sensitivity at lower concentrations. A significant shift in charge transfer resistance was detected as bacterial concentrations increased from 10^2 to 10^7 CFU/mL. The statistical significance of the response peaked at bacterial counts of up to 10^5 CFI/mL before declining, likely due to the saturation of the CIP cavities as the number of bacterial cells surpassed the binding capacity.

Statistical analysis indicated that the sensor's dynamic range extended from 10^2 to 10^7 CFU/mL, based on the significant differences in consecutive readout signals within this interval. This range surpassed that of previous studies using CIP-MWs [137]. A linear regression analysis within this dynamic range yielded a goodness of fit (R^2) value of 0.99, with a calculated sensitivity of 72.5 μS per CFU/mL, which is 10 times greater than the sensitivities reported in earlier research on conductometric *E. coli* detection using CIP-MWs [137].This broad linear detection range can facilitate the analysis of samples of unknown concentration via a simple dilution series, eliminating the need for sample concentration or pre-treatment steps. This versatility makes our approach particularly suitable for applications in clinical, food, and environmental industries. Furthermore, employing the 3-sigma and 10-sigma methods [192], the sensor's LOD and LOQ were estimated to be 2×10^2 CFU/mL and 1.4×10^4 CFU/mL, respectively. These sensor characteristics were much lower than those obtained with the conductometric technique reported previously for microfluidic CIP-based bacteria sensors, representing a marked improvement in sensitivity.

Our established impedimetric microfluidic CIP-MW-based sensor achieves detection ranges and limits that are competitive with or superior to those of existing biosensors that use biological receptors for whole bacteria detection [161]. However, our proposed sensor has the advantage of

the CIP's durability and cost-efficiency over their biological counterparts [174]. Unlike biological recognition elements, such as aptamers, antibodies, and bacteriophages, which are often sensitive and lose functionality, CIPs maintain stability and performance. Additionally, the production of CIP-based films is controllable and facile, and the material is inexpensive, biocompatible, and biodegradable. The developed sensor's performance surpasses that of other CIP-based bacterial sensing methods such as frequency-based techniques using quartz crystal microbalance (QCM) [168,173]. Furthermore, impedimetric sensing offers several added advantages over QCM techniques. Unlike QCM, which relies on precise frequency measurements and can be complex and costly, impedimetric sensing simplifies the detection process by directly measuring changes in electrical impedance. This approach is particularly beneficial for detecting low concentrations of analytes, where QCM's frequency shifts can become less accurate and more difficult to measure. Additionally, impedimetric sensors are often more robust, less sensitive to environmental variations such as temperature and viscosity changes, and generally more adaptable for a wide range of applications. These factors make impedimetric sensing a more versatile and cost-effective alternative for various biosensing needs [176]. This validates the suitability of integrating an EIS-based microfluidic biosensing strategy with CIPs for the creation of pathogen sensors with high sensitivity, presenting a genuine alternative to conventional methods. Bringing together the advantages of biosensors and CIPs, this method is promising for pathogen detection, offering the advantages of enhanced sensitivity, selectivity, simplicity, low cost, and stability.

5.3.4. Specificity of the CIP-MW based microfluidic sensor

To investigate the specificity of the CIP-MWs in the developed sensor, *Listeria* cells were used as the target microorganism, while the template for CIP preparation was *E. coli.* Fig. 5-11 shows the

results performed in triplicates experiments. As seen in Fig. 5-11A, using *E. coli* as the target microorganism results in a significant (P-Value=0.0008) increase in the normalized post-incubation charge transfer resistance shift of the sensor. However, in the case of using non-template microorganism as the target, i.e., *Listeria (*Fig. 5-11B) cells, the difference in the sensor's normalized post-incubation charge transfer resistance is non-significant (P-Value=0.42). Considering the size and shape of these two microorganisms, which are similar in shape and size, we can conclude that our sensor is specific to the imprinted bacteria microorganism, even if cells with similar shapes and morphologies are used in the sensor.

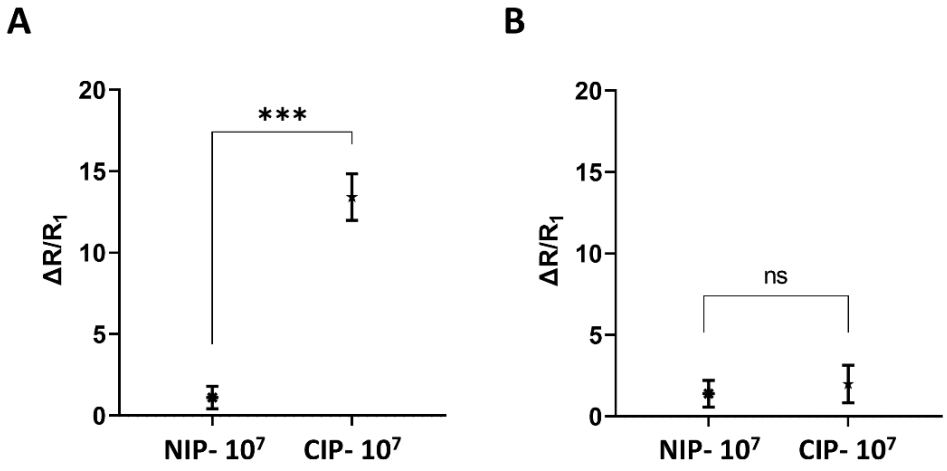

*Fig. 5-11. Results of the developed CIP-MWs based sensor's specificity test where different microorganism was used as the target, while the template for CIP preparation was E. coli. The target cells are A) E. coli, and B) Listeria with count of 10^7 CFU/mL. Error bars are standard deviations (SD) and ns: non-significant, and ***: P-Value <0.001.*

5.3.5. Conclusion

A low-cost, miniaturized, and label-free microfluidic biosensor for *E. coli* bacteria detection based on CIPs was designed and fabricated. The sensing capacity of the resulting CIP-based biosensor toward the target bacteria was assessed by the EIS characterization technique. The developed

biosensor, employing CIP-MWs as working electrodes in PDMS microchannels, demonstrated enhanced sensitivity to bacterial presence. Using EIS measurements, an increase in the charge transfer resistance of CIP-MWs after exposure to bacteria was detected, enabling quantification between 10^2 and 10^7 CFU/mL with detection and quantification limits of 2×10^2 CFU/mL and 1.4×10^4 CFU/mL, respectively. The wide linear detection range of the reported biosensor can enable the analysis of real samples without pre-treatment or concentration steps. Furthermore, the sensor showed specificity towards the imprinted cells when exposed to other bacteria microorganisms, i.e., Listeria. With its potential for cost-effectiveness, durability, portability, and real-time monitoring, the developed sensor presents a promising solution for waterborne pathogen detection at the PoN.

Chapter 6

6. Thesis Summary and Prospect

6.1. Thesis Summary

6.1.1. Selection of Functional Monomers for CIP Synthesis

This research selected the non-covalent approach to synthesizing CIPs since it has a more straightforward experimental procedure, especially when dealing with BAs. Also, there are a variety of appropriate monomers available to use in this approach. In terms of selecting the functional monomers, we relied on previously published works that have synthesized highly effective CIPs for selective recognition of BAs [53]–[56], [66], [193].

The selected functional monomers are Acrylamide (AAM), Methacrylic acid (MAA), Methyl methacrylate (MMA), and N-vinylpyrrolidone (VP). As mentioned earlier, MAA is widely used in CIP formulations because of its ability to act as a hydrogen bond donor and acceptor. Our selected formulation has three additional functional monomers with different side chains, which provide both polar and non-polar functionalities in the synthesized CIP to obtain a stable interaction with the template molecule during self-assembly formation between CIP and template. Therefore, the addition of various suitable functional monomers can improve the template-CIP complex formation during the self-assembly process, thus improving the binding efficiency and selectivity of the resulting CIPs.

6.1.2. CIP-MW Fabrication and Optimization

The fabrication of CIP-MWs, along with optimization of the coating parameters (uniformity, thickness, and stability) was explained in detail in chapter 3. Compared to classical bulk imprinting, thin surface-imprinted CIP films can form a high surface density of imprinted cavities and low heterogeneity with geometrical constrictions fewer than bulk imprinting. This strategy provides a high control over the imprinting, enabling the effective template removal and binding of the target analyte in CIP coatings [20], [155]–[157]**.** As expected, the extraction reaction efficiently removed the imprinted cells from the CIP layer and exposed the bacilli-like surfaces complementary to *E. coli*.

6.1.3. Rebinding Performance

To evaluate the rebinding performance of the other optimized CIP compositions consisting of single, two and three functional monomers (1,2, and 3 monomer CIP/NIP-MWs) were prepared and tested with the bacterial solution with the initial concentration of 10^4 cells/mL. Comparing the bacterial rebinding performance of SS-MWs, CIP-MWs and NIPs-MWs revealed that the binding capacity of CIP-MWs is significantly higher than the NIP-MWs of the same functional monomer composition. The higher binding capacity is achieved by increasing the copolymer types from 1 to 4, which can be attributed to the addition of various functional side chains that helps to provide a more stable template-polymer complex during self-assembly and imprinting of relatively large *E. coli* bacterial cell surfaces with various functionalities. Especially addition of the fourth functional monomer (VP) has resulted in a dramatic increase in the binding performance of CIP-MWs. This can be attributed to VP's relatively large molecular structure featuring a steric hindrance effect, which helps in synthesizing a stable complex. VP also presents hydrophobic and hydrophilic

surface functionalities that can interact with different functional groups on the large surface of bacterial cells [194]. However, the amount of this functional monomer in the copolymer system of CIP-MWs is limited to the optimized quantification and increasing its ratio in CIP composition will decrease the uniformity of NIP/CIP coatings on SS-MWs based on the coating optimization results.

After studying the binding performance of synthesized CIP-MWs, we studied the effect of initial bacteria count on rebinding to CIP-MWs by measuring their rebinding capacity to *E. coli* cells in aqueous suspensions, which was discussed in chapter 4 in details.

6.1.4. Bacterial Specificity and Selectivity

The specificity of CIP-MWs was investigated by exposing the CIP-MWs imprinted with *E. coli* as the template to suspensions of three different bacteria microorganisms, including *E. coli*, *Sarcina* and *Listeria innocua* at an initial count of 10^4 CFU/mL, which was discussed in chapter 4 in details. It was shown that CIP-MWs imprinted with *E. coli* cells could capture a significant number of *E. coli* compared to SS-MWs and NIP-MWs. However, their bacteria-capturing performance did not significantly differ from the NIP-MWs (p-values >0.05) when exposed to other non-specific bacteria targets, i.e., *Sarcina* and *Listeria*. This reveals the specific capturing behavior of our CIP-MWs towards the *E. coli* template cells used in the imprinting process. In all cases, a significant difference was observed between the capturing efficiency of SS-MWs and NIP-MWs, which can be attributed to the non-specific adsorption of bacteria to polymeric coatings.

6.1.5. Influence of Bacteria Gram Type on Imprinting Efficacy

In another milestone, which was reported in chapter 4, the influence of bacteria gram type on imprinting efficacy was investigated. For this, gram-positive bacteria (*Sarcina*) were used as templates during imprinting, and the rebinding experiments were performed by exposing the resulted CIP-MWs to same target as imprinted bacteria. It was observed that bacteria capturing efficiency had dropped significantly in the case of using *Sarcina* cells. Also, the specific binding, which can be considered the difference in bacteria capturing efficiency of NIP-MWs and CIP-MWs, became less significant for the *Sarcina*-imprinted polymers. The reason for the lower binding capacity to Sarcina bacteria could be due to the larger size of this bacteria (1.8-3 microns in diameter). Also, according to literature, *Sarcina* bacteria has cuboid shape. Because of the cuboidal shape, *Sarcina* tends to form packets often in tetrads but occasionally in cubes of eight cells, which increases the size of colonies. As a result of increased size of colonies, more surface area of the wire could be occupied with fewer bacteria cells. Another possibility for decreased BCE when using *Sarcina* bacteria could be due to changing bacterium types from gram-negative to gram-positive. This change in bacteria type results in their different cell walls and proteins. So, one reason for lower bacteria capturing efficiency with *Sarcina* could be its different cell wall chemistry that could introduce different interactions with polymer/MW and reduce the number of imprinted cavities. Gram-positive bacteria have a greater volume of peptidoglycan (a polymer of amino acids and sugars that create the cell wall of all bacteria in their cell membranes), which is what makes the thick outer covering. This thick outer covering, or membrane, can absorb a lot of foreign material [160]. SEM imaging revealed that the morphology of CIP-MWs imprinted with *Sarcina* cells differs from the previously fabricated CIP-MWs with *E. coli*-OP50 cells. The surface of CIP-MWs was bubble-shape coatings, which did not change significantly after washing with

template removal solutions. So, a reason for decrease BCE could be not efficient removal of entrapped bacteria, therefore a smaller number of cavities for rebinding assays. To investigate further, we hypothesized that different gram-types of bacteria could play an important role in imprinting and capturing efficiency. We tested this hypothesis by using another gram-negative bacterium, *Salmonella*, for imprinting. Results of rebinding assays obtained with this experiment were in good agreement with the results obtained for *E. coli* OP50, which confirms the validity of our hypothesis.

6.1.6. Integration with Microfluidic Biosensors

In the third objective, CIP-MWs were integrated with miniaturized microfluidic sensing platforms to evaluate the capability of the developed CIP-based microfluidic biosensor to selectively capture and detect BAs. The affinity of CIP-MWs was assessed by exposing *E. coli* bacteria solutions to the synthesized CIP-MWs on the microfluidic device. The effectiveness of the biosensor's binding to target microorganisms was investigated using electrical transduction in two sub-objectives: based on conductometric measurements and impedimetric measurements. For this, we first showed the integration of CIP-MWs in a low-cost microfluidic sensor for conductometric detection of CIP-bacteria binding events. Resistance changes normalization and the subsequent analysis of the sensor's dose-response curve revealed the limits of detection and quantification of 2.1×10^5 CFU/mL and 7.3×10^5 CFU/mL, respectively. Experiments using competing cells showed specificity of the sensor towards the imprinted *E. coli* cells.

To further improve the sensor performance, the sensor design was next changed to a three-electrode configuration and impedimetric measurements were conducted to evaluate the AC characteristics of the electrochemical cell with CIP-MWs as working electrodes. Impedimetric

biosensors operate based on the interaction between analytes and bioreceptors, resulting in alterations in capacitance and electron transfer resistance across the surface of a working electrode. We reported further improvement of the sensor performance, by modification of the sensor design and utilizing EIS measurements. The measured electrochemical spectrum was fitted with an equivalent electrical circuit, and the charge-transfer resistance as the relevant concentration dependent parameter was measured before and after exposure to bacteria. The experiments revealed a 10-fold increase in the charge-transfer resistance of CIP-MWs after exposure to bacteria with a cell count of 10^5 CFU/mL, compared to NIP-MWs. This notable increase was attributed to the attachment of bacteria cells to selective cavities on CIP coatings, disrupting the transfer of redox ions between the electrolyte and the electrode surface. The charge-transfer resistance changes normalization and the subsequent analysis of the sensor's dose-response curve between 0 to 10^7 CFU/mL bacteria revealed the limits of detection and quantification of 2×10^2 CFU/mL and 1.4×10^4 CFU/mL, respectively. The dynamic range of the sensor was 10^2 to 10^7 CFU/mL. The sensor's specificity against a different bacterial microorganism, i.e., *Salmonella* was assessed. The improvement in sensitivity and detection limit of the EIS-based sensor distinguished it from previous work based on conductometric transducers. The measured charge transfer resistance in this technique correlates with electrode surface phenomena, providing a more refined assessment than the total cell resistance measured in previously reported DC method. Thus, the proposed sensor has the potential to offer a cost-effective, durable, portable, and real-time solution for the detection of waterborne pathogens.

6.2. Thesis Prospects

In this study, we investigated the performance of CIPs for the selective detection of *E. coli* bacteria using microfluidic-based sensor platforms. While the findings presented in this thesis demonstrate the effectiveness of these sensors in providing rapid and cost-effective bacterial detection, several additional avenues for future research remain. Based on the current work presented in this thesis, the technology is at Technology Readiness Level (TRL) 4 (Technology validated in the lab), as the CIP-MWs have been synthesized and successfully tested in laboratory conditions, including integration into microfluidic devices for bacterial capture and detection. Moving forward, after incorporating the proposed improvements the technology could advance to TRL 7 (System prototype demonstration in an operational environment). This would involve testing the technology under real-world conditions to evaluate its performance, scalability, and reliability, ultimately bringing it closer to commercialization. The following sections will discuss some of these potential future directions in more detail.

6.2.1. Limitations and Challenges Associated with the Proposed Platform and Future Research Direction

Despite the various advantages offered by the CIP-based bacterial detection sensors and the methodologies discussed in this thesis, we recognize that several limitations must be addressed for these systems to become fully applicable and efficient for widespread use in clinical, environmental, and food safety diagnostics. While these sensors present a significant improvement over traditional methods in terms of cost, speed, and portability, further development is required to ensure they are suitable for end-users without technical expertise or specialized training.

One of the primary challenges lies in the long-term stability and reusability of the CIP sensors. Although initial results show good bacterial capture efficiency, the ability to regenerate the sensor after multiple uses has not been explored. The removal of the bacterial template and reusability of the sensor can make this technology more cost-effective and practical for routine use, especially in field applications where sensor replacement may not be feasible. Future research should focus on developing effective template removal solutions that can regenerate the CIP coating without compromising its structural integrity or binding capacity.

One of the key challenges is the impact of bacterial microorganism variability on the efficiency of the imprinting process and the subsequent bacterial capturing efficiency (BCE). Specifically, when *Sarcina* bacteria, a gram-positive bacterium, were used as templates for imprinting, the sensor's BCE was significantly lower compared to when gram-negative bacteria, such as *E. coli OP50*, were used. This discrepancy in performance could be attributed to several factors, including the larger size and cuboidal shape of *Sarcina* bacteria, which tend to form colonies with a greater surface area, thus reducing the number of bacteria captured per unit area on the MWs. Furthermore, the different cell wall compositions between gram-positive and gram-negative bacteria, particularly the thick peptidoglycan layer in gram-positive bacteria, likely contributes to reduced interactions between the bacteria and the CIP-MWs. This may result in less effective imprinting and a lower number of imprinted cavities available for bacterial capture. The effect of bacterial morphology and cell wall chemistry on imprinting efficacy highlights the need for more precise control over the imprinting process, particularly when dealing with different bacterial types. The challenge is that bacterial surfaces exhibit a high degree of heterogeneity, and the interactions between CIPs and bacterial cell wall components can vary depending on the microorganism. Future work should explore how to modify the CIP composition and polymerization conditions to

account for variations in bacterial gram-type, shape and size, ensuring more consistent and efficient bacterial capture across a broader range of target species. Moreover, while the addition of multiple MWs in rebinding experiments improved the BCE for *Sarcina*, this solution may not be scalable, and further studies should investigate how the number of MWs or cavities could be optimized for different target bacteria.

Moreover, the presence of non-target bacteria or environmental contaminants could interfere with the binding process, reducing the overall accuracy of detection. Exploring competitive assays and improving the sensor's ability to discriminate between bacterial targets and non-specific binding is crucial for enhancing the sensor's real-world applicability.

Although the sensor is effective within a certain concentration range, the LOD could be further reduced to increase its sensitivity, particularly for applications in environmental monitoring where bacterial concentrations are often lower. This could be achieved by optimizing the functionalization of the CIP coatings, increasing their binding affinity, or incorporating nanomaterials to enhance the electrical conductivity and detection capabilities. Nanomaterials could also help improve the sensor's response time and sensitivity, allowing for more precise detection of bacterial targets at lower concentrations. Integrating nanomaterials with MIP-based electrochemical sensors has been shown to have the potential to increase the electrochemical signal's intensity, and therefore, the sensor's sensitivity. The nanomaterials can be used either as electroactive agents to facilitate signal generation, or act as carriers themselves to accumulate higher amount of electroactive targets and deliver them more easily to electrodes surface [195]. Nanomaterials such as silver and gold nanoparticles graphene, graphene oxide, carbon nanotubes (CNTs), carbon dots, and MXene have been used for this purpose. For instance, gold nanoparticles

were utilized by Kan et al. [196] to increase the electrical conductivity of MIPs (approximately 30 times), which in turn led to a wider linear range and lower LOD of the sensor.

Among different nanomaterials, MXenes have become one of the best alternatives for fabricating sensors to detect various analytes, like cancer biomarkers, cardiovascular diseases, pesticides, heavy metals, and antibiotics. Due to the numerous advantageous properties of MXenes such as a high surface area, outstanding electrical conductivity, increased functionality, adjustable characteristics, and remarkable ion-intercalation capabilities, they have been identified as a promising nanomaterial for electrochemical sensing [197]. Due to their unique properties, MXenes have been combined with MIPs during the recent years to form MIP-MXene nanocomposites. Integrating MIPs and MXenes have been claimed to improve the MIP-based sensor's sensitivity and selectivity since they can catalyze electrochemical mechanisms, enhance electron mobility, enhance the output signal, and increase electrode surface area [197].

While the integration of CIP-MWs with microfluidic platforms offers great potential for real-time detection, the scalability and throughput of the system still present challenges. Currently, the platform supports a low throughput of bacterial tests, which is sufficient for proof-of-concept but not yet suitable for high-throughput applications that would be required in clinical diagnostics or large-scale environmental monitoring. The incorporation of parallel sensor arrays or multi-sample processing features would be necessary to enhance throughput. Additionally, the current design of the microfluidic channels and the sensor's mechanical properties should be refined to optimize the flow dynamics, reduce clogging, and improve bacterial interaction with the CIP-coated microwires.

Further improvements can be made to the microfluidic design itself. Current designs rely on relatively simple channels and electrochemical transducers. Future research could involve the

optimization of dimensions and channel designs, and development of more sophisticated multi-stage microfluidic systems capable of sample pre-processing (e.g., filtration, enrichment, or concentration), bacteria isolation, and real-time detection all within a single device. Such a lab-on-chip (LOC) system would enable more effective and comprehensive pathogen screening, especially for complex samples with low bacterial concentrations.

The cost-efficiency of the proposed microfluidic sensors has been a key design consideration; however, more robust fabrication techniques are needed to improve device longevity and performance. For instance, gold electrodes could be used to replace stainless steel electrodes, ensuring more durable and reliable sensors for prolonged use in real-world conditions.

Further, the data analysis process remains time-consuming, particularly for large datasets generated by bacterial detection assays. Although standard software tools like Excell, Minitab, and GraphPad were used for analysis, developing a customized MATLAB or Python-based solution for automated tracking and quantification could streamline the process, improve consistency, and enhance throughput.

Finally, the throughput of the current platform is limited by the number of bacterial samples that can be processed in parallel. Currently, each test involves a relatively low number of bacterial samples, which does not meet the high demands of commercial and clinical screening. In future iterations, throughput can be increased by parallelizing sensor arrays or employing motorized stages for automated sample positioning, thus reducing analysis time per sample and enhancing the overall scalability of the platform.

7. Appendix A

7.1. NIP and CIP Removal Procedure

After complete polymerization of the NIP and CIP prepolymer solutions in the presence of salinized MWs, the tubes were cut to remove the intact polymer with the MW immobilized inside (Fig. A1-left). To remove the MW, the powdery polymer around it was gently peeled off, and the MW was released. It was observed that a thin layer of the polymer was uniformly attached to the surface of the MW (Fig. A1-1-middle), and its uniformity and thickness were studied following the procedures described in the paper (Fig. A1-right).

Fig. A1. Left) Polymerized CIP with a MW immobilized inside it after removal from the containing tube. Middle) Different CIP-MWs after removal from the polymer bulk. The coated and bare sides of MWs are labeled. Right) Diameter of five replicated 4-CIP-MW samples showing reproducible CIP coatings[149]. *Reprinted with permission from American Chemical Society.*

7.2. Measurement of Stainless Steel Microwire (SS-MW) Diameter

Measurements of MWs' diameter were conducted using a custom-developed macro in Image-J software. An optical microscope (DMIL LED Inverted Microscope, Leica, Germany) was used to

image MWs (Fig. A2-A). The images were then converted to greyscale to increase contrast. Using ImageJ's Canny edge detection function [198], the MW edges were detected by marking pixels above a threshold (Fig. A2-B). Canny edge detection is a proven method for detecting edges and was used here due to its speed, robustness, and sensitivity [199]. Following this, the macro selected 100 random points on one detected edge (customizable inside the macro code), from which it determined the shortest distance to the other edge (Fig. A2-C). For all the points, the macro measures the distance from each point on the line to all the points on the other line in pixels and then chooses the shortest distance. Finally, it reports individual measurements, along with the average and standard deviation (SD) of the diameter measurements in an output CSV file. The measurements were converted to a length scale based on pixel size for further analysis.

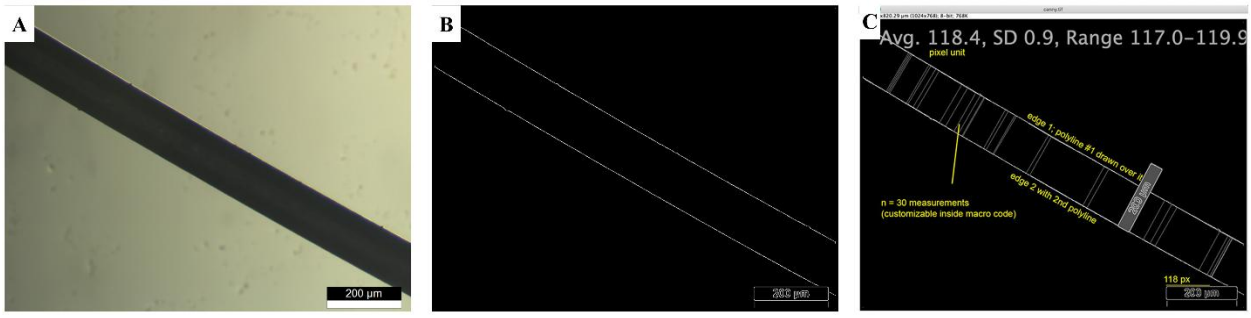

Fig. A2. The image processing method used for the measurement of MW diameter. A) The optical image of MW, B) The output image of the Canny edge detection step with contoured lines showing the edges of the MW, C) Distance measurements done across the MW diameter using the developed ImageJ macro (n=30 is shown here) [149]. *Reprinted with permission from American Chemical Society.*

7.3. Optimized Single-Monomer NIP Coatings

To fabricate uniform NIP coatings based on each of the FMs used in our studies, we conducted RSM optimization. Table A1 shows the optimized values for each recipe for synthesizing NIP-MWs based on each FMs, and Fig. A3 shows the coated NIP-MWs using these optimized recipes.

Table A1. Optimal recipes for single-monomer NIPs on SS-MWs.

Important Factors	**FM**	**FM: Cross-linker Ratio**	**Solvent**	**Polymerization Time (h)**	**Polymerization Temperature (°C)**
Levels	MAA	1:4.76	Acetonitrile	11.6	63
	AAM	1:1	Acetonitrile	9.25	70
	VP	1:6	Toluene	12	60
	MMA	1:6	Acetonitrile	11.25	68

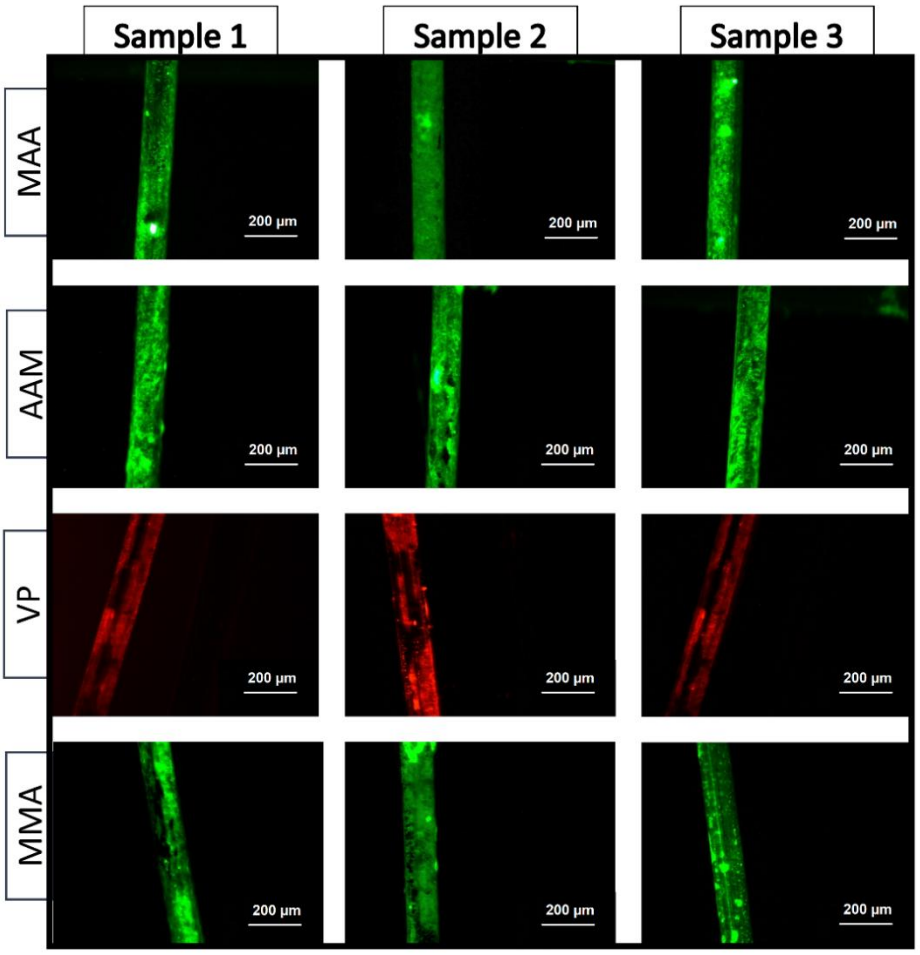

Fig. A3. Fluorescent images of NIP coatings using optimized compositions predicted by the RSM model. Rows from top to bottom show the optimal NIP-MWs synthesized from monomers MAA, AAM, VP, and MMA, respectively. Nile Red with red fluorescent protein (RFP) imaging was used in the recipe with VP as FM, while all other recipes had Rhodamine 110 with a green fluorescent protein (GFP) as a fluorescent dye [149]. *Reprinted with permission from American Chemical Society.*

7.4. Optimization of Complex CIP Compositions using Mixture Design of Experiment (DOE)

The immobilization of more complex MIPs with various FMs was optimized by utilizing a mixture DOE, which is a specific class of RSM. The mixture under study in this DOE comprises a variety of compounds that add up to a constant total [200]. In this method, the quality of the mixture is a function of the proportions of its components, so it is possible to predict the optimal proportions of each compound to get the desired response. The design equation for the performed mixture design can be written as Equation A1:

$$x_1M_1 + x_2M_2 + x_3M_3 + x_4M_4 = 1 \quad ; \qquad 0<x1, x2, x3, x4<1 \tag{A1}$$

Where M_i are the four FMs and x_i, represents the proportional factors.

Fig. A4 demonstrates the contour plots generated from analyzing the results of mixture DOE for the thickness and uniformity. The coefficient of determination (R^2) values obtained by this analysis were 98.41 for thickness, 99.12 for uniformity, and 99.7 for stability, indicating that the mixture model fits the experimental data well.

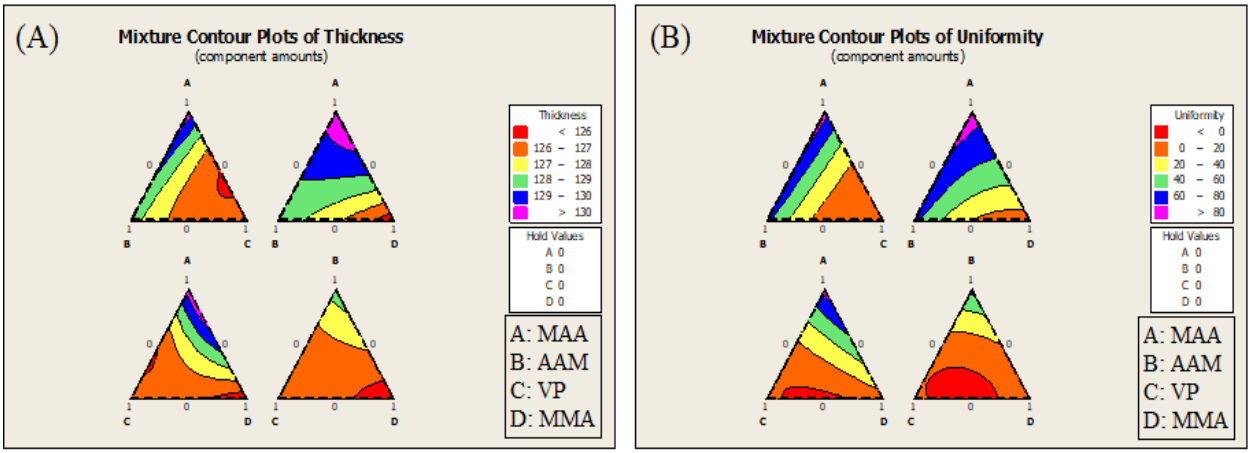

Fig. A4. Contour plots from analysis of the results of mixture DOE for the (A) thickness and (B) uniformity of coating. Contour plots demonstrate a two-dimensional view of the response surface for each triple blend, where all the points with the same responses are connected (contour lines)[149]. *Reprinted with permission from American Chemical Society.*

7.5. Validation of The Mixture Design of Experiment

The mixture analysis was validated by using the response optimization approach to predict the proportions of FMs required for NIP coatings with not only the maximum but also the minimum coating qualities and uniformities. The predicted compositions were tested in three replicates each, as shown in Fig. A5**,** for the best (top row) and the worst (bottom row) multiplexed NIP coating recipes**.**

The results of multiplexed NIP coating experiments were in good agreement with the predictions. Uniform duplex, triplex and quadruplex monomer NIP coatings were successfully achieved on SS-MWs (Fig. 75, top row). Under conditions where the model predicted the least coating qualities, the experiments followed the model and resulted in no NIP coatings on the MWs (Fig. 75, bottom row).

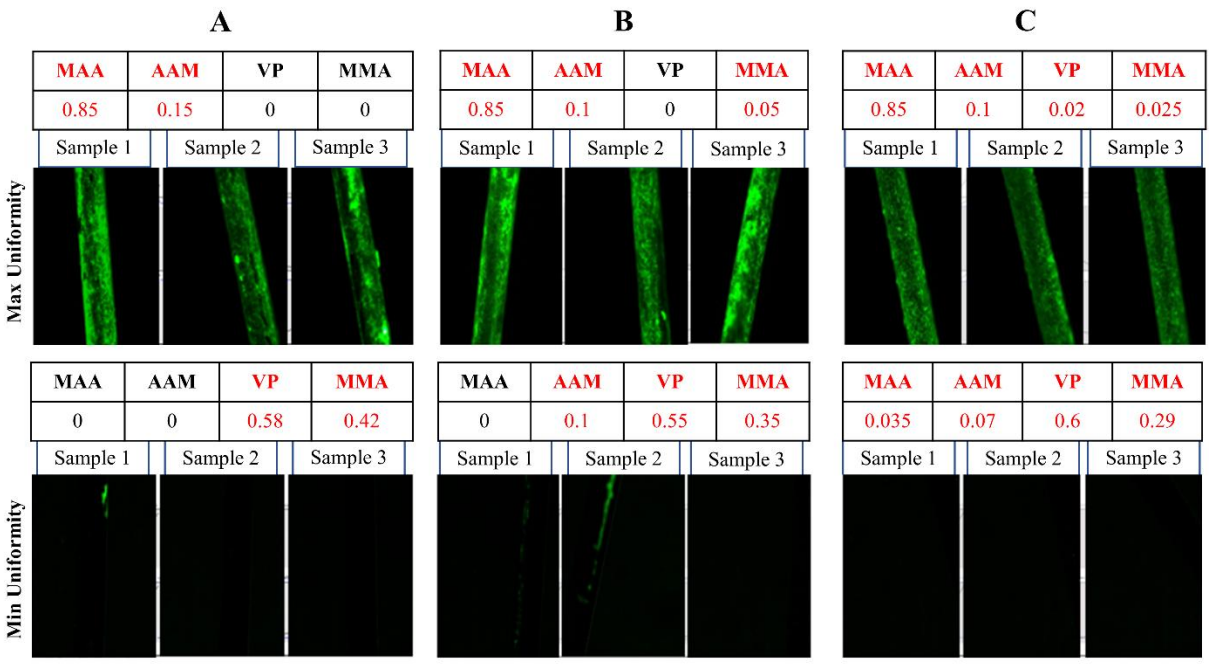

Fig. A5. Fluorescent images of NIP coatings using predicted compositions for validation of mixture model. The top and bottom rows demonstrate the results using suggested compositions for obtaining coatings with the highest and lowest NIP quality and uniformity, respectively. A) two-monomer, B) three-monomer, and C) four-monomer compositions are shown (with three replicates for each case). The tables above the images include the normalized proportions of each functional monomer, i.e., they add up to a constant total of 1[149]. *Reprinted with permission from American Chemical Society.*

7.6. SEM Images of the 4-CIP-MWs Before and After Bacteria Template Removal

Lower magnification SEM images of the 4-CIP-MWs before and after bacteria template removal are shown in Fig. 76, showing the high density and homogeneous distribution of bacterial cavities.

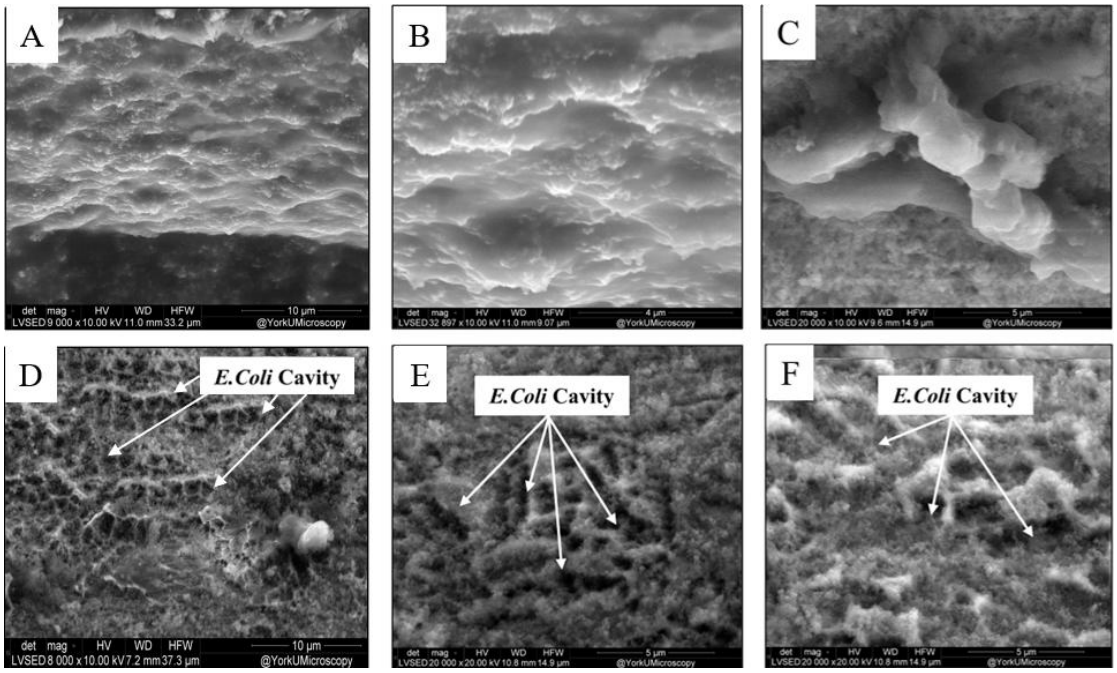

Fig. A6. SEM images of the 4-CIP-MWs before (A-C) and after (D-E) template removal[149]. *Reprinted with permission from American Chemical Society.*

7.7. Trypan Blue Staining

Trypan blue staining was used to examine the viability of bacterial cells after exposure to our CIP preparation recipe. 10 μL of *E. coli* OP50 cells with an initial count of 10^5 CFU/mL were mixed with an equal volume of 0.4% trypan blue and incubated at room temperature for 5 mins. After cleaning a hemocytometer slide and the chamber surface with 70% ethanol, 10 μL of stained cells were placed into the hemocytometer chamber. The microscopic images of the bacterial cells before and after trypan blue staining are shown in Fig. 77, at 40x magnification. The images show that indeed the bacteria die after exposure to our CIP preparation recipe but do not lyse in this process. However, based on the SEM images and the rebinding assays, which show a significant rebinding performance of CIP-MWs compared to NIP-MWs, we believe that the bacteria morphology has not changed significantly after exposure to polymerization conditions. Thus, since

the binding mechanism relies on the complementary shape, the formed cavities on the CIP coatings had a similar shape and size to the dead template bacteria that could rebind to the native cells.

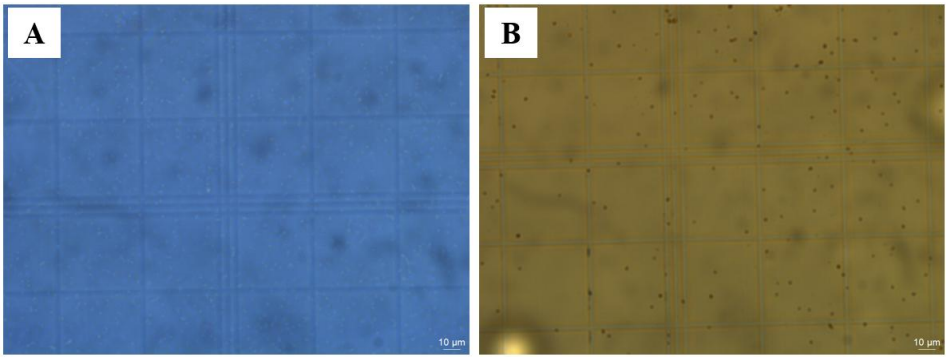

Fig. A7. Trypan Blue staining of bacteria cells before and after exposure to the CIP preparation recipe [149]. *Reprinted with permission from American Chemical Society.*

8. Appendix B

8.1. Effect of Incubation Time on Bacteria Capturing of CIP-MWs Inside the Microfluidic Sensor

The fluorescent images of CIP-MWs in the microfluidic channel after running a GFP-tagged *E. coli* bacteria suspensions at 10^8 CFU/mL in the time intervals of 10, 20, 30 and 40 mins are shown in Fig. B1-A, along with the control experiment performed by running only buffer solution at the same time intervals (Fig. B1-B). It can be seen that by increasing the incubation time to 30 mins, there is a significant increase in the fluorescent signals on the MW's surface while running the bacteria suspension through the sensor. However, the experiments revealed that increasing the incubation time to 40 mins did not significantly increase the fluorescent signal. Images from the control experiment (Fig. B1-B) taken while running the pure buffer confirm that the increase in the fluorescent signal while running bacteria suspension is only due to capturing of GFP bacteria to the CIP-MW.

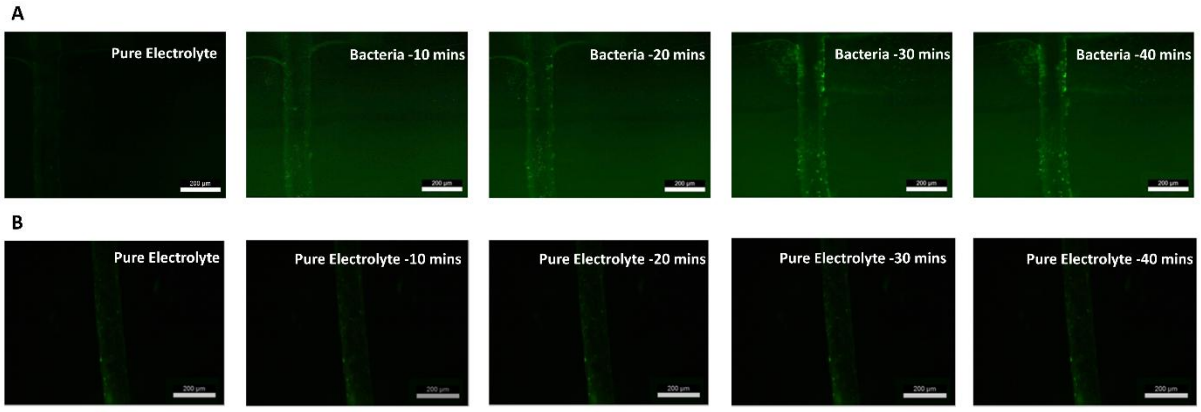

Fig. B1. A) Fluorescent images of CIP-MWs in the microfluidic channel after running buffer (first column) and bacteria suspension in 10 mins intervals. B) Fluorescent images of CIP-MWs by running only buffer solution at the same time intervals (control experiment).

8.2. Determination of Stable and Plateaued Response

The constant of proportionality between the applied current and voltage obtained by the device is resistance. This is dependent on the applied current, step duration for stabilization, type of base solution, wire material, wire coating polymer, and the geometry of the device. These parameters have been kept constant among repeating trials. The device has been characterized for the specific base solution (3ppm saline solution) and geometry identified in the main paper. The response curve (current vs voltage) can be separated into two different sections. The first part (Fig. B2-A) has an exponential increase that is obtained as a result of the instability and very high resistance created at low current application (10 nA). The second component, highlighted in purple, comprises the remaining curve is linear. This linearity translates to a constant resistance value that is expected with a linear increase in current application and is the characterizing metric of the device. Plotting the resistance vs time curve (Fig. B2-B), one can identify the exact moment of resistance stabilization that would result in a clear plateau, expected for the design of this device [167].

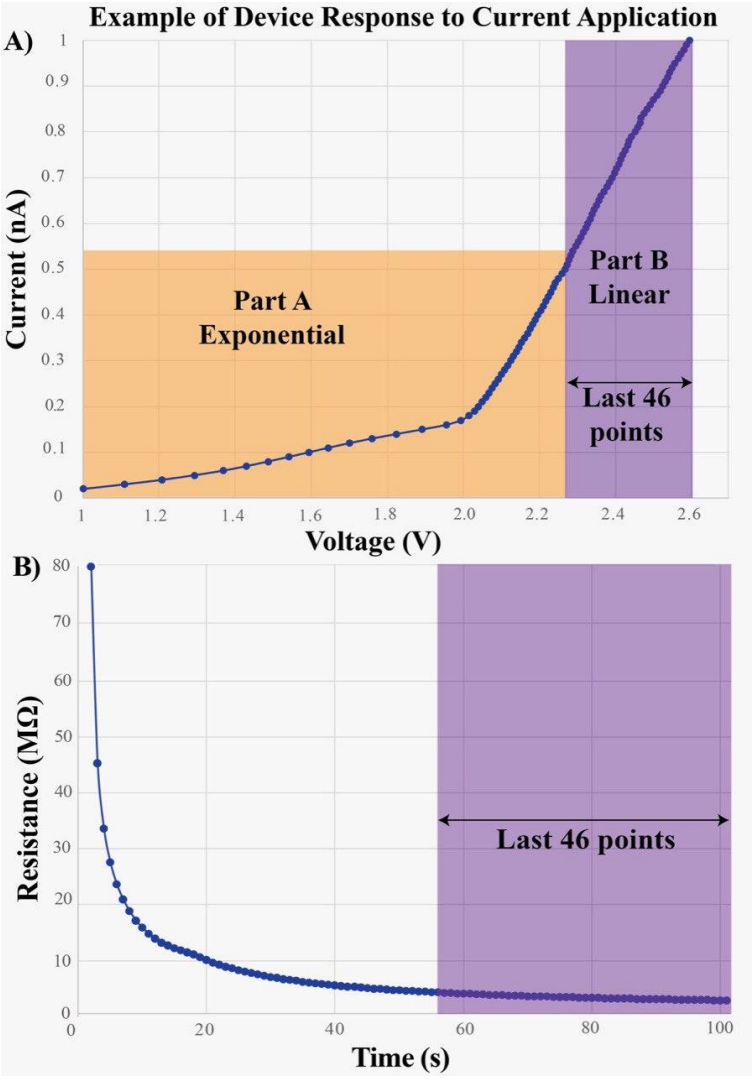

Fig. B2. A) The current vs voltage response obtained on the Kickstart software upon application of current. B) The corresponding resistance response of the device vs time. Highlighted in purple is the plateau region used to determine the resistance of the device.

```
excelFileName = 'Copy of April 21-MIP CONC-PLA.xlsx';
numSheets = 7;%number of sheets
numColumns = 10; % number of columns per page
% Import data from the Excel file
for j=1:numSheets
sheetData = xlsread(excelFileName, j);

%Plot the data set
for i = 1:10
    hold;
plot(sheetData(:, i+1),sheetData(:, 1))
hold;
i=i+1;
end
release;
%Calculate the moving average
% Window size for the moving average
windowSize = 5;

% Initialize an array to store the moving average
movingAverages = zeros(1, 100 - windowSize + 1);
for h=2:numColumns
transposedData = transpose(sheetData(:, h));
% Calculate the moving average
for i = 1:(101 - windowSize + 1)
    window = transposedData(i:i + windowSize - 1);
    movingAverages(i) = mean(window);
end

%Determine if the difference between the consecutive moving average is above of below
% the threshold of 1%.
for i=1:95
    if abs(movingAverages(i)-movingAverages(i+1))/(movingAverages(i))<0.01
      if i+floor(windowSize/2)<30
         i=i+1;
      else
          if i+floor(windowSize+1/2)>56
              fprintf("plateau not reached");
          end
           i+floor(windowSize/2)
        break
       end

    else
        i=i+1;
    end
end
end
```

Fig. B3. MATLAB code used to determine the initial plateau.

References

[1] D. Ivnitski, I. Abdel-Hamid, P. Atanasov, and E. Wilkins, “Biosensors for detection of pathogenic bacteria,” *Biosens. Bioelectron.*, vol. 14, no. 7, pp. 599–624, 1999.

[2] P. Rajapaksha, A. Elbourne, S. Gangadoo, R. Brown, D. Cozzolino, and J. Chapman, “A review of methods for the detection of pathogenic microorganisms,” *Analyst*, vol. 144, no. 2, pp. 396–411, 2019.

[3] S. Hameed, L. Xie, and Y. Ying, “Conventional and emerging detection techniques for pathogenic bacteria in food science: A review,” *Trends Food Sci. Technol.*, vol. 81, pp. 61–73, 2018.

[4] M. Ferone, A. Gowen, S. Fanning, and A. G. M. Scannell, “Microbial detection and identification methods: bench top assays to omics approaches,” *Compr. Rev. Food Sci. Food Saf.*, vol. 19, no. 6, pp. 3106–3129, 2020.

[5] A. Saravanan *et al.*, “Methods of detection of food-borne pathogens: a review,” *Environ. Chem. Lett.*, vol. 19, no. 1, pp. 189–207, 2021.

[6] J. W.-F. Law, N.-S. Ab Mutalib, K.-G. Chan, and L.-H. Lee, “Rapid methods for the detection of foodborne bacterial pathogens: principles, applications, advantages and limitations,” *Front. Microbiol.*, vol. 5, p. 770, 2015.

[7] E. Sheikhzadeh, S. Eissa, A. Ismail, and M. Zourob, “Diagnostic techniques for COVID-19 and new developments,” *Talanta*, vol. 220, no. May, p. 121392, 2020, doi: 10.1016/j.talanta.2020.121392.

[8] V. Sagan *et al.*, “Monitoring inland water quality using remote sensing: potential and limitations of spectral indices, bio-optical simulations, machine learning, and cloud

computing," *Earth-Science Rev.*, vol. 205, p. 103187, 2020, doi: https://doi.org/10.1016/j.earscirev.2020.103187.

[9] S. Kurbanoglu, C. Erkmen, and B. Uslu, "Frontiers in electrochemical enzyme based biosensors for food and drug analysis," *TrAC Trends Anal. Chem.*, vol. 124, p. 115809, 2020, doi: https://doi.org/10.1016/j.trac.2020.115809.

[10] P. Weerathunge *et al.*, "Ultrasensitive colorimetric detection of murine norovirus using NanoZyme aptasensor," *Anal. Chem.*, vol. 91, no. 5, pp. 3270–3276, 2019.

[11] J. Li, J. Shen, and R. Qi, "Electrochemiluminescence sensing platform for microorganism detection," *Biosaf. Heal.*, vol. 4, no. 2, pp. 61–63, 2022, doi: https://doi.org/10.1016/j.bsheal.2022.02.002.

[12] J. Shen, T. Zhou, and R. Huang, "Recent Advances in Electrochemiluminescence Sensors for Pathogenic Bacteria Detection," *Micromachines* , vol. 10, no. 8. 2019. doi: 10.3390/mi10080532.

[13] P. Zhang, Y.-P. Chen, W. Wang, Y. Shen, and J.-S. Guo, "Surface plasmon resonance for water pollutant detection and water process analysis," *TrAC Trends Anal. Chem.*, vol. 85, pp. 153–165, 2016.

[14] E. Elcin and H. A. Öktem, "Whole-cell fluorescent bacterial bioreporter for arsenic detection in water," *Int. J. Environ. Sci. Technol.*, vol. 16, no. 10, pp. 5489–5500, 2019, doi: 10.1007/s13762-018-2077-0.

[15] C. Fricke, H. Harms, and T. Maskow, "Rapid calorimetric detection of bacterial contamination: influence of the cultivation technique," *Front. Microbiol.*, vol. 10, p. 2530, 2019.

[16] E. T. S. G. da Silva, D. E. P. Souto, J. T. C. Barragan, J. de F. Giarola, A. C. M. de

Moraes, and L. T. Kubota, “Electrochemical biosensors in point-of-care devices: recent advances and future trends,” *ChemElectroChem*, vol. 4, no. 4, pp. 778–794, 2017.

[17] T. S. Bedwell and M. J. Whitcombe, “Analytical applications of MIPs in diagnostic assays: future perspectives,” *Anal. Bioanal. Chem.*, vol. 408, no. 7, pp. 1735–1751, 2016, doi: 10.1007/s00216-015-9137-9.

[18] J. Riu and B. Giussani, “Electrochemical biosensors for the detection of pathogenic bacteria in food,” *TrAC Trends Anal. Chem.*, vol. 126, p. 115863, 2020.

[19] N. Razmi, M. Hasanzadeh, M. Willander, and O. Nur, “Recent progress on the electrochemical biosensing of Escherichia coli O157: H7: Material and methods overview,” *Biosensors*, vol. 10, no. 5, p. 54, 2020.

[20] M. Amiri, A. Bezaatpour, H. Jafari, R. Boukherroub, and S. Szunerits, “Electrochemical methodologies for the detection of pathogens,” *ACS sensors*, vol. 3, no. 6, pp. 1069–1086, 2018.

[21] J. Song, M. G. Mauk, B. A. Hackett, S. Cherry, H. H. Bau, and C. Liu, “Instrument-free point-of-care molecular detection of Zika virus,” *Anal. Chem.*, vol. 88, no. 14, pp. 7289–7294, 2016.

[22] S. Afsahi *et al.*, “Novel graphene-based biosensor for early detection of Zika virus infection,” *Biosens. Bioelectron.*, vol. 100, pp. 85–88, 2018.

[23] A. Khoshroo, M. Mavaei, M. Rostami, B. Valinezhad-Saghezi, and A. Fattahi, “Recent advances in electrochemical strategies for bacteria detection,” *BioImpacts BI*, vol. 12, no. 6, p. 567, 2022.

[24] D. Refaat *et al.*, “Strategies for molecular imprinting and the evolution of MIP nanoparticles as plastic antibodies—synthesis and applications,” *Int. J. Mol. Sci.*, vol. 20,

no. 24, 2019, doi: 10.3390/ijms20246304.

[25] J. Xu *et al.*, "Molecularly imprinted polymer nanoparticles as potential synthetic antibodies for immunoprotection against HIV," *ACS Appl. Mater. Interfaces*, vol. 11, no. 10, pp. 9824–9831, 2019.

[26] M. J. Whitcombe *et al.*, "The rational development of molecularly imprinted polymer-based sensors for protein detection," *Chem. Soc. Rev.*, vol. 40, no. 3, pp. 1547–1571, 2011, doi: 10.1039/c0cs00049c.

[27] R. Khan, A. Mohammad, and A. Asiri, *Advanced biosensors for health care applications*. Elsevier, 2019.

[28] Y. eren Saylan, O. Erdem, S. Unal, and A. Denizli, "An alternative medical diagnosis method: biosensors for virus detection," *Biosensors*, vol. 9, no. 2, p. 65, 2019.

[29] G. Guan, B. Liu, Z. Wang, and Z. Zhang, "Imprinting of molecular recognition sites on nanostructures and its applications in chemosensors," *Sensors*, vol. 8, no. 12, pp. 8291–8320, 2008, doi: 10.3390/s8128291.

[30] M. S. Cheng and C.-S. Toh, "Novel biosensing methodologies for ultrasensitive detection of viruses," *Analyst*, vol. 138, no. 21, pp. 6219–6229, 2013.

[31] G. Xing, W. Zhang, N. Li, Q. Pu, and J.-M. Lin, "Recent progress on microfluidic biosensors for rapid detection of pathogenic bacteria," *Chinese Chem. Lett.*, vol. 33, no. 4, pp. 1743–1751, 2022, doi: https://doi.org/10.1016/j.cclet.2021.08.073.

[32] K. I. K. Wang *et al.*, "Toward embedded laboratory automation for smart lab-on-a-chip embryo arrays," *Biosens. Bioelectron.*, vol. 48, pp. 188–196, 2013, doi: 10.1016/j.bios.2013.04.033.

[33] T. Karasu, E. Özgür, and L. Uzun, "MIP-on-a-chip: Artificial receptors on microfluidic

platforms for biomedical applications," *J. Pharm. Biomed. Anal.*, vol. 226, p. 115257, Mar. 2023, doi: 10.1016/J.JPBA.2023.115257.

[34] R. Pol, F. Céspedes, D. Gabriel, and M. Baeza, "Microfluidic lab-on-a-chip platforms for environmental monitoring," *TrAC Trends Anal. Chem.*, vol. 95, pp. 62–68, 2017, doi: https://doi.org/10.1016/j.trac.2017.08.001.

[35] L. N. Thwala, S. C. Ndlovu, K. T. Mpofu, M. Y. Lugongolo, and P. Mthunzi-Kufa, "Nanotechnology-based diagnostics for diseases prevalent in developing countries: current advances in point-of-care tests," *Nanomaterials*, vol. 13, no. 7, p. 1247, 2023.

[36] S. M. Scott and Z. Ali, "Fabrication methods for microfluidic devices: An overview," *Micromachines*, vol. 12, no. 3, p. 319, 2021.

[37] N. Bhattacharjee, A. Urrios, S. Kang, and A. Folch, "The upcoming 3D-printing revolution in microfluidics," *Lab Chip*, vol. 16, no. 10, pp. 1720–1742, 2016, doi: 10.1039/C6LC00163G.

[38] R. Antony, M. S. Giri Nandagopal, N. Sreekumar, and N. Selvaraju, "Detection principles and development of microfluidic sensors in the last decade," *Microsyst. Technol.*, vol. 20, no. 6, pp. 1051–1061, 2014, doi: 10.1007/s00542-014-2165-0.

[39] S. A. Jaywant and K. Mahmood Arif, "A comprehensive review of micro fluidic water quality monitoring sensors," *Sensors (Switzerland)*, vol. 19, no. 21, 2019, doi: 10.3390/s19214781.

[40] G. Vasapollo *et al.*, "Molecularly imprinted polymers: Present and future prospective," *Int. J. Mol. Sci.*, vol. 12, no. 9, pp. 5908–5945, 2011, doi: 10.3390/ijms12095908.

[41] F. Puoci *et al.*, *Molecularly imprinted polymers (PIMs) in biomedical applications*. INTECH Open Access Publisher, 2010.

[42] O. S. Ahmad, T. S. Bedwell, C. Esen, A. Garcia-Cruz, and S. A. Piletsky, “Molecularly imprinted polymers in electrochemical and optical sensors,” *Trends Biotechnol.*, vol. 37, no. 3, pp. 294–309, 2019.

[43] S. Akgönüllü and A. Denizli, “Molecular imprinting-based sensors: Lab-on-chip integration and biomedical applications,” *J. Pharm. Biomed. Anal.*, vol. 225, p. 115213, 2023, doi: https://doi.org/10.1016/j.jpba.2022.115213.

[44] L. Yang, K. Ge, M. F. Qadir, X. Wang, Y. Gu, and Y. Yang, “MIPs-Based Sensors and Biosensors for Environmental Monitoring BT - Molecularly Imprinted Polymers as Artificial Antibodies for the Environmental Health: A Step Towards Achieving the Sustainable Development Goals,” S. Patra and M. Sillanpaa, Eds. Cham: Springer Nature Switzerland, 2024, pp. 167–200. doi: 10.1007/978-3-031-58995-9_7.

[45] X. Zhang *et al.*, “A novel electrochemical sensor based on electropolymerized molecularly imprinted polymer and gold nanomaterials amplification for estradiol detection,” *Sensors Actuators B Chem.*, vol. 200, pp. 69–75, 2014.

[46] F. Breton *et al.*, “Virtual imprinting as a tool to design efficient MIPs for photosynthesis-inhibiting herbicides,” *Biosens. Bioelectron.*, vol. 22, no. 9, pp. 1948–1954, 2007, doi: https://doi.org/10.1016/j.bios.2006.08.017.

[47] S. Rajpal, P. Mishra, and B. Mizaikoff, “Rational in silico design of molecularly imprinted polymers: current challenges and future potential,” *Int. J. Mol. Sci.*, vol. 24, no. 7, p. 6785, 2023.

[48] R. Yu, H. Zhou, M. Li, and Q. Song, “Rational selection of the monomer for molecularly imprinted polymer preparation for selective and sensitive detection of 3-methylindole in water,” *J. Electroanal. Chem.*, vol. 832, no. October 2018, pp. 129–136, 2019, doi:

10.1016/j.jelechem.2018.10.043.

[49] X. Shi, A. Wu, G. Qu, R. Li, and D. Zhang, “Development and characterisation of molecularly imprinted polymers based on methacrylic acid for selective recognition of drugs,” *Biomaterials*, vol. 28, no. 25, pp. 3741–3749, 2007.

[50] J. Fu, L. Chen, J. Li, and Z. Zhang, “Current status and challenges of ion imprinting,” *J. Mater. Chem. A*, vol. 3, no. 26, pp. 13598–13627, 2015.

[51] F. Navarro-Villoslada, B. San Vicente, and M. a C. Moreno-Bondi, “Application of multivariate analysis to the screening of molecularly imprinted polymers for bisphenol A,” *Anal. Chim. Acta*, vol. 504, no. 1, pp. 149–162, 2004.

[52] L. Chen, S. Xu, and J. Li, “Recent advances in molecular imprinting technology: Current status, challenges and highlighted applications,” *Chem. Soc. Rev.*, vol. 40, no. 5, pp. 2922–2942, 2011, doi: 10.1039/c0cs00084a.

[53] T. Wangchareansak, A. Thitithanyanont, D. Chuakheaw, M. P. Gleeson, P. A. Lieberzeit, and C. Sangma, “Influenza A virus molecularly imprinted polymers and their application in virus sub-type classification,” *J. Mater. Chem. B*, vol. 1, no. 16, pp. 2190–2197, 2013, doi: 10.1039/c3tb00027c.

[54] W. Sukjee *et al.*, “An influenza A virus agglutination test using antibody-like polymers,” *J. Biomater. Sci. Polym. Ed.*, vol. 28, no. 15, pp. 1786–1795, 2017, doi: 10.1080/09205063.2017.1338503.

[55] T. Wangchareansak, A. Thitithanyanont, D. Chuakheaw, M. P. Gleeson, P. A. Lieberzeit, and C. Sangma, “A novel approach to identify molecular binding to the influenza virus H5N1: Screening using molecularly imprinted polymers (MIPs),” *Medchemcomm*, vol. 5, no. 5, pp. 617–621, 2014, doi: 10.1039/c3md00272a.

[56] C. Sangma, P. A. Lieberzeit, and W. Sukjee, “H5N1 virus plastic antibody based on molecularly imprinted polymers,” in *Synthetic Antibodies*, Springer, 2017, pp. 381–388.

[57] B. Sellergren, “Polymer-and template-related factors influencing the efficiency in molecularly imprinted solid-phase extractions,” *TrAC Trends Anal. Chem.*, vol. 18, no. 3, pp. 164–174, 1999.

[58] L. Ye, R. Weiss, and K. Mosbach, “Synthesis and characterization of molecularly imprinted microspheres,” *Macromolecules*, vol. 33, no. 22, pp. 8239–8245, 2000.

[59] K. Yoshimatsu, K. Reimhult, A. Krozer, K. Mosbach, K. Sode, and L. Ye, “Uniform molecularly imprinted microspheres and nanoparticles prepared by precipitation polymerization: The control of particle size suitable for different analytical applications,” *Anal. Chim. Acta*, vol. 584, no. 1, pp. 112–121, 2007.

[60] L. Chen, X. Wang, W. Lu, X. Wu, and J. Li, “Molecular imprinting: perspectives and applications,” *Chem. Soc. Rev.*, vol. 45, no. 8, pp. 2137–2211, 2016, doi: 10.1039/C6CS00061D.

[61] E. Abdollahi, A. Khalafi-Nezhad, A. Mohammadi, M. Abdouss, and M. Salami-Kalajahi, “Synthesis of new molecularly imprinted polymer via reversible addition fragmentation transfer polymerization as a drug delivery system,” *Polymer (Guildf).*, vol. 143, pp. 245–257, 2018, doi: 10.1016/j.polymer.2018.03.058.

[62] M. D. Attieh, “Enzymatically initiated synthesis of biomimetic receptors based on molecularly imprinted polymers by free radical polymerization.” Université de Technologie de Compiègne; Université Libanaise, 2016.

[63] A. Biffis, G. Dvorakova, and A. Falcimaigne-Cordin, “Physical forms of MIPs,” *Mol. Imprinting*, pp. 29–82, 2012.

[64] M. Włoch and J. Datta, “Synthesis and polymerisation techniques of molecularly imprinted polymers,” in *Comprehensive analytical chemistry*, vol. 86, Elsevier, 2019, pp. 17–40.

[65] A. A. Malik, C. Nantasenamat, and T. Piacham, “Molecularly imprinted polymer for human viral pathogen detection,” *Mater. Sci. Eng. C*, vol. 77, pp. 1341–1348, 2017.

[66] S. Klangprapan, B. Choke-arpornchai, P. A. Lieberzeit, and K. Choowongkomon, “Sensing the classical swine fever virus with molecularly imprinted polymer on quartz crystal microbalance,” *Heliyon*, vol. 6, no. 6, p. e04137, 2020, doi: 10.1016/j.heliyon.2020.e04137.

[67] D.-F. Tai, C.-Y. Lin, T.-Z. Wu, J.-H. Huang, and P.-Y. Shu, “Artificial receptors in serologic tests for the early diagnosis of dengue virus infection,” *Clin. Chem.*, vol. 52, no. 8, pp. 1486–1491, 2006.

[68] D.-F. Tai, C.-Y. Lin, T.-Z. Wu, and L.-K. Chen, “Recognition of dengue virus protein using epitope-mediated molecularly imprinted film,” *Anal. Chem.*, vol. 77, no. 16, pp. 5140–5143, 2005.

[69] K. K. Dar, S. Shao, T. Tan, and Y. Lv, “Molecularly imprinted polymers for the selective recognition of microorganisms,” *Biotechnol. Adv.*, vol. 45, no. July, p. 107640, 2020, doi: 10.1016/j.biotechadv.2020.107640.

[70] A.-M. Poller, E. Spieker, P. A. Lieberzeit, and C. Preininger, “Surface Imprints: Advantageous Application of Ready2use Materials for Bacterial Quartz-Crystal Microbalance Sensors,” *ACS Appl. Mater. Interfaces*, vol. 9, no. 1, pp. 1129–1135, Jan. 2017, doi: 10.1021/acsami.6b13888.

[71] J. Pan, X. Xue, J. Wang, H. Xie, and Z. Wu, “Recognition property and preparation of

Staphylococcus aureus protein A-imprinted polyacrylamide polymers by inverse-phase suspension and bulk polymerization," *Polymer (Guildf).*, vol. 50, no. 11, pp. 2365–2372, 2009, doi: https://doi.org/10.1016/j.polymer.2009.04.004.

[72] Y. Long *et al.*, "Novel polymeric nanoparticles targeting the lipopolysaccharides of Pseudomonas aeruginosa," *Int. J. Pharm.*, vol. 502, no. 1, pp. 232–241, 2016, doi: https://doi.org/10.1016/j.ijpharm.2016.02.021.

[73] N. Gupta, K. Shah, and M. Singh, "An epitope-imprinted piezoelectric diagnostic tool for Neisseria meningitidis detection," *J. Mol. Recognit.*, vol. 29, no. 12, pp. 572–579, Dec. 2016, doi: https://doi.org/10.1002/jmr.2557.

[74] C. Liang *et al.*, "A virus-MIPs fluorescent sensor based on FRET for highly sensitive detection of JEV," *Talanta*, vol. 160, pp. 360–366, 2016.

[75] K. He *et al.*, "Highly selective recognition and fluorescent detection of JEV via virus-imprinted magnetic silicon microspheres," *Sensors Actuators B Chem.*, vol. 233, pp. 607–614, 2016.

[76] C.-H. Lu *et al.*, "Sensing HIV related protein using epitope imprinted hydrophilic polymer coated quartz crystal microbalance," *Biosens. Bioelectron.*, vol. 31, no. 1, pp. 439–444, 2012.

[77] B. Yang, H. Gong, C. Chen, X. Chen, and C. Cai, "A virus resonance light scattering sensor based on mussel-inspired molecularly imprinted polymers for high sensitive and high selective detection of Hepatitis A Virus," *Biosens. Bioelectron.*, vol. 87, pp. 679–685, 2017.

[78] L. Uzun, R. Say, S. □nal, and A. Denizli, "Hepatitis B surface antibody purification with hepatitis B surface antibody imprinted poly (hydroxyethyl methacrylate-N-methacryloyl-l-

tyrosine methyl ester) particles," *J. Chromatogr. B*, vol. 877, no. 3, pp. 181–188, 2009.

[79] Z. Altintas, J. Pocock, K.-A. Thompson, and I. E. Tothill, "Comparative investigations for adenovirus recognition and quantification: Plastic or natural antibodies?," *Biosens. Bioelectron.*, vol. 74, pp. 996–1004, 2015.

[80] M. Jenik *et al.*, "Sensing picornaviruses using molecular imprinting techniques on a quartz crystal microbalance," *Anal. Chem.*, vol. 81, no. 13, pp. 5320–5326, 2009.

[81] A. Aherne, C. Alexander, M. J. Payne, N. Perez, and E. N. Vulfson, "Bacteria-mediated lithography of polymer surfaces," *J. Am. Chem. Soc.*, vol. 118, no. 36, pp. 8771–8772, 1996.

[82] C. Alexander and E. N. Vulfson, "Spatially functionalized polymer surfaces produced via cell mediated lithography." Wiley Online Library, 1997.

[83] S. D. Harvey *et al.*, "Preparation and evaluation of spore-specific affinity-augmented bio-imprinted beads," *Anal. Bioanal. Chem.*, vol. 386, no. 2, pp. 211–219, 2006.

[84] T. Zhou, X. Shen, S. Chaudhary, and L. Ye, "Molecularly imprinted polymer beads prepared by Pickering emulsion polymerization for steroid recognition," *J. Appl. Polym. Sci.*, vol. 131, no. 1, 2014.

[85] T. Zhou, K. Zhang, T. Kamra, L. Bülow, and L. Ye, "Preparation of protein imprinted polymer beads by Pickering emulsion polymerization," *J. Mater. Chem. B*, vol. 3, no. 7, pp. 1254–1260, 2015.

[86] X. Shen *et al.*, "Bacterial imprinting at Pickering emulsion interfaces," *Angew. Chemie Int. Ed.*, vol. 53, no. 40, pp. 10687–10690, 2014.

[87] M. Darder *et al.*, "Algae–silica systems as functional hybrid materials," *J. Mater. Chem.*, vol. 20, no. 42, pp. 9362–9369, 2010.

[88] M. Jia, Z. Zhang, J. Li, X. Ma, L. Chen, and X. Yang, “Molecular imprinting technology for microorganism analysis,” *TrAC Trends Anal. Chem.*, vol. 106, pp. 190–201, 2018.

[89] S. A. Zaidi, “Bacterial Imprinting Methods and Their Applications: An Overview,” *Crit. Rev. Anal. Chem.*, pp. 1–10, 2020.

[90] O. Hayden and F. L. Dickert, “Selective microorganism detection with cell surface imprinted polymers,” *Adv. Mater.*, vol. 13, no. 19, pp. 1480–1483, 2001.

[91] F. L. Dickert and O. Hayden, “Bioimprinting of polymers and sol- gel phases. Selective detection of yeasts with imprinted polymers,” *Anal. Chem.*, vol. 74, no. 6, pp. 1302–1306, 2002.

[92] M.-H. Lee, J. L. Thomas, M.-H. Li, C.-P. Shih, J.-S. Jan, and H.-Y. Lin, “Recognition of Rhodobacter sphaeroides by microcontact-imprinted poly (ethylene-co-vinyl alcohol),” *Colloids Surfaces B Biointerfaces*, vol. 135, pp. 394–399, 2015.

[93] T. Cohen, J. Starosvetsky, U. Cheruti, and R. Armon, “Whole cell imprinting in sol-gel thin films for bacterial recognition in liquids: Macromolecular fingerprinting,” *Int. J. Mol. Sci.*, vol. 11, no. 4, pp. 1236–1252, 2010.

[94] K. Fu *et al.*, “Rapid and selective recognition of Vibrio parahaemolyticus assisted by perfluorinated alkoxysilane modified molecularly imprinted polymer film,” *RSC Adv.*, vol. 10, no. 24, pp. 14305–14312, 2020.

[95] J. Pan, W. Chen, Y. Ma, and G. Pan, “Molecularly imprinted polymers as receptor mimics for selective cell recognition,” *Chem. Soc. Rev.*, vol. 47, no. 15, pp. 5574–5587, 2018, doi: 10.1039/c7cs00854f.

[96] X. Xie, Y. Bu, and S. Wang, “Molecularly imprinting: a tool of modern chemistry for analysis and monitoring of phenolic environmental estrogens,” *Rev. Anal. Chem.*, vol. 35,

no. 2, pp. 87–97, 2016.

[97] N. Idil, M. Hedstrm, A. Denizli, and B. Mattiasson, “Whole cell based microcontact imprinted capacitive biosensor for the detection of Escherichia coli,” *Biosens. Bioelectron.*, vol. 87, pp. 807–815, 2017.

[98] S. Pardeshi and S. K. Singh, “Precipitation polymerization: a versatile tool for preparing molecularly imprinted polymer beads for chromatography applications,” *Rsc Adv.*, vol. 6, no. 28, pp. 23525–23536, 2016.

[99] Y. Saylan and A. Denizli, “Molecularly imprinted polymer-based microfluidic systems for point-of-care applications,” *Micromachines*, vol. 10, no. 11, p. 766, 2019.

[100] B. Regan, F. Boyle, R. O’Kennedy, and D. Collins, “Evaluation of molecularly imprinted polymers for point-of-care testing for cardiovascular disease,” *Sensors*, vol. 19, no. 16, p. 3485, 2019.

[101] K. Takimoto, E. Takano, Y. Kitayama, and T. Takeuchi, “Synthesis of monodispersed submillimeter-sized molecularly imprinted particles selective for human serum albumin using inverse suspension polymerization in water-in-oil emulsion prepared using microfluidics,” *Langmuir*, vol. 31, no. 17, pp. 4981–4987, 2015.

[102] C.-C. Hong, C.-P. Chen, J.-C. Horng, and S.-Y. Chen, “Point-of-care protein sensing platform based on immuno-like membrane with molecularly-aligned nanocavities,” *Biosens. Bioelectron.*, vol. 50, pp. 425–430, 2013.

[103] E. Kellens *et al.*, “Micro-patterned molecularly imprinted polymer structures on functionalized diamond-coated substrates for testosterone detection,” *Biosens. Bioelectron.*, vol. 118, pp. 58–65, 2018, doi: https://doi.org/10.1016/j.bios.2018.07.032.

[104] R. Schirhagl, J. Qian, and F. L. Dickert, “Immunosensing with artificial antibodies in

organic solvents or complex matrices," *Sensors Actuators B Chem.*, vol. 173, pp. 585–590, 2012.

[105] S. Harz, M. Schimmelpfennig, B. Tse Sum Bui, N. Marchyk, K. Haupt, and K. Feller, "Fluorescence optical spectrally resolved sensor based on molecularly imprinted polymers and microfluidics," *Eng. Life Sci.*, vol. 11, no. 6, pp. 559–565, 2011.

[106] J. Liu *et al.*, "Electrochemical microfluidic chip based on molecular imprinting technique applied for therapeutic drug monitoring," *Biosens. Bioelectron.*, vol. 91, pp. 714–720, 2017.

[107] P. S. Sharma *et al.*, "Synthesis and application of a 'plastic antibody' in electrochemical microfluidic platform for oxytocin determination," *Biosens. Bioelectron.*, vol. 100, pp. 251–258, 2018.

[108] C.-C. Hong, C.-C. Lin, C.-L. Hong, Z.-X. Lin, M.-H. Chung, and P.-W. Hsieh, "Handheld analyzer with on-chip molecularly-imprinted biosensors for electrical detection of propofol in plasma samples," *Biosens. Bioelectron.*, vol. 86, pp. 623–629, 2016.

[109] G. M. Birnbaumer *et al.*, "Detection of viruses with molecularly imprinted polymers integrated on a microfluidic biochip using contact-less dielectric microsensors," *Lab Chip*, vol. 9, no. 24, pp. 3549–3556, 2009.

[110] S. Ansari and S. Masoum, "Molecularly imprinted polymers for capturing and sensing proteins: Current progress and future implications," *TrAC Trends Anal. Chem.*, vol. 114, pp. 29–47, 2019.

[111] Z. Iskierko, P. S. Sharma, K. Bartold, A. Pietrzyk-Le, K. Noworyta, and W. Kutner, "Molecularly imprinted polymers for separating and sensing of macromolecular compounds and microorganisms," *Biotechnol. Adv.*, vol. 34, no. 1, pp. 30–46, 2016.

[112] K. Ren and R. N. Zare, “Chemical Recognition in Cell-Imprinted Polymers,” *ACS Nano*, vol. 6, no. 5, pp. 4314–4318, May 2012, doi: 10.1021/nn300901z.

[113] R. Schirhagl, E. W. Hall, I. Fuereder, and R. N. Zare, “Separation of Bacteria with Imprinted Polymeric Films,” *Analyst*, vol. 137, p. 1495, 2012.

[114] A. R. Koohpaei, S. J. Shahtaheri, M. R. Ganjali, A. R. Forushani, and F. Golbabaei, “Application of multivariate analysis to the screening of molecularly imprinted polymers (MIPs) for ametryn,” *Talanta*, vol. 75, no. 4, pp. 978–986, 2008.

[115] C. Herdes and L. Sarkisov, “Computer simulation of volatile organic compound adsorption in atomistic models of molecularly imprinted polymers,” *Langmuir*, vol. 25, no. 9, pp. 5352–5359, 2009.

[116] M. Valtchev, B. S. Palm, M. Schiller, and U. Steinfeld, “Development of sulfamethoxazole-imprinted polymers for the selective extraction from waters,” *J. Hazard. Mater.*, vol. 170, no. 2–3, pp. 722–728, 2009.

[117] O. Hayden, R. Bindeus, C. Hadersp□ck, K.-J. Mann, B. Wirl, and F. L. Dickert, “Mass-sensitive detection of cells, viruses and enzymes with artificial receptors,” *Sensors Actuators B Chem.*, vol. 91, no. 1–3, pp. 316–319, 2003.

[118] X. Hu *et al.*, “Molecularly imprinted polymer coated on stainless steel fiber for solid-phase microextraction of chloroacetanilide herbicides in soybean and corn,” *J. Chromatogr. A*, vol. 1217, no. 38, pp. 5875–5882, 2010, doi: https://doi.org/10.1016/j.chroma.2010.07.011.

[119] Y. Hu, Y. Wang, X. Chen, Y. Hu, and G. Li, “A novel molecularly imprinted solid-phase microextraction fiber coupled with high performance liquid chromatography for analysis of trace estrogens in fishery samples,” *Talanta*, vol. 80, no. 5, pp. 2099–2105, 2010, doi:

10.1016/j.talanta.2009.11.015.

[120] X. Hu, G. Dai, J. Huang, H. Jin, Y. Yu, and Y. Liang, “Preparation and Characterization of Metolachlor Molecularly Imprinted Polymer Coating on Stainless Steel Fibers for Solid-Phase Microextraction,” *Anal. Lett.*, vol. 44, no. 7, pp. 1358–1370, May 2011, doi: 10.1080/00032719.2010.511743.

[121] H. Shaikh, N. Memon, M. I. Bhanger, S. M. Nizamani, and A. Denizli, “Core-shell molecularly imprinted polymer-based solid-phase microextraction fiber for ultra trace analysis of endosulfan I and II in real aqueous matrix through gas chromatography-micro electron capture detector,” *J. Chromatogr. A*, vol. 1337, pp. 179–187, 2014, doi: 10.1016/j.chroma.2014.02.035.

[122] T. Zhao, X. Guan, W. Tang, Y. Ma, and H. Zhang, “Preparation of temperature sensitive molecularly imprinted polymer for solid-phase microextraction coatings on stainless steel fiber to measure ofloxacin,” *Anal. Chim. Acta*, vol. 853, pp. 668–675, 2015.

[123] R. Mirzajani and F. Kardani, “Fabrication of ciprofloxacin molecular imprinted polymer coating on a stainless steel wire as a selective solid-phase microextraction fiber for sensitive determination of fluoroquinolones in biological fluids and tablet formulation using HPLC-UV detection,” *J. Pharm. Biomed. Anal.*, vol. 122, pp. 98–109, 2016, doi: 10.1016/j.jpba.2016.01.046.

[124] J. Ma, X. Huang, and S. Wei, “Preparation and application of chlorpyrifos molecularly imprinted solid-phase microextraction probes for the residual determination of organophosphorous pesticides in fresh and dry foods,” *J. Sep. Sci.*, vol. 41, no. 15, pp. 3152–3162, 2018.

[125] Y. Lu, L. Lü, J. He, and T. Zhao, “Preparation of hydrophilic molecularly imprinted solid-

phase microextraction fiber for the selective removal and extraction of trace tetracyclines residues in animal derived foods," *J. Sep. Sci.*, vol. 43, no. 11, pp. 2172–2179, 2020.

[126] S. Ilyas, A. E. Simonson, and W. Asghar, "Emerging point-of-care technologies for sickle cell disease diagnostics," *Clin. Chim. Acta*, vol. 501, pp. 85–91, 2020.

[127] K. Chon, J. Moon, S. Kim, S.-D. Kim, and J. Cho, "Bio-particle separation using microfluidic porous plug for environmental monitoring," *Desalination*, vol. 202, no. 1–3, pp. 215–223, 2007.

[128] X. Mei, J. Yang, X. Yu, Z. Peng, G. Zhang, and Y. Li, "Wearable molecularly imprinted electrochemical sensor with integrated nanofiber-based microfluidic chip for in situ monitoring of cortisol in sweat," *Sensors Actuators B Chem.*, vol. 381, p. 133451, 2023.

[129] K. Raj M and S. Chakraborty, "PDMS microfluidics: A mini review," *J. Appl. Polym. Sci.*, vol. 137, no. 27, p. 48958, 2020.

[130] O. Erkmen, "Practice 4 - Pure culture techniques," O. B. T.-L. P. in M. Erkmen, Ed. Academic Press, 2021, pp. 41–50. doi: https://doi.org/10.1016/B978-0-323-91017-0.00002-0.

[131] A. C. Ogodo, D. I. Agwaranze, M. Daji, and R. E. Aso, "Chapter 13 - Microbial techniques and methods: basic techniques and microscopy," C. Egbuna, K. C. Patrick-Iwuanyanwu, M. A. Shah, J. C. Ifemeje, and A. B. T.-A. T. in B. Rasul, Eds. Academic Press, 2022, pp. 201–220. doi: https://doi.org/10.1016/B978-0-12-822654-4.00003-8.

[132] S. E. DeVilbiss, M. K. Steele, L.-A. H. Krometis, and B. D. Badgley, "Freshwater salinization increases survival of Escherichia coli and risk of bacterial impairment," *Water Res.*, vol. 191, p. 116812, 2021.

[133] Y. Meride and B. Ayenew, "Drinking water quality assessment and its effects on residents

health in Wondo genet campus, Ethiopia," *Environ. Syst. Res.*, vol. 5, no. 1, pp. 1–7, 2016.

[134] M. Kutz, *Applied plastics engineering handbook: processing and materials*. William Andrew, 2011.

[135] B. N. Miles, A. P. Ivanov, K. A. Wilson, F. Dogan, D. Japrung, and J. B. Edel, "Single molecule sensing with solid-state nanopores: Novel materials, methods, and applications," *Chem. Soc. Rev.*, vol. 42, no. 1, pp. 15–28, 2013, doi: 10.1039/c2cs35286a.

[136] M. L. McHugh, "Multiple comparison analysis testing in ANOVA.," *Biochem. medica*, vol. 21, no. 3, pp. 203–209, 2011, doi: 10.11613/bm.2011.029.

[137] S. Akhtarian, A. Doostmohammadi, D.-E. Archonta, G. Kraft, S. K. Brar, and P. Rezai, "Microfluidic Sensor Based on Cell-Imprinted Polymer-Coated Microwires for Conductometric Detection of Bacteria in Water," *Biosensors*, vol. 13, no. 10, p. 943, 2023.

[138] S. Akhtarian, S. Kaur Brar, and P. Rezai, "Electrochemical Impedance Spectroscopy-Based Microfluidic Biosensor Using Cell-Imprinted Polymers for Bacteria Detection," *Biosensors*, vol. 14, no. 9. 2024. doi: 10.3390/bios14090445.

[139] P. E. McKnight and J. Najab, "Mann-Whitney U Test," *The Corsini Encyclopedia of Psychology*. p. 1, Jan. 30, 2010. doi: https://doi.org/10.1002/9780470479216.corpsy0524.

[140] R. Wang *et al.*, "Rapid, sensitive and label-free detection of pathogenic bacteria using a bacteria-imprinted conducting polymer film-based electrochemical sensor," *Talanta*, vol. 226, p. 122135, 2021, doi: https://doi.org/10.1016/j.talanta.2021.122135.

[141] T. Sajini and B. Mathew, "A brief overview of molecularly imprinted polymers: highlighting computational design, nano and photo-responsive imprinting," *Talanta Open*, vol. 4, p. 100072, 2021.

[142] E. Caro, N. Masqué, R. M. Marcé, F. Borrull, P. A. G. Cormack, and D. C. Sherrington,

"Non-covalent and semi-covalent molecularly imprinted polymers for selective on-line solid-phase extraction of 4-nitrophenol from water samples," *J. Chromatogr. A*, vol. 963, no. 1–2, pp. 169–178, 2002.

[143] J. Zhang, Y. Wang, and X. Lu, "Molecular imprinting technology for sensing foodborne pathogenic bacteria," *Anal. Bioanal. Chem.*, vol. 413, no. 18, pp. 4581–4598, 2021, doi: 10.1007/s00216-020-03138-x.

[144] D. R. Kryscio and N. A. Peppas, "Critical review and perspective of macromolecularly imprinted polymers," *Acta Biomater.*, vol. 8, no. 2, pp. 461–473, 2012.

[145] E. Spieker and P. A. Lieberzeit, "Molecular Imprinting Studies for Developing QCM-sensors for Bacillus Cereus," *Procedia Eng.*, vol. 168, pp. 561–564, 2016, doi: https://doi.org/10.1016/j.proeng.2016.11.525.

[146] P. A. Levin and E. R. Angert, "Small but mighty: cell size and bacteria," *Cold Spring Harb. Perspect. Biol.*, vol. 7, no. 7, p. a019216, 2015.

[147] PubChem, "PubChem Compound Summary for CID 4093, Methacrylic acid," *National Center for Biotechnology Information*.

[148] PubChem, "PubChem Compound Summary for CID 6579, Acrylamide," *National Center for Biotechnology Information*.

[149] S. Akhtarian, A. Doostmohammadi, K. Youssef, G. Kraft, S. Kaur Brar, and P. Rezai, "Metal Microwires Functionalized with Cell-Imprinted Polymer for Capturing Bacteria in Water," *ACS Appl. Polym. Mater.*, vol. 5, no. 5, pp. 3235–3246, 2023.

[150] X. Hu, J. Pan, Y. Hu, Y. Huo, and G. Li, "Preparation and evaluation of solid-phase microextraction fiber based on molecularly imprinted polymers for trace analysis of tetracyclines in complicated samples," *J. Chromatogr. A*, vol. 1188, no. 2, pp. 97–107,

2008, doi: 10.1016/j.chroma.2008.02.062.

[151] X. Hu, J. Pan, Y. Hu, and G. Li, “Preparation and evaluation of propranolol molecularly imprinted solid-phase microextraction fiber for trace analysis of β-blockers in urine and plasma samples,” *J. Chromatogr. A*, vol. 1216, no. 2, pp. 190–197, 2009.

[152] X. Hu, Y. Hu, and G. Li, “Preparation and Characterization of Prometryn Molecularly Imprinted Solid-Phase Microextraction Fibers,” *Anal. Lett.*, vol. 40, no. 4, pp. 645–660, Mar. 2007, doi: 10.1080/00032710600966127.

[153] M. Tayefi, M. Razavi-Nouri, and A. Sabet, “Using conmicroorganismed mixture design method for optimizing the properties of organoclay filled ethylene-octene copolymer nanocomposites,” *Mater. Res. Express*, vol. 7, no. 1, 2019, doi: 10.1088/2053-1591/ab61aa.

[154] N. Perez Moral and A. G. Mayes, “Molecularly imprinted multi layer core shell nanoparticles a surface grafting approach,” *Macromol. Rapid Commun.*, vol. 28, no. 22, pp. 2170–2175, 2007.

[155] N. Yasmeen, M. Etienne, P. S. Sharma, S. El-Kirat-Chatel, M. B. Hel□, and W. Kutner, “Molecularly imprinted polymer as a synthetic receptor mimic for capacitive impedimetric selective recognition of Escherichia coli K-12,” *Anal. Chim. Acta*, vol. 1188, p. 339177, 2021.

[156] Z. She, K. Topping, M. H. Shamsi, N. Wang, N. W. C. Chan, and H.-B. Kraatz, “Investigation of the utility of complementary electrochemical detection techniques to examine the in vitro affinity of bacterial flagellins for a toll-like receptor 5 biosensor,” *Anal. Chem.*, vol. 87, no. 8, pp. 4218–4224, 2015.

[157] Y. eren Saylan, O. Erdem, N. Cihangir, and A. Denizli, “Detecting fingerprints of

waterborne bacteria on a sensor," *Chemosensors*, vol. 7, no. 3, p. 33, 2019.

[158] S. L. Walker, J. E. Hill, J. A. Redman, and M. Elimelech, "Influence of growth phase on adhesion kinetics of Escherichia coli D21g," *Appl. Environ. Microbiol.*, vol. 71, no. 6, pp. 3093–3099, 2005.

[159] A. Doostmohammadi, K. Youssef, S. Akhtarian, G. Kraft, S. K. Brar, and P. Rezai, "Polymer Molecularly Imprinted Polymer (MIP) Based Core-Shell Microspheres for Bacteria Isolation," *Polymer (Guildf).*, 2021.

[160] S. Shahriari, M. Monajjemi, and K. Zare, "Increasing the efficiency of some antibiotics on penetrating bacteria cell membrane," *Ukr. J. Ecol.*, vol. 8, no. 1, pp. 671–679, 2018.

[161] A. Ahmed, J. V Rushworth, N. A. Hirst, and P. A. Millner, "Biosensors for whole-cell bacterial detection," *Clin. Microbiol. Rev.*, vol. 27, no. 3, pp. 631–646, 2014.

[162] R. Arreguin-Campos *et al.*, "Biomimetic sensing of Escherichia coli at the solid-liquid interface: From surface-imprinted polymer synthesis toward real sample sensing in food safety," *Microchem. J.*, vol. 169, p. 106554, 2021, doi: https://doi.org/10.1016/j.microc.2021.106554.

[163] N. L. Bragazzi, D. Amicizia, D. Panatto, D. Tramalloni, I. Valle, and R. Gasparini, "Chapter Six - Quartz-Crystal Microbalance (QCM) for Public Health: An Overview of Its Applications," vol. 101, R. B. T.-A. in P. C. and S. B. Donev, Ed. Academic Press, 2015, pp. 149–211. doi: https://doi.org/10.1016/bs.apcsb.2015.08.002.

[164] T. A. Sergeyeva, S. A. Piletsky, A. A. Brovko, E. A. Slinchenko, L. M. Sergeeva, and A. V El'Skaya, "Selective recognition of atrazine by molecularly imprinted polymer membranes. Development of conductometric sensor for herbicides detection," *Anal. Chim. Acta*, vol. 392, no. 2–3, pp. 105–111, 1999.

[165] H. Noh *et al.*, “Precise evaluation of liquid conductivity using a multi-channel microfluidic chip and direct-current resistance measurements,” *Sensors Actuators B Chem.*, vol. 297, p. 126810, 2019.

[166] J. K. Park, J. C. Ryu, W. K. Kim, and K. H. Kang, “Effect of electric field on electrical conductivity of dielectric liquids mixed with polar additives: DC conductivity,” *J. Phys. Chem. B*, vol. 113, no. 36, pp. 12271–12276, 2009.

[167] M. J. Farshchi Heydari, N. Tabatabaei, and P. Rezai, “Low-Cost Resistive Microfluidic Salinity Sensor for High-Precision Detection of Drinking Water Salt Levels,” *ACS Omega*, vol. 7, no. 18, pp. 15529–15539, May 2022, doi: 10.1021/acsomega.2c00268.

[168] A. Ostovan *et al.*, “Greenificated molecularly imprinted materials for advanced applications,” *Adv. Mater.*, vol. 34, no. 42, p. 2203154, 2022.

[169] K. A. Charles and N. O. Matthew, *Fundamentals of electric circuits*. McGraw-hill Education, 2017.

[170] L. Xu, P. C. Ivanov, K. Hu, Z. Chen, A. Carbone, and H. E. Stanley, “Quantifying signals with power-law correlations: A comparative study of detrended fluctuation analysis and detrended moving average techniques,” *Phys. Rev. E*, vol. 71, no. 5, p. 51101, 2005.

[171] S. Tokonami *et al.*, “Label-free and selective bacteria detection using a film with transferred bacterial configuration,” *Anal. Chem.*, vol. 85, no. 10, pp. 4925–4929, 2013.

[172] S. El Ichi *et al.*, “Microconductometric immunosensor for label-free and sensitive detection of Gram-negative bacteria,” *Biosens. Bioelectron.*, vol. 54, pp. 378–384, 2014.

[173] X. Zhang *et al.*, “Conductometric sensor for viable Escherichia coli and Staphylococcus aureus based on magnetic analyte separation via aptamer,” *Microchim. Acta*, vol. 187, pp. 1–10, 2020.

[174] P. Qi, Y. Wan, and D. Zhang, “Impedimetric biosensor based on cell-mediated bioimprinted films for bacterial detection,” *Biosens. Bioelectron.*, vol. 39, no. 1, pp. 282–288, 2013.

[175] Y. Chen *et al.*, “Recent advances in rapid pathogen detection method based on biosensors,” *Eur. J. Clin. Microbiol. Infect. Dis.*, vol. 37, pp. 1021–1037, 2018.

[176] E. Yilmaz, D. Majidi, E. Ozgur, and A. Denizli, “Whole cell imprinting based Escherichia coli sensors: A study for SPR and QCM,” *Sensors Actuators B Chem.*, vol. 209, pp. 714–721, 2015.

[177] E. I. Prest, F. Hammes, M. C. M. Van Loosdrecht, and J. S. Vrouwenvelder, “Biological stability of drinking water: controlling factors, methods, and challenges,” *Front. Microbiol.*, vol. 7, p. 45, 2016.

[178] E. Canale-Parola, “Sarcina,” *Bergey’s Man. Syst. Archaea Bact.*, pp. 1–9, 2015.

[179] D. Elfadil, A. Lamaoui, F. Della Pelle, A. Amine, and D. Compagnone, “Molecularly imprinted polymers combined with electrochemical sensors for food contaminants analysis,” *Molecules*, vol. 26, no. 15, p. 4607, 2021.

[180] L. E. Ahangar and M. A. Mehrgardi, “Amplified detection of hepatitis B virus using an electrochemical DNA biosensor on a nanoporous gold platform,” *Bioelectrochemistry*, vol. 117, pp. 83–88, 2017, doi: 10.1016/j.bioelechem.2017.06.006.

[181] H. S. Magar, R. Y. A. Hassan, and A. Mulchandani, “Electrochemical Impedance Spectroscopy (EIS): Principles, Construction, and Biosensing Applications.,” *Sensors (Basel).*, vol. 21, no. 19, Oct. 2021, doi: 10.3390/s21196578.

[182] T. Pajkossy and R. Jurczakowski, “Electrochemical impedance spectroscopy in interfacial studies,” *Curr. Opin. Electrochem.*, vol. 1, no. 1, pp. 53–58, 2017, doi:

https://doi.org/10.1016/j.coelec.2017.01.006.

[183] M. de Pauli *et al.*, “Capacitance spectra extracted from EIS by a model-free generalized phase element analysis,” *Electrochim. Acta*, vol. 320, p. 134366, 2019, doi: https://doi.org/10.1016/j.electacta.2019.06.059.

[184] M. Barreiros dos Santos, J. P. Agusil, B. Prieto-Simón, C. Sporer, V. Teixeira, and J. Samitier, “Highly sensitive detection of pathogen Escherichia coli O157:H7 by electrochemical impedance spectroscopy,” *Biosens. Bioelectron.*, vol. 45, pp. 174–180, 2013, doi: https://doi.org/10.1016/j.bios.2013.01.009.

[185] L. Yang and R. Bashir, “Electrical/electrochemical impedance for rapid detection of foodborne pathogenic bacteria,” *Biotechnol. Adv.*, vol. 26, no. 2, pp. 135–150, 2008, doi: https://doi.org/10.1016/j.biotechadv.2007.10.003.

[186] J. S. Daniels and N. Pourmand, “Label-Free Impedance Biosensors: Opportunities and Challenges,” *Electroanalysis*, vol. 19, no. 12, pp. 1239–1257, Jun. 2007, doi: https://doi.org/10.1002/elan.200603855.

[187] C. Ruan, L. Yang, and Y. Li, “Immunobiosensor chips for detection of Escherichia c oli O157: H7 using electrochemical impedance spectroscopy,” *Anal. Chem.*, vol. 74, no. 18, pp. 4814–4820, 2002.

[188] A. Doostmohammadi *et al.*, “Molecularly imprinted polymer (MIP) based core-shell microspheres for bacteria isolation,” *Polymer (Guildf).*, vol. 251, p. 124917, 2022.

[189] I. K. Bigdeli, M. Yeganeh, M. T. Shoushtari, and M. K. Zadeh, “Chapter 23 - Electrochemical impedance spectroscopy (EIS) for biosensing,” in *Micro and Nano Technologies*, S. Thomas, T. A. Nguyen, M. Ahmadi, A. Farmani, and G. B. T.-N. for S. M. Yasin, Eds. Elsevier, 2021, pp. 533–554. doi: https://doi.org/10.1016/B978-0-12-

823358-0.00025-3.

[190] F. Moghtader, G. Congur, H. M. Zareie, A. Erdem, and E. Piskin, “Impedimetric detection of pathogenic bacteria with bacteriophages using gold nanorod deposited graphite electrodes,” *RSC Adv.*, vol. 6, no. 100, pp. 97832–97839, 2016.

[191] A. Doostmohammadi, K. Youssef, S. Akhtarian, G. Kraft, and P. Rezai, “Fluorescent bacteria detection in water using cell imprinted polymer (CIP) coated microparticles in a magnetophoretic microfluidic device,” *Talanta*, vol. 268, p. 125290, 2024, doi: https://doi.org/10.1016/j.talanta.2023.125290.

[192] J. C. Miller and J. N. Miller, “Statistics and Chemometrics for Analytical Chemistry . Gosport.” United Kingdom: Pearson Prentice-Hall, 2010.

[193] T. Wangchareansak, C. Sangma, K. Choowongkomon, F. Dickert, and P. Lieberzeit, “Surface molecular imprints of WGA lectin as artificial receptors for mass-sensitive binding studies,” *Anal. Bioanal. Chem.*, vol. 400, no. 8, pp. 2499–2506, 2011, doi: 10.1007/s00216-011-4952-0.

[194] D. Mastropietro, K. Park, and H. Omidian, “4.23 Polymers in Oral Drug Delivery,” P. B. T.-C. B. I. I. Ducheyne, Ed. Oxford: Elsevier, 2017, pp. 430–444. doi: https://doi.org/10.1016/B978-0-12-803581-8.09291-2.

[195] C. Malitesta, E. Mazzotta, R. A. Picca, A. Poma, I. Chianella, and S. A. Piletsky, “MIP sensors–the electrochemical approach,” *Anal. Bioanal. Chem.*, vol. 402, pp. 1827–1846, 2012.

[196] X. Kan, T. Liu, H. Zhou, C. Li, and B. Fang, “Molecular imprinting polymer electrosensor based on gold nanoparticles for theophylline recognition and determination,” *Microchim. Acta*, vol. 171, pp. 423–429, 2010.

[197] A. Singhal *et al.*, “MXene-modified molecularly imprinted polymers as an artificial bio-recognition platform for efficient electrochemical sensing: progress and perspectives,” *Phys. Chem. Chem. Phys.*, vol. 24, no. 32, pp. 19164–19176, 2022, doi: 10.1039/D2CP02330J.

[198] J. Canny, “A computational approach to edge detection,” *IEEE Trans. Pattern Anal. Mach. Intell.*, no. 6, pp. 679–698, 1986.

[199] A. Vancleef, D. Maes, T. Van Gerven, L. C. J. Thomassen, and L. Braeken, “Flow-through microscopy and image analysis for crystallization processes,” *Chem. Eng. Sci.*, vol. 248, p. 117067, 2022, doi: https://doi.org/10.1016/j.ces.2021.117067.

[200] P. K. Bellairu, S. Bhat, and E. V Gijo, “Modelling and optimisation of natural fibre reinforced polymer nanocomposite: application of mixture-design technique,” *Multidiscip. Model. Mater. Struct.*, 2020.